INVESTIGATION OF MOLYBDENUM LIMITATION ON MICROBES IN A NITRATE- AND METAL-CONTAMINATED SITE AT OAK RIDGE RESERVATION

by

XIAOXUAN GE

(Under the Direction of Michael W. W. Adams)

ABSTRACT

Anthropogenic nitrate contamination is a serious problem in many natural environments. Nitrate removal by microbial action is dependent on molybdenum (Mo), which is required by nitrate reductase in denitrification and dissimilatory nitrate reduction to ammonium. The contaminated area at Oak Ridge Reservation (ORR) is an extreme acidic environment contaminated by nitrate, various metals, etc. In this study, it was demonstrated that Fe and Al mineral formation that occurs as the pH of acidic synthetic groundwater is increased, decreases soluble Mo to low picomolar concentrations, a process proposed to mimic environmental diffusion of acidic contaminated groundwater. Analysis of ORR sediments revealed recalcitrant Mo in the contaminated core that co-occurred with Fe and Al, consistent with Mo scavenging by Fe/Al precipitates. ORR strain *Bacillus* strain EB106-08-02-XG196 isolated from contaminated sediment is more tolerant to multiple metals (Cd, Ni, Cu, Co, Mn and U) but also exhibits more robust growth compared to control strains under low molybdate concentrations (< 1 nM), including *Pseudomonas fluorescens* N2E2 from a pristine ORR environment. Molybdate is taken up by the molybdate binding protein, ModA, of the molybdate ATP-binding cassette transporter. ModA of XG196 is phylogenetically distinct from those of other characterized ModA proteins. Isothermal titration calorimetry analysis showed XG196 ModA molybdate binding constant ($K_D$) is 2.2 nM,

about one order of magnitude lower than those of *P. fluorescens* N2E2 (27.0 nM) and *E. coli* K12 (25.0 nM). XG196 ModA also showed higher affinity for molybdate than for tungstate ($K_D$ 11 nM), whereas the ModA proteins from *P. fluorescens* N2E2 and *E. coli* K12 ModA had similar affinities for the two oxyanions. This high molybdate affinity coupled with resistance to multiple metals gives strain XG196 a competitive advantage in Mo-limited environments contaminated with high concentrations of metals and nitrate, as found at ORR. Nitrous oxide ($N_2O$), a greenhouse gas, can be produced in ORR by nitrification, denitrification, chemodenitrification. Effects of ORR environment-related metals (Mo, Cu, Cd, Co, Ni, U and metal mix) on $N_2O$ emission were demonstrated by ORR strains *Rhodanobacter* R12 and *Acidovorax* 3H11 in this study.

INDEX WORDS: molybdenum limitation, Fe/Al precipitation, the Oak Ridge Reservation, nitrate contamination, nitrate reduction, *Bacillus sp.* XG196, Illumina sequencing, high molybdate affinity ModA, ITC, nitrous oxide, metal effects.

# INVESTIGATION OF MOLYBDENUM LIMITATION ON MICROBES IN A NITRATE- AND METAL-CONTAMINATED SITE AT OAK RIDGE RESERVATION

by

XIAOXUAN GE

BS, Shandong Normal University, China, 2011

MS, University of Chinese Academy of Sciences, China, 2015

A Dissertation Submitted to the Graduate Faculty of The University of Georgia in Partial Fulfillment of the Requirements for the Degree

DOCTOR OF PHILOSOPHY

ATHENS, GEORGIA

2020

# INVESTIGATION OF MOLYBDENUM LIMITATION ON MICROBES IN A NITRATE- AND METAL-CONTAMINATED SITE AT OAK RIDGE RESERVATION

by

XIAOXUAN GE

| | |
|---|---|
| Major Professor: | Michael W. W. Adams |
| Committee: | Mary Ann Moran |
| | Jorge C. Escalante |
| | Elizabeth Ann Ottesen |

Electronic Version Approved:

Ron Walcott
Dean of the Graduate School
The University of Georgia
December 2020

# DEDICATION

This dissertation is dedicated to my family in China that has been supporting and encouraging me throughout these years at UGA. To my parents, Zhenmei Guo and Jindong Ge for your selfless love, support and understanding for me studying abroad. To my brother, Shunxin Ge (Gray) for being such a wonderful brother, my best friend and taking cate of mom and dad all these years. To my beloved husband, Jian Wang (Jackie), for his endless love, patience and support in every way in my life. To my dearest baby, Alex, for giving me the chance to be a mom, the greatest title in this world.

ACKNOWLEDGEMENTS

I am thankful to all those who supported me these years. Special thanks to Dr. Michael W. W. Adams for his wonderful mentorship, support and encouragement. His passion, talent and valuable experience inspire me so much and guide me to be a better scientist. I appreciate the support and feedback provided by committee members Dr. Jorge Escalante, Dr. Mary Ann Moran and Dr. Elizabeth Ann Ottesen.

I would like to thank Dr. Michael P. Thorgersen for sharing his valuable research experiences and great ideas with me. My special thanks to Farris L. Poole for his support, instructions and informative discussions. I would like to thank Dr. Gerrit JAN Schut for his help and sharing his parenthood experience. I would also like to thank my lab mates in Adams lab who are very supportive and are important parts of my doctoral journey.

Lastly, I would like to thank my family and close friends for their love and support, which have motivated me in many different ways.

TABLE OF CONTENTS

Page

LIST OF TABLES

Page

LIST OF FIGURES

Page

# CHAPTER 1

# INTRODUCTION AND LITERATURE REVIEW

## Nitrogen cycle

Nitrogen (N) in one of the six most important elements in living organisms, which also includes carbon (C), hydrogen (H), oxygen (O), phosphorus (P) and sulfur (S) (1, 2). The nitrogen cycle, which involves the processes by which multiple nitrogen chemical forms interconvert between the environment and the living organisms, is also one of the most important biogeochemical cycles in nature (3, 4). Microorganisms play very important roles in dinitrogen gas fixation, nitrification, denitrification, dissimilatory nitrate reduction to ammonium and anaerobic ammonium oxidation, which together constitute the microbial nitrogen cycle (Figure 1.1) (5-7). Dinitrogen gas fixation is the process that converts nitrogen gas, which is about 78% of the earth atmosphere, to ammonium, nitrite and nitrate and then to organic compounds (8-10). This is the step that converts dinitrogen to available forms for the biosphere. The majority of dinitrogen gas fixation is carried out by microorganisms called diazotrophs (10, 11). Nitrification is the oxidation of ammonia to nitrite and then to nitrate (3, 4, 6). This is an aerobic process performed by some autotrophic bacteria and archaea in soil and marine environments (3, 4, 6). Denitrification is a series of reactions that reduce nitrate to nitrite ($NO_2^-$), nitric oxide (NO), nitrous oxide ($N_2O$) and finally dinitrogen ($N_2$), completing the nitrogen cycle. Denitrification in nature is mainly carried out by facultative anaerobic bacteria under anaerobic conditions as one kind of respiration. Dissimilatory nitrate reduction to ammonium (DNRA) is another form of anaerobic respiration that reduces nitrate to nitrite and ammonium (3, 4, 6). DNRA happens in prokaryotes and some eukaryotic microorganisms. DNRA only coverts nitrogen to bioavailable forms, which is different

with denitrification that reduce nitrate to dinitrogen as the end product. Anaerobic ammonium oxidation (Anammox) is a comproportionation reaction that coverts nitrite and ammonium ions to dinitrogen and water (12, 13). Anammox has been found in various natural ecosystems, including freshwater sediments and marine environments (13-16). Anammox plays an important role in removing reactive nitrogen, like gases nitrogen oxides ($NO_x$), ammonia ($NH_3$), nitrous oxide ($N_2O$), nitrite ($NO_2^-$) as well as nitrate ($NO_3^-$) and return dinitrogen to the atmosphere (17, 18).

In the microbial nitrogen cycle, there are several processes that are dependent on molybdenum-containing enzymes. These are nitrogenase in the dinitrogen fixation, nitrate reductase in the reduction of nitrate to nitrite and nitrite oxidoreductase in the oxidation of nitrite to nitrate (Figure 1.1) (19-22). Limitations of dinitrogen fixation and nitrate reduction has been reported because of lacking bioavailable molybdenum in various environments (23-26), and this issue will be further discussed in following sections.

**Nitrate contamination in natural water systems**

Nitrate comes from many sources because of natural activities and human activities. In nature, nitrate can be produced by dinitrogen fixation performed by bacteria, decaying plants, and human and animal manure (27). Human activities like fertilizer usage in agriculture, nitrogen compounds emitted by industry and automobiles contribute a large amount of nitrate to soil and natural water systems (27-29). Some bacteria are diazotrophs, together with blue-green algae and some fungi, in that they can assimilate dinitrogen from the atmosphere and use it as their sole N source (27). Nitrogen assimilation by microorganisms is the major natural mechanism which converts nitrogen gas available to animals and plants. The degradation of plant and animal tissues by microorganisms can also release ammonium or nitrate to soil and groundwater (3, 4, 6). Another source of nitrate in nature is by the degradation of nitrate and ammonium salts, like sodium nitrate, ammonium nitrate, ammonium chloride, etc. In addition, natural precipitations can also bring

ammonia and nitrate down to soil and water systems on earth (3, 4, 6). Ammonia from different sources can be oxidized to nitrate by the process of nitrification and contribute to the nitrate pool in nature.

The agricultural activities of human beings is considered as the most important anthropogenic source of nitrate, and other activities like industry pollution and automobile emission, etc. can also contribute to nitrate contamination to soil and groundwater (27, 30). The main contamination source of nitrate from agriculture is overuse of nitrogen-containing fertilizers, such as anhydrous ammonia, urea and ammonium nitrate (27, 30). Ammonia is the most basic form of nitrogen fertilizer because it is cheap, stable in soil and has a relatively high nitrogen content (27, 30). Between 2000 and 2014, nitrogen fertilizer consumption showed strong growth with an increase of 35% and reached about 110.4 Tg (teragrams, 1 Tg = 1,000,000 tons), of which China (31%), India (30%) and the United States (15%) made up about 57% of the global consumption market share (31). In the United States, 13.0 Tg of nitrogen fertilizer was consumed in 2015, which is about 59% of total plant nutrients based on the USDA webpage updated in 2019 (Fertilizer Use and Price, https://www.ers.usda.gov/data-products/fertilizer-use-and-price.aspx). Nitrogen use efficiency (NUE) is an indicator of nutrient management performance in agriculture. It is represented by the ratio of the sum of the nitrogen content in all harvested products and the sum of all nitrogen inputs (nitrogen fertilizers, animal manure, microbial nitrogen fixation, etc.) in certain systems (32). It has been estimated that the global average NUE was 47% in 2009 and 42% in 2010 (33, 34). NUE generally in developed countries (USA and Canada 68%, Europe 52%) is higher than developing countries (China 25%, India 30%) because of fertilizer best management practices (31). These data indicate that more than 50% of applied nitrogen fertilizer does not get utilized by plants and remains in the soil and in groundwater. Ammonia will turn into nitrate eventually as a result of oxidation by bacterial ammonia oxidizers, which can remain in

groundwater for decades (35, 36). Many studies have pointed out that synthetic nitrogen fertilizers are the major nitrate contamination source to groundwater (27, 30, 37).

The maximum contaminant level (MCL) for nitrate (as the nitrate ion) is 10 mg/L as N (44.27 mg of nitrate/L) in drinking water according to the standard of the U.S. Environmental Protection Agency's (EPA) and 11.3 mg/L as N (50 mg of nitrate/L) in WHO guideline (38). Nitrate concentration in natural groundwater is typically less than 2 mg/L (39). Higher nitrate concentrations in groundwater were reported in areas of nitrogen fertilizer application in Iran (8 to 20 mg of nitrate /L) (38), in locations with N-fertilizer applied in large quantities in China (300 mg of nitrate/L) (40), in rural agricultural district in India (450 mg/L) (41), in a heavy metal contaminated area in the United States (230 mg/L) (26). Groundwater is an important drinking water source for human beings. It is the source of domestic water for 50% of the US population and for 90% of the people living in rural area (27). In 2006, 1.9 million people in the US were predicted to use drinking water from private wells with $\geq$ 5 mg/L nitrate (42).

High nitrate persistence can increase nitrate eutrophication, a phenomena that water becomes overly enriched with minerals and nutrients which induce excessive growth of algae, death of zooplankton and fish (dead zones), and hypoxia (18, 43). Dead zones have now been reported for more than 400 water systems, which affects more than 245,000 square kilometers (43). Hypoxia can result in the death of fish and invertebrates, loss of habitat and enhanced susceptibility to diseases for resident organisms, and change of predator–prey interactions in river, lakes and marine systems (44-46). High consumption of nitrate can be detrimental to human health and is known to cause many problems, like cancer, adverse reproductive outcomes, thyroid disease and methemoglobinemia in infants and adults (47-49).

**Nitrate reduction**

Two dissimilatory nitrate reduction pathways, denitrification and DNRA, are the two major processes in nature that can reduce nitrate from the environment, mainly carried out by microorganisms. In denitrification, nitrate ($NO_3^-$) is first reduced to nitrite ($NO_2^-$) by dissimilatory nitrate reductase, next nitrite is reduced to nitric oxide (NO) by nitrite reductase (NO-forming), then to nitrous oxide ($N_2O$) by nitric oxide reductase. The last step is the reduction of nitrous oxide to dinitrogen ($N_2$) by nitrous oxide reductase. All four reactions usually take place under anaerobic conditions (50) but denitrification is also observed under aerobic conditions in some microorganisms (51-53). DNRA pathway is another form of nitrate-dependent anaerobic respiration but in this case nitrate is reduced to nitrite by nitrite reductase and then nitrite is reduced to ammonium ($NH_4^+$) by nitrite reductase (54). Assimilatory nitrate reduction also occurs in prokaryotes, in which nitrate is reduced nitrite and then to ammonium while nitrite is the intermediate. Assimilatory nitrate reduction is not sensitive to $O_2$, but can be inhibited by ammonia and organic nitrogen (55, 56). Thus it is believed to happen mainly in aerobic habitats, where ammonium is not high (55).

Three different types of nitrate reductase have been widely studied and described in detail. These are respiratory nitrate reductases (NAR), periplasmic nitrate reductases (NAP), and assimilatory nitrate reductases (NAS) (57, 58). The NARs are composed by three subunits, NarG (112–140 kDa), NarH (52–64 kDa) and NarI (19–25 kDa), and is one kind of anaerobic nitrate respiration (Figure 1.2 Left) (59-61). Crystal structures and other studies has revealed NarG and NarH are anchored to the membrane side by NarI, which is a transmembrane subunit (60). NarG is the catalytic subunit and contains a molybdenum cofactor (molybdo-bis(pyranopterin guanine dinucleotide), Mo-bisMGD) at its active site and one iron-sulfur cluster ([4Fe-4S]). NarH is an electron-transfer subunit, which contains three [4Fe-4S] clusters and one [3Fe-4S] cluster. The

membrane anchor subunit NarI contains two heme b cofactors (Figure 1.1). A probable electron-transfer pathway is that menaquinol ($MQH_2$) is oxidized by NarI, which passes electrons to NarH by two hemes and also release two $H^+$ to the periplasm. NarH then passes electrons via iron-sulfur clusters to the Mo-bisMGD reactive site in NarG and reduces nitrate to nitrite (Figure 1.1 left) (61).

Periplasmic nitrate reductases (NAP) are composed of one large subunit NapA (80-90 kDa) and one small subunit NapB (about 17 kDa) located in periplasm (Figure 1.2 middle) (58). NapA contains a Mo-bisMGD cofactor and an FeS center, while NapB contains two c-type cytochromes (62, 63). NapAB also requires by NapH (with two iron-sulfur clusters), NapG (with four iron-sulfur clusters) and NapC (with four c-type cytochromes), to enable the nitrate reduction process. In this case, NapA is the catalytic subunit and reduce nitrate to nitrite by its catalytic Mo-bisMGD using electrons passed from other proteins. Two electron transfer pathways have been proposed. In the first, ubiquinol ($UQH_2$) is oxidized by NapHGC and electrons are transferred to NapAB, meanwhile two $H^+$ are translocated to the periplasm. This process has also been reported to translocate two more $H^+$ out of the cell (64). In the second pathway, $MQH_2$ is oxidized by NapC (which is unable to use $UQH_2$) and transfer two electrons to NapAB and also release two $H^+$ (Figure 1.2 middle) (58).

Assimilatory nitrate reductases (NAS) are located in cytoplasm in different bacteria. The catalytic subunit, like NasA in *Klebsiella oxytoca* and NasC in *Bacillus subtilis*, or NarB in *Synechococcus sp.* PCC7942, all have an active site containing a Mo-bisMGD cofactor. However, they are quite different in molecular properties and the nature of their electron transfer centers. As shown in Figure 1.2, Nas from *Klebsiella oxytoca* and *Bacillus subtilis* are heterodimers made up of a large catalytic subunit NasA with one Mo-bisMGD, one [4Fe-4S] and one [2Fe-2S] and a small subunit NasC with FAD, which uses NAD(P)H as an electron donor. In contrast, the catalytic

subunit of *Bacillus subtilis* NasC contains the Mo-bisMGD cofactor and only one [4Fe-4S] center, whereas its small subunit NasB has two [2Fe-2S] centers and one FAD cofactor. Monomeric NarB in *Synechococcus sp.* PCC7942 only has one [4Fe-4S] besides the Mo catalytic center and uses ferredoxin (Fd) as electron donor (57, 58). All nitrate reductase catalytic units described above have Mo cofactors as the active sites, the nature of which will be discussed in detail in the following sections.

**Molybdenum and Mo cofactor enzymes**

Molybdenum (Mo) has an atomic number of 42 and is a required trace element for most life forms. Most molybdenum compounds have a low solubility in water but molybdate ($MoO_4^{2-}$) is quite soluble and thus widely distributed (65). Mo has various oxidation states (from +2 to +6) but only the oxidation states of +4, +5, and +6 are biologically important and used for oxidation-reduction reactions in different enzymes (66). Mo plays an important role in biosphere as Mo enzymes are found in bacteria, plants, and animals and are involved in a wide range of reactions in nitrogen, carbon and sulfur metabolism (20-22). Mo is an essential element for all higher eukaryote organisms but not in all bacteria (67). Tungsten (W), which is generally regarded as an antagonist of Mo, is required in some enzymes rather than Mo, especially in archaea. The physiological oxidation states of W are also +4, +5, and +6 (7). There are five distinct enzyme families that use Mo (and in some cases W), and they are nitrogenase (Mo only, although some can use iron or vanadium), the xanthine oxidase family (Mo only), the sulfite oxidase family (Mo only), the DMSO reductase family (most use Mo, a few use W) and the WOR family (W only, with one example known that uses Mo) (68).

Two main types of Mo cofactors are found in nature that have developed to control the redox state and catalytic power of Mo (69). The first type of Mo-containing cofactor is the iron-molybdenum cofactor or FeMo-co that contains seven iron atoms in addition to Mo ($MoFe_7S_9C$,

Figure 1.3B) and is found in nitrogenase (69). This is a critical step in the nitrogen cycle as it converts the atmospheric dinitrogen into the bioavailable form ammonium. The second type is the molybdenum cofactor which is mononuclear and lacks any other metal. The Mo atom bound to the cis-dithiolene (–S–C=C–S–) group of an organic cofactor termed molybdopyranopterin (MPT) (Figure 1.3A). Terminal oxo or sulfur groups, or sulfur and/or selenium atoms from amino acid side-chains complete the Mo coordination sphere (Figure 1.3B) (7). Non-nitrogenase Mo-enzymes are grouped into three families: the xanthine oxidase (XO) family, the sulfite oxidase (SO) family and the dimethylsulfoxide (DMSO) reductase family.

More than 50 different Mo cofactor enzymes are found in nature (19-21, 69). Members of the XO and SO families have one MPT molecule. The difference between them is that the third Mo–S ligand of sulfite oxidase is provided by a cysteine (Cys) and third Mo–X ligand of xanthine oxidase is either S, Se, O or S-Cu-S (Figure 1.3B). By contrast, enzymes of the DMSOR family have two MPT molecules coordinated to one Mo and form a Mo bis-MPT guanine dinucleotide cofactor (Mo-bisMGD; Figure 1.3B). In addition to the four S atoms from the two MPTs, the coordination sphere of the Mo is completed by terminal S, Se or O, or via Asp (O), Ser (O), Cys (S), SeCys (Se) and $H_2O$ (OH) (69, 70). The XO family includes enzymes such as xanthine dehydrogenase (XDH) from the photosynthetic bacterium *Rhodobacter capsulatus*. This enzyme is cytoplasmic and catalyzes the oxidation of hypoxanthine to xanthine then to uric acid with $NAD^+$ as the electron acceptor. XDH in *R. capsulatus* is composed of XdhA and XdhB subunits ($\alpha_2\beta_2$). The N-terminal domain of XdhA binds two iron-sulfur [2Fe-2S] clusters while its C-terminal domain binds one FAD. XdhB is the Mo cofactor binding subunit, which sits between two domains (Mo1 domain and Mo2 domain) (71). The electrons are transferred from the Mo cofactor to the two [2Fe-2S] clusters then to FAD and finally to $NAD^+$ (72).

Sulfite oxidase in *Starkeya novella* (formerly *Thiobacillus novellus*) catalyzes the oxidation of sulfite to sulfate in some phototrophic and chemotrophic sulfur-oxidizing microorganisms. This enzyme is located in the periplasm and is a heterodimer (αβ), with one subunit (SorA) containing the Mo cofactor while the other (SorB) contain a cytochrome (73). One type of nitrate reductase, Nas, belongs to this family while the other two, Nap and Nar, belong to the DMSOR family (74). Enzymes of the DMSOR family are widely spread in prokaryotes (72, 75) and can contain just one Mo bis-(pyranopterin guanine dinucleotide) or Mo-bisPGD cofactor (as in trimethylamine- N-oxide reductase (TorA), dimethyl sulfoxide reductase (DorA) and biotin sulfoxide reductase (BisC)), one Mo-bisPGD cofactor and a heme (periplasmic nitrate reductase NapAB), or be even more complex in the form of multisubunit membrane-bound proteins (formate dehydrogenase-N (FdnGHI), dimethylsulfoxide reductase (DmsABC) and nitrate reductase (NarGHI)) (72, 76, 77). Enzymes of the DMSOR family catalyze a number of reactions essential to the carbon, nitrogen, sulfur, arsenic, and selenium biogeochemical cycles (75). Phylogenetic analysis showed that the formylmethanofuran dehydrogenase subunit (FwdB/FmdB), which reduces $CO_2$ to formate in hydrogenotrophic methanogenesis, is the most ancient lineage in DMSOR family and selenocysteine is the ancestral ligand for the Mo atom (75).

Rather than Mo, some bacteria and many anaerobic archaea require tungsten (W) in the form of tungstate ($WO_4^{2-}$). W (atomic number 74) is in the same group as Mo in the Periodic Table and they have very similar chemical properties. W is usually regarded as an antagonist of Mo and is typically taken up by Mo-dependent microbes leading to the production of inactive W-containing molybdoenzymes or molybdoenzymes lacking Mo or W (78). In the earth's crust Mo and W are similarly abundant but molybdate is about 10,000-fold more abundant than tungstate in seawater (W: 0.054 nM, Mo: 104 nM) (78). W concentrations in freshwater systems and generally higher an order of magnitude higher than in in seawater (79). W is bound to W containing enzymes

as tungstate, in which two MPT molecules coordinated to one W and form a W bis-MPT guanine dinucleotide cofactor (W-bisMGD) by the four S atoms from the two MPTs and S, Se or O, or via Asp (O), Ser (O), Cys (S), SeCys (Se) and $H_2O$ (OH) (Figure 1.3B) (69, 70).

Representative W-containing enzymes that are unable to use Mo include the AOR family of enzymes found in the prototypical hyperthermoophillic archaeon, *Pyrococcus furiosus.* This organism contains five members of this family, all of which have been purified and characterized to various degrees. They are aldehyde ferredoxin oxidoreductase (AOR) (80, 81), glyceraldehyde-3-phosphate ferredoxin oxidoreductase (GAPOR) (82), formaldehyde ferredoxin oxidoreductase (FOR) (83), the fourth tungsten-containing oxidoreductase (WOR4) (84) and the fifth tungsten-containing oxidoreductase (WOR5) (85). AOR has a broad substrate specificity but is most active with aldehydes derived from amino acids (86, 87). GAPOR has one known substrate, which is glyceraldehyde-3-phosphate, and it functions in the unusual glycolytic pathway that is present in *P. furiosus* (82, 88). C4 to C6 semi- and dialdehydes are the best substrates for FOR (83). No activity has been identified for WOR4, it may play a role in $S^0$ reduction as it could not be purified without $S^0$ in the medium (84). WOR5 has a broad substrate specificity and can use aliphatic and aromatic aldehydes as substrates (85). In addition, W-specific enzymes also include *G. metallireducens* benzoyl-CoA reductase (BCR) (7) and *Pelobacter acetylenicus* acetylene hydratase (AH) (89). There are also a group of enzymes that are catalytically active with Mo but are also able to incorporate W and are also active with this metal. These include formate dehydrogenase (FDH) (90, 91), tungsten-containing formylmethanofuran dehydrogenase (FWD) (92), thiosulfate reductase (TSR) (93), dimethyl sulfoxide reductase (DMSOR) (94), membrane-bound nitrate reductase (NAR) (95) and periplasmic nitrate reductase (NAP) (96) found in specific strains (70).

**Molybdate uptake and transport**

Mo is taken up into microbial cells in form of molybdate ($MoO_4^{2-}$) and this can occur via three different transport systems. For example, in *E. coli,* molybdate can enter the cytoplasm by a high-affinity ATP-binding cassette (ABC) transporter, by a sulfate ABC transporter or by a non-specific anion transporter (65, 66, 97). Most organisms use the high-affinity molybdate ABC transporter as the sulfate ABC and the non-specific anion transporter have much lower affinities for molybdate (98). There are two types of ABC system able to transport molybdate, one of which can also transport tungstate, in addition to a tungstate-specific transporter. These are referred to as ModABC, WtpABC and TupABC, respectively and are each composed of three proteins, a periplasmic binding protein A, a membrane protein B and the ATPase C (97). Of these, most microorganisms use the ModABC system and this is also the best studied. A crystal structure of ModABC transporter complex from *Archaeoglobus fulgidus* has been solved to 3.1 Å resolution which has one ModA subunit, two ModB subunits and two ModC subunits ($ModAB_2C_2$, PDB: 2ONK) (Figure 1.4) (99). The *E. coli* ModA system is encoded by the *modABCDEF* operon and is well studied. ModA (275 amino acids) is a monomer and binds molybdate with a stoichiometry of 1:1. The structure of *E. coli* ModA has been solved with resolution at 1.75 Å (PDB: 1AMF) (100). ModB (229 amino acids) is highly hydrophobic and forms a membrane channel. ModC (352 amino acids) which contains an ATP-binding domain and is assumed to provide energy for molybdate transport by the ABC complex. ModE (262 amino acids) depresses the expression of *modABC* by binding to its operator region when it binds Mo, while the functions of ModD (231 amino acids) ModF (490 amino acids) are unknown (97). The ModA proteins of *Xanthomonas axonopodis pv. citri* 306 (PDB: 2H5Y, $MoO_4^{2-}$), *E. coli* K12 (PDB: 1AMF, $MoO_4^{2-}$), *Vibrio cholerae* serotype O1 ATCC 39315 (PDB:4RXL, $WO_4^{2-}$) and *Azotobacter vinelandii* (PDB: 1ATG, $WO_4^{2-}$) have been determined, in which molybdate or tungstate was bounded (Figure 4.3

and 3.5) (100-102). The tungsten-utilizing microorganisms take up tungstate using a transporter (WtpA) and the structures of WtpA from *Methanosarcina acetivorans* ATCC 35395 (PDB: 3CFX, $WO_4^{2-}$), *Methanocaldococcus jannaschii* ATCC 43067 (PDB: 3CFZ, $WO_4^{2-}$), *Pyrococcus furiosus* ATCC 43587 (PDB: 3CG1, $WO_4^{2-}$), *Archaeoglobus fulgidus* ATCC 49558 (PDB: 3CIJ, $WO_4^{2-}$) and *P. horikoshii* ATCC 700860 (PDB: 3CG3, $WO_4^{2-}$) are known, all of which bind one tungstate ion (103).

The affinity of the ModABC system appears to vary with different organisms. The ModA of *E. coli* has a high specificity and affinity for molybdate with $K_D$ values reported in the range of 20-27 nM (104, 105). In contrast, the value for the ModA of *Xanthomonas axonopodis pv. citri* (strain 306) is 290 ± 100 nM (106) while that for the protein from *Bradyrhizobium japonicum* was in the 100 nM range (107). Molybdate is also transported by tungstate transport protein A, or WtpA, which is part of a different ABC transporter system that uses both tungstate and molybdate. WtpA is found in organisms that lack ModA and is common in archaea. WtpA from hyperthermophilic archaeon *Pyrococcus furiosus* has a much higher affinity for tungstate ($K_D$ of 17 ± 7 pM) than that for molybdate ($K_D$ of 11 ± 5 nM) with a 1:1 stoichiometry as measured by isothermal titration calorimetry (ITC) (108). The third transporter that transports tungstate but not molybdate is the tungstate binding protein TupABC. TupA of *Desulfovibrio alaskensis* G20 has very strong affinity for tungstate ($K_D$ of 6.30 ± 0.02 pM) (109) and its structure has also been determined (PDB: 5MY5) (109).

**Molybdenum limitation**

Mo is found at concentrations of about 1–10 mg/kg in most rocks and soils (65). Mo in form of molybdate ($MoO_4^{2-}$) is the most abundant transition metal in seawater and its concentration is a very stable in the ocean (about 100 nM) (110) but its concentration varies in different freshwaters from several pM to several μM (78, 111, 112). The 2011 WHO Guidelines for

Drinking-Water Quality (fourth edition) advised a health-based value of 70 µg/L (730 nM) for Mo but it is also mentioned in the guideline that it is not necessary to set a formal guideline value as Mo generally occurs at very low concentrations in drinking-water (65, 112). Low environmental and/or dietary Mo can result in health problems in humans, oral, esophageal and gastric cancers are reported because of decreased reduction of nitrate and nitrosamine (113-116). Low Mo could affect animal or human health by affecting molybdenum enzymes like aldehyde oxidase, sulfite oxidase and xanthine oxidase especially in early life stage, in utero stage and the postnatal developmental period (117).

Even though Mo concentrations are naturally low in environments as described above, they can be lower in some environments because molybdate can be further removed from the environment. For example, molybdate is precipitated from sea water in the form of molybdenum-iron-sulfur compounds as $HS^-$, thiols, and humic-bound thiol groups and thus Mo forms covalent bonds to transition metals (especially Fe) and organic molecules via S bridges (118). Molybdate is also known to bind to insoluble organic matter in top soils by plant-derived tannins and tannin-like compounds and bind to both iron oxides and natural organic matter in deeper soils (119, 120). Magnesium–aluminum layered double hydroxides precipitated from reaction between magnesium chloride and synthetic sodium aluminate solution can also absorb transition metal oxyanions like molybdate from solution into hydrotalcite (121). The precipitation of common cations magnesium ($Mg^{2+}$) and iron ($Fe^{3+}$) as $MgFeCO_3$-type hydrotalcite-like layered double hydroxide has high affinity for solute like molybdate (122). Molybdate can also adsorb directly to insoluble minerals such as ferrihydrite ($Fe_2O_3 \bullet xH_2O$) and gibbsite ($Al(OH)_3$) as a pH-dependent process when the pH increases from pH 3.1 to 6.3 for Fe precipitates, or from pH 5.5 to 6.7 for Al precipitates (121-125). However, it is not clear if any of the different Mo depleting mechanisms are effective enough to affect specific bioactivities in natural environments.

**Nitrate and metal contamination in ORR**

There is a very special contaminated site at the Oak Ridge Reservation (ORR) in Tennessee, USA. The US government disposed of millions of liters of waste containing nitric acid and toxic metals at this site between 1951 and 1983. The waste generated from uranium operations at the Y-12 Plant and was discarded into four unlined earthen reservoirs referred to as the S-3 ponds with ~9.5 million liters in each of the four ponds (126). Nitrate generated from nitric acid is a major contaminant in these ponds. In 1978, the pH values of the ponds ranged from 0.8 to 5.3 and contained nitrate at concentrations up to 74 g/L (1.2 M; (126)). Metals present included iron up to 1.2 g/L (about 21.4 mM), aluminum up to 4.8 g/L (about 177.8 mM), magnesium up to 0.67 g/L (about 27.6 mM) and uranium up to 0.32 g/L(about 1.3 mM) (126). In 1983, in an effort to clean-up the waste site and slow the leaching of contaminants, the pH in the S-3 ponds was adjusted to about 9 (126, 127). The precipitates and sludge that formed from this process were allowed to settle and the liquid waste was removed, treated and discharged into a nearby river (126). In 1988 the 1-meter-thick sludge that remained contained high concentrations of aluminum, calcium, and iron was stabilized with coarse aggregates and the S-3 ponds were filled and capped with a parking lot (127). In 1997, an analysis of the groundwater in 46 wells surrounding the parking lot revealed that there was a plume of nitrate that extended approximately 1 km to a depth of over 100 meters (128, 129). In the most recent survey at ORR in 2015, groundwater from wells in the contamination plume were still at low pH and contained high concentrations of nitrate (up to 230 mM) and various metals measured by our laboratory. The metals included uranium (up to 580 μM), aluminum (up to 20.7 mM), manganese (up to 3.1 mM), nickel (up to 157 μM), cobalt (up to 30 μM), cadmium (up to 10 μM), copper (up to 15 μM), chromium (up to 11 μM), lead (up to 0.5 μM) and thorium (up to 8 μM) (130). Interestingly, of 26 metals analyzed, molybdenum (Mo) was the metal that

had a noticeably lower median concentration (<<1 nM) in the highly contaminated wells than in pristine wells (up to 330 nM (26)).

**Microorganisms in ORR**

Many studies have been done to examine the relationships between microorganisms and the extremely contaminated environment in ORR from various perspectives. Geochemical analysis of groundwater samples from a total of 69 wells showed large ranges of environmental variables including uranium from 0 to 55.3 mg/L (average, 1.5 mg/L), nitrate from 0 to 11,648 mg nitrate-N/L (average, 641 mg $NO_3^-$-N/L), pHs from 3 to 10.5 (average, pH 6.9), $CO_2$ from 0 to 29,739 mg/L (average, 476 mg/L), $N_2O$ from 0 to 1.2 mg/L (average, 0.1 mg/L), $CH_4$ from 0 to 0.6 mg/L (average, close to 0 mg/L), and $H_2S$ from 0 to 4.2 mg/L (average, 0.1 mg/L), cell counts from 3.5 $\times 10^2$ to 1.8 $\times 10^6$ cells/ml (average, 1.2 $\times 10^5$ cells/ml), dissolved organic carbon (DOC) from 0.2 to 128.2 mg/L (average, 7.8 mg/L) and dissolved inorganic carbon (DIC) from 9.4 to 179.2 mg/L (average, 58.3 mg/L) (131). Metagenome analysis indicated that the abundance of ~95% of genes decreased in uranium and nitrate contaminated samples. For example, genes encoding enzymes involved in sulfur (S) cycling (e.g., *dsrA* and *sqr*), cytochrome and hydrogenase decreased as uranium increased in groundwater; some functional genes did not decrease significantly with increasing nitrate concentrations like denitrification related genes (e.g., *nirK* and *nosZ*), dissimilatory nitrate reduction (e.g., *napA*), and assimilatory nitrate reduction (e.g., *nasA*) genes; the abundance of some *dsrA*-bearing uncultured sulfate reducing bacteria increased significantly as uranium increased and increased levels of abundance of cytochrome and hydrogenase gene variants were also observed. Also, the microbial biomass increased significantly with increased nitrate concentrations (131). These observations suggest that sulfate and nitrate reducers may be dominant in the ORR contaminated environment. In the nitrate-contaminated areas at ORR, nitrous oxide ($N_2O$) was detected (as high as 1.2 mg/L) (131), which could be produced by the nitrate

reducers that dominant in the microbial community. $N_2O$ is a greenhouse gas and also contributes to stratospheric ozone destruction (132, 133). $N_2O$ can be produced by 1) biotic process that reduce nitrite produced in nitrification or denitrification and 2) abiotic process chemodenitrification. In denitrification $N_2O$ is produced by reduction of nitrite in anoxic conditions or by nitrification in presence of $O_2$ when $NH_4^+$ present (134, 135). In chemodenitrification, reactive intermediates like $NH_2OH$, $NO_2^-$ produced in nitrogen cycle pathways may engage in chemical reactions that yield $N_2O$, especially in the presence of $Fe^{2+}/Fe^{3+}$, $Mn^{4+}$, organic matter or at acidic pH ($\leq 5$) (134, 136, 137). However, it is unclear how contaminating metals affect $N_2O$ production in ORR.

In an in-field bioreactor study at ORR, researchers monitored the shifts of microbial communities from uncontaminated groundwater but incubated with filtered groundwater from a contaminated well enriched in various contaminants like chloride, nitrate, uranium, and sulfate. The results showed a loss of members of the *Bacteroidetes*, *Acidobacteria*, *Chloroflexi*, and *Betaproteobacteria*, but enrichment in the iron- and nitrate-reducing *Ferribacterium* and parasitic *Bdellovibrio* (138). It has also been shown that changes in the concentrations of dissolved organic matter (DOM) can affect microbial community significantly, tannin- and protein-like compounds play roles in early stages of ORR groundwater microbial community incubation, while the availability of lipid- and lignin-like compounds are more related with community composition and development in later stages (139). Also, complex natural organic C (sediment NOM or bacterial cell lysate) can enhance the growth of more diverse bacteria than simple organic C sources (140). These results greatly aid in the design of experiments for microbial cultivation and isolation under laboratory conditions.

Metal analysis of groundwater samples from contaminated wells and background wells revealed that metal contaminants, like U, Al, Mn, Ni, Co, Cd, Cu, Cr, Pb and Th, are higher in contaminated wells (26). Nitrate-reducing microorganisms are enriched and isolated from both

groundwater and sediments at the Oak Ridge Reservation (ORR) using concentrations of nitrate and metals similar to the contaminated environment at ORR, seven new metal-resistant, nitrate-reducing strains show various pH ranges for growth, carbon source preferences, and degrees of resistance to individual and combinations of metals (141). The one notable exception in ORR groundwater metal analysis is Mo, which is present at lower concentrations in contaminated wells (26). Hence, a fundamental question is, does Mo limitation affect biological nitrate reduction as microorganisms must use Mo as a cofactor for key enzymes in nitrate reducing pathways? And how do the contaminated metals affect the nitrate reducing organisms in ORR? These issues are addressed in the proposed research.

**Research objectives**

The main goal of this work is to examine the relationship between nitrate-reducing bacteria and the contamination in the form of metals and nitrate in the ORR environment. In particular, what are the mechanisms that enable microorganisms to survive in this unique extreme environment. In Chapter 2, the results of an investigation to determine if Mo availability to microbes is a limiting factor is described. This is obviously significant because Mo is required for biological nitrate reduction in nature. I show here that Mo limitation in the highly contaminated groundwater is a result of precipitation of iron- and aluminium-based minerals when the pH increases during the spreading of the acidic and contaminated groundwater into non-contaminated environments. In addition to reproducing this in the laboratory, evidence is presented for direct mineral-based precipitation of Mo in ORR contaminated sediments. In Chapter 3, the draft genome of a metal resistant nitrate-reducing *Bacillus* strain that I isolated from ORR contaminated sediment was described. In Chapter 4, I describe how I elucidated the mechanism by which a metal resistant nitrate-reducing *Bacillus* strain that I isolated from ORR was able to survive under extreme Mo-limitation. In Chapter 5, I describe how the effects of the essential metal Mo and of

various contaminating metals affected $N_2O$ production by two strains isolated by our collaborators from the ORR groundwater. Taken together, all of these results show that both essential (Mo) and toxic metals can have very important effects on the metabolism of nitrate in natural environments.

**Figures and Tables**

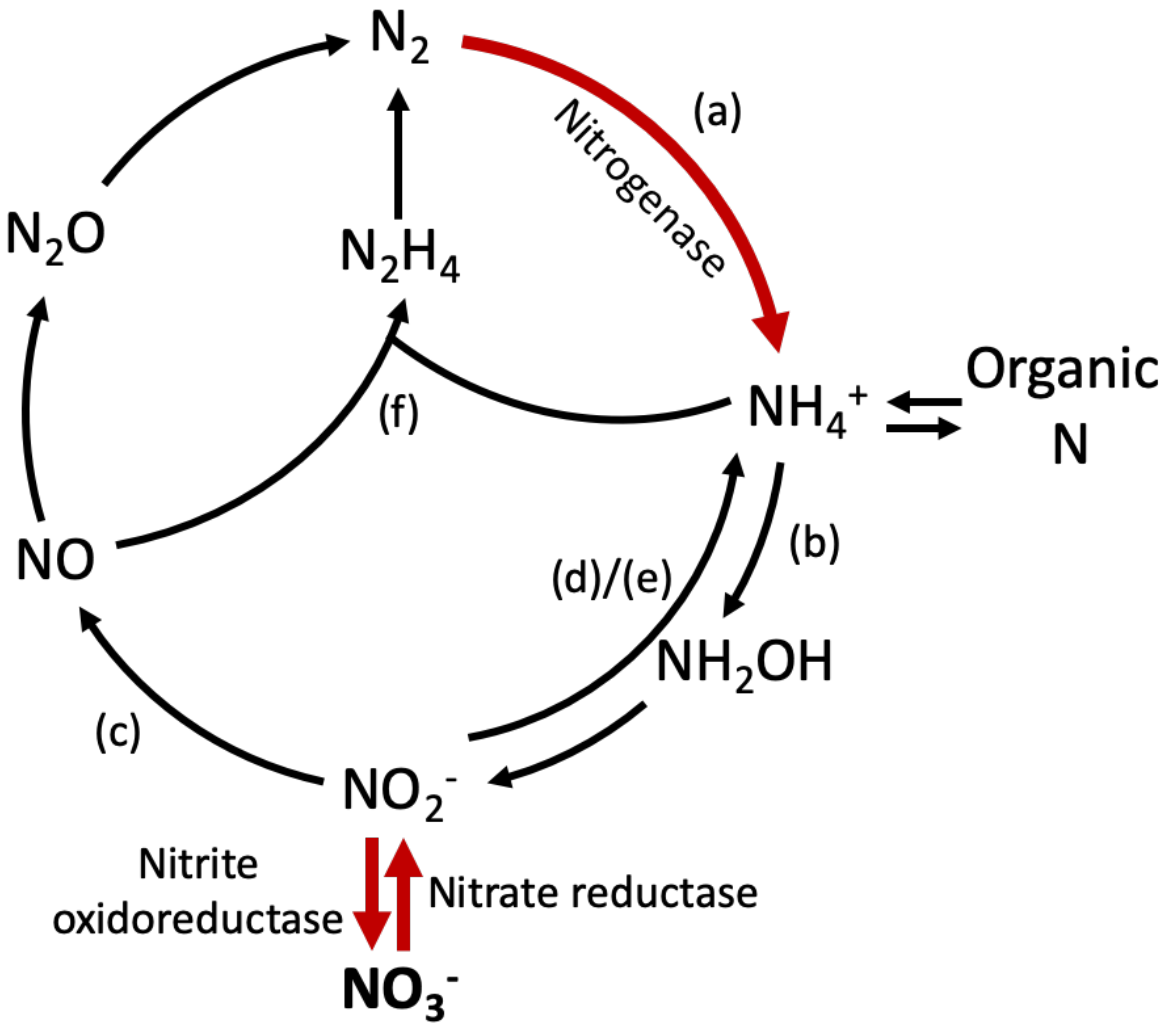


Figure 1.1 The microbial nitrogen cycle. (a) dinitrogen gas fixation; (b) nitrification; (c) denitrification; (d) dissimilatory nitrate reduction to ammonium; (e) assimilatory nitrate reduction; and (f) anaerobic ammonium oxidation. The steps catalyzed by molybdenum-containing enzymes are highlighted with red thick arrows. The reactions catalyzed by nitrogenase, nitrate reductase and nitrite oxidoreductase are indicated.

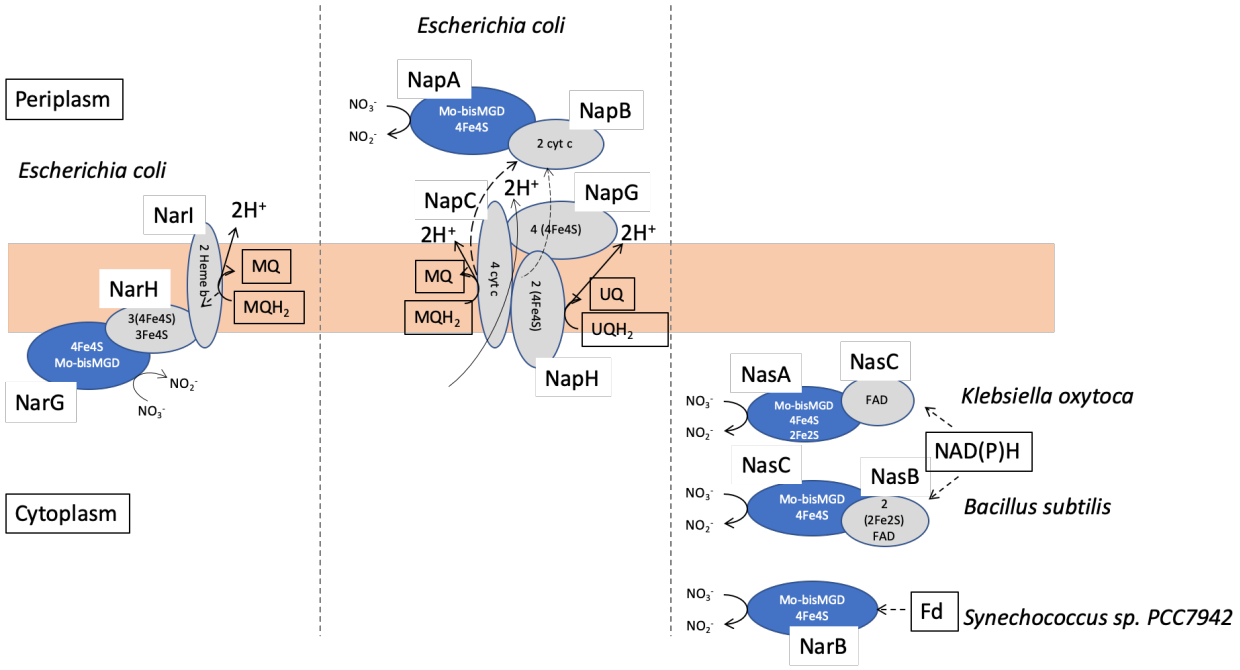


Figure 1.2 Nitrate reduction by three types of nitrate reductase in representative microbial strains. The catalytic subunits of respiratory nitrate reductases (NAR), periplasmic nitrate reductases (NAP), and assimilatory nitrate reductases (NAS) are shown as blue ovals. Additional subunits and related enzymes are shown as grey ovals. Cofactors of all enzymes are indicated, and electron flow is indicated by dashed arrows. The abbreviations are: Mo bis-MPT guanine dinucleotide cofactor (Mo-bisMGD), menaquinol ($MQH_2$), menoquinone (MQ), Cytochrome c (cyt c), ubiquinone (UQ), ubiquinol ($UQH_2$), flavin adenine dinucleotide (FAD), Ferredoxin (Fd). Figure adapted from (57, 58).

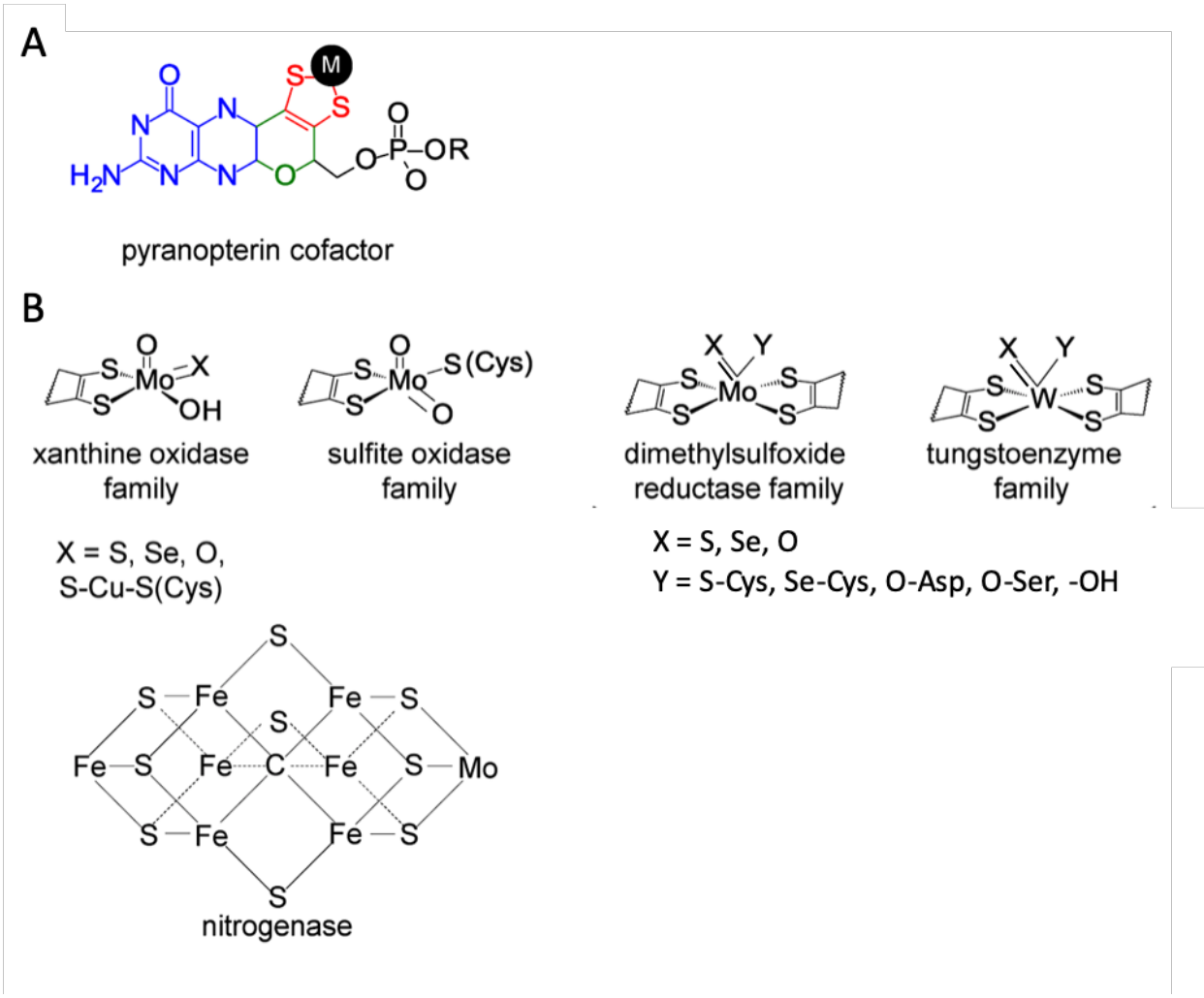


Figure 1.3 Structures of Mo/W cofactors. (A) the pyranopterin cofactor and (B) the coordination of the Mo (and W) atom in the different classes of molybdoenzyme. Figure modified from (7, 70).

# CHAPTER 2

# IRON- AND ALUMINUM- INDUCED DEPLETION OF MOLYBDENUM IN ACIDIC ENVIRONMENTS IMPEDES THE NITROGEN CYCLE[1]

[1]Xiaoxuan Ge, Brian J. Vaccaro, Michael P. Thorgersen, Farris L. Poole, Erica L. Majumder, Grant M. Zane, Kara B. De León, W. Andrew Lancaster, Ji Won Moon, Charles J. Paradis, Frederick von Netzer, David A. Stahl, Paul D. Adams, Adam P. Arkin, Judy D. Wall, Terry C. Hazen, and Michael W. W. Adams. (2019). *Environmental Microbiology*, 21(1):152-163. Reprinted here with permission of the publisher.

## Abstract

Anthropogenic nitrate contamination is a serious problem in many natural environments. Nitrate removal by microbial action is dependent on the metal molybdenum (Mo), which is required by nitrate reductase for denitrification and dissimilatory nitrate reduction to ammonium. The soluble form of Mo, molybdate ($MoO_4^{2-}$), is incorporated into and adsorbed by iron (Fe) and aluminum (Al) (oxy)hydroxide minerals. Herein we used Oak Ridge Reservation (ORR) as a model nitrate-contaminated acidic environment to investigate whether the formation of Fe- and Al- precipitates could impede microbial nitrate removal by depleting Mo. We demonstrate that Fe and Al mineral formation that occurs as the pH of acidic synthetic groundwater is increased, decreases soluble Mo to low picomolar concentrations, a process proposed to mimic environmental diffusion of acidic contaminated groundwater. Analysis of ORR sediments revealed recalcitrant Mo in the contaminated core that co-occurred with Fe and Al, consistent with Mo scavenging by Fe/Al precipitates. Nitrate removal by ORR isolate *Pseudomonas fluorescens* N2A2 is virtually abolished by Fe/Al precipitate-induced Mo depletion. The depletion of naturally-occurring Mo in nitrate- and Fe/Al-contaminated acidic environments like ORR or acid mine drainage sites has the potential to impede microbial-based nitrate reduction thereby extending the duration of nitrate in the environment.

## Introduction

Nitrate contamination has become a serious environmental issue due to the extensive use of nitrate-containing fertilizers in agriculture as well as through the release of nitrate-containing industrial wastes (27). The natural nitrate concentration in groundwater is typically less than 2 mg/L (39) and the U.S. Environmental Protection Agency's (EPA) maximum contaminant level (MCL) for nitrate (as the nitrate ion) in drinking water is 50 mg/L (0.80 mM). High nitrate concentrations can be detrimental to health and is known to cause methemoglobinemia in infants and adults (47, 48). In 2006, 1.9 million people in the US were predicted to use drinking water from private wells with ≥5 mg/L (0.08 mM) nitrate (42). Additionally, nitrate persistence in rivers can increase nitrate eutrophication near major river outlets resulting in algal blooms, hypoxia, and dead zones (18, 43).

Mo is a key element in the global nitrogen cycle (Figure 2.1A). It is the catalyst in three enzyme-based processes, $N_2$-fixation (nitrogenase), nitrification (nitrite oxidoreductase), denitrification (nitrate reductase) and dissimilatory nitrate reduction to ammonium (DNRA; nitrate reductase) (20). In fact, low environmental and/or dietary Mo appears to promote oral (113), esophageal (114, 115) and gastric (116) cancers in humans due to decreased reduction of nitrate and nitrosamine. In natural environments, the concentration of Mo can limit the efficiency of key Mo-dependent reactions (23, 24). Thus, natural or anthropogenic processes that deplete aquatic environments of Mo may have profound effects on the rate of steps in the global nitrogen cycle (20).

The major soluble form of Mo in natural environments is as the oxyanion molybdate ($MoO_4^{2-}$) (142). However, there are several ways in which soluble molybdate can be removed from the environment, including by binding to existing insoluble minerals or by being incorporated into insoluble minerals as they are formed. For example, molybdate is precipitated from sea water in

the form of molybdenum-iron-sulfur compounds present in black shales and sea sediments (118). Molybdate is also known to bind to insoluble organic matter in top soils (119). In addition, molybdate can be incorporated into hydrotalcite minerals that are formed by the precipitation of iron (Fe) and aluminum (Al) oxy/hydroxides (121-123). Molybdate can also adsorb directly to insoluble minerals such as ferrihydrite ($Fe_2O_3.xH_2O$) and gibbsite ($Al(OH)_3$) (124, 125). This Mo depletion process caused by iron or aluminum minerals is pH-dependent where molybdate concentration decreases as the pH increases from pH 3.1 to 6.3 for Fe precipitates, or from pH 5.5 to 6.7 for Al precipitates (121-125). However, it is not clear if these mechanisms are effective at depleting molybdate from solution in a regime that limits Mo bioavailability in natural environments (26).

At Oak Ridge Reservation (ORR) in Tennessee, USA between 1951 and 1983, the US government disposed of millions of liters of waste containing nitric acid and toxic metals. The waste generated from uranium operations at the Y-12 Plant was discarded into four unlined earthen reservoirs referred to as the S-3 ponds (~9.5 million liters per pond) (126). In 1978, the pH values of the ponds ranged from 0.8 to 5.3 and contained nitrate at concentrations up to 1.2 M (126). Metals present included iron up to 21 mM, aluminum up to 178 mM and uranium up to 1.3 mM (126). In 1983, in an effort to clean-up the waste site, the pH in the S-3 ponds was adjusted to about 9 (126, 127). The sludge that formed was allowed to settle and the liquid waste was removed (126). In 1988 the 1-m-thick sludge was stabilized with coarse aggregates and the S-3 ponds were filled and capped with a parking lot (127). In 1997, an analysis of the groundwater in 46 wells surrounding the parking lot revealed that there was a plume of nitrate that extended approximately 1 km to a depth of over 100 m (128, 129). In the most recent survey at ORR in 2015, groundwater from wells in the contamination plume were still at low pH range (pH 3 to 5) and contained high concentrations of nitrate (up to 230 mM) and various metals, including uranium (up to 0.6 mM)

(26, 130). Interestingly, of 26 metals analyzed, molybdenum (Mo) was the only metal that had a lower median concentration (<<1 nM) in the highly contaminated wells compared to pristine wells (up to 330 nM) (26). In essence, the highly contaminated wells were depleted in Mo and the reason for Mo depletion and its possible biological effects are the focus of the present study.

In the ORR contaminated environment many factors could limit microbial activity including low pH, fluctuations in dissolved oxygen and the availability of reduced carbon (143-145). We previously proposed that low concentrations of Mo observed in the contaminated environment could limit microbial nitrate reduction (26). Herein we seek to examine the cause of Mo-depletion in the contaminated environment. We propose an environmental model in which molybdate depletion is a result of adsorption and/or incorporation of Mo into Fe and Al minerals that form as the pH of contaminated acidic groundwater increases through mixing with the surrounding neutral groundwater and sediment (Figure 2.1B). Evidence supporting the Fe- and Al-dependent Mo-depletion model is provided including synthetic groundwater studies and metal analysis of vertical soil cores drilled in an ORR non-contaminated site and a contaminated area near the S-3 ponds. Importantly, we demonstrate that Fe- and Al- induced Mo- depletion results in a Mo concentration regime that limits microbial nitrate reduction by the ORR groundwater isolate *Pseudomonas fluorescens* strain N2A2.

## Results

### Concentrations of nitrate, Mo, Al and Fe in ORR groundwater

In a previous study, groundwater samples from 93 ORR wells were analyzed for multiple geochemical parameters (130). The concentrations of nitrate, Al, Fe and Mo, as well as the pH of those groundwater samples are re-analyzed and plotted in Figure 2.2. There is a subset of groundwater samples from wells located near the S-3 ponds that are highly contaminated with nitrate (>1 mM) and are very acidic (pH < 4). These samples have much lower Mo concentrations (<<1 nM) compared to samples from pristine wells, located over 3 km from the S-3 ponds, (pH>6 and nitrate concentration <0.80 mM), where Mo concentrations reach up to 300 nM (Figure 2.2A and Figure S2.1). The groundwater samples from these highly contaminated wells have Fe concentrations less than 3 μM while Al concentrations are as high as 20 mM (Figure 2.2B and Figure 2.2C).

### Abiotic depletion of trace $MoO_4^{2-}$ with $Fe^{3+}$ or $Al^{3+}$ precipitation

To test our Mo depletion model in the laboratory, Fe or Al treatment experiments were carried out with synthetic groundwater to determine if we could simulate Mo removal by $Fe^{3+}$ and $Al^{3+}$ precipitation. Specifically, the synthetic groundwater contained oxyanions that might compete with molybdate (3.1 mM $HCO_3^-$ and 15.2 mM $SO_4^{2-}$), together with cations (8.9 mM $Mg^{2+}$) known to promote the formation of Fe- and Al-based minerals (hydrotalcites). These oxyanions and cations were added at concentrations mimicking what was measured in highly contaminated groundwater samples from wells near the S-3 ponds (130). Both the Fe and Fe+Al treatments were extremely efficient in depleting the synthetic groundwater of molybdate. As shown in Figure 2.3A, the $Fe(NO_3)_3$ (20 mM) introduced a high concentration of contaminating Mo (47 nM) to the synthetic groundwater. When the pH was adjusted from 2.3 to 4.0, almost all Fe was removed from the solution, with only about 12 μM of the 20 mM remaining after Fe treatment and about 13

μM after Fe+Al treatment. At the same time, the Mo was depleted to below the detection limit (<5 pM) of the ICP-MS instrument after both Fe and Fe+Al treatments. When the pH was increased to 6.7, only 0.28 μM and 0.47 μM Fe remained in solution after Fe and Fe+Al treatments, respectively. Correspondingly, the Mo concentrations measured were 170 pM and 556 pM. We determined that the additional Mo was introduced as a contaminant from the trace grade NaOH that was used to adjust the pH (Figure 2.3A, left panel). It should be noted that the solubility of molybdate is independent of pH over this range (pH 4.0-6.7) and is unaffected by the pH adjustment in the control solutions (without added Fe, Figure 2.3B).

Al was not as efficient as Fe or Fe+Al at removing low concentrations of Mo from synthetic groundwater at pH 4.0 or at 6.7. Addition of Al (as the nitrate salt) introduced only 3.5 nM Mo as a contaminant. When the pH was increased to 4.0 after Al addition (from pH 3.8), only a small fraction of the Al precipitated changing the concentration from 19.7 mM to 15.3 mM. Accordingly, the Mo concentration decreased from 3.5 to 2.2 nM. Increasing the pH to 6.7 dramatically increased Al precipitation with only 6.1 μM remaining in solution (from 15.3 mM), but the Mo concentration only decreased to 1.7 nM (from 2.2 nM; we estimate that 10% of this difference was introduced as a contaminant from the NaOH) (Figure 2.3A, middle panel). As shown in Figure 2.3A, when both Al and Fe were present in synthetic groundwater, the results appeared to be additive and there were no dramatic synergistic effects caused by both metals precipitating from the same solution, especially at pH 4.0, only about 1.0 mM Al precipitated out of 10.3 mM present in the synthetic groundwater.

Several anions, including $NO_3^-$, $HCO_3^-$, $SO_4^{2-}$ and $Cl^-$, are present in the ORR groundwater (130) and were added to the synthetic groundwater in the experiments above. In this case, the synthetic groundwater contained one of the following ions: sulfate (15.2 mM), bicarbonate (3.0 mM), phosphate (5.0 mM) or chloride (10.5 mM) or a combination of sulfate (15.2 mM),

bicarbonate (3.0 mM) and chloride (10.5 mM) (Table S2.1). As shown in Figure S2.2A, depletion of Mo by Fe treatment was more or less independent of the presence of the anions, as all Mo concentrations decreased from approximately 50 nM to less than 400 pM. However, sulfate inhibited molybdate depletion in Al treatment as the Mo concentration was 2.2 nM (sulfate only) and 3.4 nM (combination of sulfate, carbonate and chloride, SCC). Hence, sulfate interferes with Mo removal by Al precipitation, but not Fe precipitation which explains why nM levels of Mo remained in Al-treated synthetic groundwater even at pH 6.7 (Figure 2.3A).

We next addressed the question of whether molybdate could also be adsorbed by pre-formed Fe or Al precipitates from synthetic groundwater. As shown in Figure 2.3B, at pH 4.0 the pre-formed Fe-precipitates scavenged Mo from solution and decreased soluble Mo from 10 nM to 200 pM. At pH 6.7 the Mo concentration decreased further to less than 5 pM (below the detection limit). The pre-formed Al-precipitates were less effective in removing Mo, decreasing the concentration to 6.9 nM at pH 4.0 and to 3.7 nM at pH 6.7. Importantly, the pre-formed Al precipitate did not impede Mo uptake by the pre-formed Fe-precipitate at pH 4.0 but they did prevent Mo adsorption by the pre-formed Fe-precipitate at pH 6.7, resulting in a concentration of remaining Mo 5-fold higher (2.0 nM) in samples with both Fe and Al precipitates (Figure 2.3B). Fe precipitation in synthetic groundwater at low pH is more efficient than Al precipitation, which is consistent with the observation that no significantly high concentrations of Fe (>10 μM) were detected in any of the contaminated wells while much higher concentrations of Al were measured (up to ~20 mM; Figure 2.2). The data presented here therefore suggest that Mo depletion in ORR groundwater is predominantly a result of both incorporation and adsorption to Fe-based oxyhydroxides precipitates, but that Al-based precipitates could also play a role.

**Co-occurrence of recalcitrant Mo with Fe and Al in contaminated ORR sediment**

In order to analyze Mo concentrations and its bioavailability in ORR sediment, a sediment core adjacent to the S-3 ponds contamination source (EB-106) and a sediment core not contaminated by the S-3 plume (EB-271) were obtained. The cores were divided into 23 cm segments by depth (800 cm and 450 cm total), which were extracted and analyzed for metals using the modified BCR three step sequential extraction procedure (144) that involves a series of increasingly harsh treatments to release metals from the sediment. As shown in Figure. S2.3A and Figure S2.3C, Mo was not detected in the weak acid extracted fractions (pH 3.0) of the first extraction step or in the reducible extraction fractions for either core. Low amounts of Mo (< 2 mg/kg and <0.7 mg/kg, respectively) were released in this final and much harsher extraction step of the contaminated and non-contaminated cores. There was some Mo in the vadose zone of both wells (100 cm depth and 194 cm depth) of the cores that may have been associated with organic matter. There were also three Mo concentration maxima centered at 501, 583 and 674 cm depth in the saturated zone of the contaminated core (Figure S2.3A and Figure S2.3B) and a feature of Mo extending into the saturated zone of the non-contaminated core from 331-444 cm depth (Figure S2.3C and Figure S2.3D).

Total metals were also measured for both sediment core segments using a separate microwave digestion procedure by nitric acid (Figure S2.3A and Figure S2.3C). Importantly, for the non-contaminated core, similar amounts of Mo were measured by the two different procedures (Figure S2.3C). Conversely, for the contaminated core, ~60% more Mo was measured in the vadose zone and approximately 2-3 fold increased Mo was measured in the 3 saturated zone maxima by the total digestion method compared to the oxidizing step of the sequential extraction procedure (Figure S2.3A). This result suggests that there is a population of highly recalcitrant Mo in the contaminated core that is only observable with total digestion of the sediment in nitric acid that is not present in the non-contaminated core.

The concentrations of Fe and Al found in the contaminated ORR sediments by the total extraction method are shown in Figure S2.3B, along with those for Mo. The Fe data show that there is one major maximum and several minor ones, and while the Al data show more variation between the triplicate environmental samples, there are clearly several major concentration maxima. Interestingly, of the three major Mo maxima in the saturated zone, two of them (501 and 583 cm) correspond to major (501 cm) and minor (583 cm) maxima for both Fe and Al. The major Mo concentration maximum at 674 cm does not appear to correlate with either of the other metals. For the non-contaminated core no significant maxima of Mo correspond to those of Fe or Al (Figure S2.3D).

**Nitrate removal limited by Mo depletion**

To test the impact of Fe- and Al-dependent Mo depletion on microbial action (Figure 2.1A), the nitrate removal activity of a denitrifying microorganism isolated from ORR groundwater, *Pseudomonas fluorescens* N2A2, was investigated after its growth medium was depleted of Mo by Fe- or Al-based precipitation (Table S2.1). The measured Mo concentrations in the growth media decreased from 32.7 nM to 400 pM as a result of Fe treatment and from 13.7 nM to 800 pM as a result of Al treatment (Table S2.2). Strain N2A2 grew very poorly in both of these Mo-depleted media compared to the standard medium containing 10 nM Mo (Figure 2.4A). However, growth was almost fully restored upon the subsequent addition of 10 nM $MoO_4^{2-}$, showing that the Fe- and Al-induced precipitation did indeed inhibit growth by removing soluble Mo (Figure 2.4A). However, Mo addition did not restore growth completely (Figure 2.4A), so it is possible that the Fe- and Al-treatments decreased the concentration of one or more of the other medium components required for optimal growth of strain N2A2 (Figure 2.4A).

While removal of soluble Mo by Fe- or Al-induced precipitation clearly impacts microbial growth, a more fundamental question is whether these processes also lead to a decrease in the

ability of the ORR microorganism to catalyze nitrate removal with nitrate reductase, a Mo dependent enzyme that also contains Fe (146). As shown in Figure 2.4B and 2.4C, this conjecture proved to be the case. N2A2 cells in the Fe-treated medium (containing 400 pM Mo) removed only 16% of the nitrate that was initially present (60 mM), while more than 95% of the nitrate was removed by cells in the untreated medium (containing 10 nM Mo). About 40% of the nitrate was removed by cells in the Al-treated medium (containing 800 pM Mo). When Mo was added back to both the Fe- and Al-treated media, more than 80% of the nitrate was removed showing that Mo depletion was the cause of the nitrate removal deficiency in Fe and Al treated media (Figure 2.4B).

Molybdenum is part of the catalytic site of nitrate reductase and the catalytic activity of the enzyme is directly related to its Mo content (69, 147). Consequently, one would expect the amount of nitrate removed by N2A2 in a given environment to be directly related to the catalytic activity of its nitrate reductase and hence its Mo content. As shown in Figure 2.4C, this expectation was the case. The total catalytic activity (units/mg of total cellular protein) of nitrate reductase was initially proportional (in early log phase, 28 h) to the Mo concentration in the medium. That is, cells had up to four-fold higher nitrate reductase activity in media that had not been Mo depleted, or that had been supplemented with Mo after Fe- or Al- treatment (Figure 2.4C). For example, the highest nitrate reductase activity is about 60 units/mg in Fe-treated media with Mo supplementation while only about 15 units/mg activity was detected in Fe-treated media at 28 h. However, the cellular production of the nitrate reductase protein is dependent upon the nitrate-content of the medium (148, 149) so in Mo-sufficient media the specific activity of the enzyme decreases as the nitrate is removed (at middle log phase, 53 h, and early stationary phase, 73 h, Figure 2.4C). In contrast, in the Fe- and Al-depleted media, the specific activities of the enzyme do not change dramatically and remain low over time. Hence, with abundant Mo, the specific activity of the nitrate reductase reflects the amount of nitrate reductase protein that is produced. In

contrast, in Fe- and Al-treated media, the measured nitrate reductase activity reflects the prevailing Mo-depletion conditions, independent of the nitrate concentration or the amount of nitrate reductase protein. Mo is therefore the key to catalytic activity and thus to efficiency in the nitrate removal process.

## Discussion

This study combines Mo depletion in acidic and metal contaminated ORR groundwater and nitrate reduction by microorganisms into one environmental model. The liquid in the S-3 ponds was highly acidic (pH < 0.8) as a result of the high concentrations of contaminating nitric acid present. The results presented herein show that $Fe^{3+}$ and $Al^{3+}$ are effective at removing molybdate from solution, even at the extremely low (<10 nM) starting concentrations found in the ORR environment. Mo removal at ORR appears to occur as a result of either adsorption onto pre-formed Fe- and Al-based oxy/hydroxides or by incorporation into Fe- and Al-based minerals that form as the pH of the acidic groundwater gradually increases (to pH > 3) as it flows into the surrounding sediment (126, 127, 130).

The sediment at ORR is rich in Fe-oxides (150, 151) and acidic dissolution of magnetite occurs in nitric acid at pH < 2.0 (152, 153). This $Fe^{3+}$ in turn would precipitate when the pH increases as a result of dilution with fresh groundwater or by interactions with carbonated soils thereby scavenging soluble Mo (127). We show here that $Fe^{3+}$ is extremely effective at removing soluble Mo from synthetic groundwater at pH values as low as 4.0, while a pH closer to neutral is required for $Al^{3+}$ to scavenge Mo. That iron rather than aluminum is the primary driver of Mo depletion in the ORR environment is consistent with our elemental analyses of the contaminated ORR wells (pH <5.0), in which the Fe concentrations are extremely low (μM range) but Al persists (mM range) and Mo is virtually undetectable. We contend that Fe precipitation at low pH has already removed Mo from the groundwater of the highly contaminated wells near the S-3 ponds. In addition, the measurement of a recalcitrant population of Mo that could only be observed when sediment was completely digested in nitric acid that was present in the contaminated but not the non-contaminated core supports our environmental model. That several of the Mo concentration

maxima (at 501 cm and 583 cm depth) observed in the contaminated core coincide with Fe and Al maxima also supports the model.

We show here that pH-induced precipitation of Fe-oxy/hydroxides, and to a lesser extent those that are Al-based, cause depletion of soluble Mo resulting in Mo concentrations in the low pM range and in many cases beyond the detection limit (<5 pM). While such low Mo concentrations are consistent with those measured in the highly contaminated groundwater at ORR, they are also at the limits of experimental design, particularly when attempting to grow microorganisms in the laboratory. Mo is a contaminant in virtually all chemicals used in microbial growth media, especially in $SO_4^{2-}$, $PO_4^{3-}$, $Fe^{3+}$ and $HCO_3^-$, which are added to Mo-depleted media. Even though we used trace grade chemicals, Mo was still introduced to the media as a contaminant at concentrations greater than 100 pM. In other words, it was nearly impossible to reproduce the extent of Mo limitation in the highly contaminated ORR groundwater in the laboratory because of unavoidable Mo contamination in commercial chemicals.

Thus, the lowest Mo concentrations we could prepare experimentally for growth experiments involving the ORR-denitrifying strain *Pseudomonas fluorescens* N2A2 were in the 100 pM range, which was sufficient to demonstrate a negative impact on nitrate reduction. Yet, the Mo concentration in highly contaminated ORR groundwater is less than 10 pM, which is at least one order of magnitude lower than what we can simulate in the laboratory. Mo availability consequently has the potential to be a major limitation for the removal of nitrate by microorganisms in the ORR environment. Other potential barriers to nitrate reduction in the contaminated ORR environment include sources of reductant for denitrification (either organic or inorganic), the acidic conditions and the effects of heavy metal contaminants. Oxygen in sediments and groundwater can also affect denitrification, because oxygen is known to inhibit the transcription or the metabolic activity of related enzymes in most denitrifying microorganisms

(146, 154). Natural microbiota can affect major geochemical cycles like the nitrogen cycle (155, 156), however inadequate metagenomic studies on sediment microbial communities in the ORR contaminated area leave unanswered questions about the relationships between these microbial communities and the environment. While denitrifiers or denitrifying communities that can survive at low pH or in the presence of certain heavy metal contaminants have been studied (157-160), conditions at the ORR site are extreme because of the complex contamination of multiple heavy metals combined with high concentrations of anions like nitrate, sulfate and chloride, as well as low pH (3 to 5). From the results presented herein, we contend that Mo limitation is another factor that could be impacting microbial nitrate reduction at ORR. Isolation of a nitrate-reducing microorganism able to grow in the presence of the high concentrations of a range of heavy metals found in some of the ORR wells, such as FW-126 (130), that is also able to utilize Mo at low pM or even fM concentrations would be of great interest.

Natural Mo concentrations in groundwater are rarely seen in the pM range like they are in the ORR contaminated groundwater. Typically, Mo concentrations range from several nM to hundreds of nM (65). However, low Mo concentrations have been observed, such as in the Wadden Sea and Boston Harbor (< 20 nM) and the Yorkshire Chalk aquifer (< 10 nM). The low Mo concentrations at these sites were proposed to be the result of Fe sedimentary mineralization and/or Mn oxide immobilization under sulfate-reducing conditions (161-163). Low Mo concentrations (< 5 nM-70 nM) resulting from the lower solubility of molybdate at low pH have also been reported in naturally acidic groundwater (pH 2.4-2.9) (164). While the ORR environment can be considered unique, acid mine drainage (AMD) forms a similar highly acidic, metal-rich environment, which is generated from the drainage of pyrite oxidation and results in sulfuric acid and ferric iron contamination (165). Like the ORR plume, AMD is neutralized by mixing and dilution with nearby

soils and groundwater. AMD can also dissolve aluminum, iron and other metals from various minerals and in general has high concentrations of $Fe^{3+}$ and/or $Al^{3+}$ (165, 166).

To date, most remediation studies of AMD have focused on how to decrease the concentrations of $Fe^{3+}$, $Al^{3+}$, $SO_4^{2-}$ and various toxic metals (167). However, we propose that anthropogenic neutralization of AMD will also deplete Mo as Fe- and/or Al-based minerals form, as occurred at the ORR site. This process could disrupt the nitrogen cycle at the AMD site by decreasing nitrate removal and/or nitrogen fixation (Figure 2.1) (23, 24, 151). In a previous study, the denitrification rate of sediment and surface water microcosms from AMD-impacted sediment decreased significantly when $Fe^{3+}/Fe^{2+}$ was added, the pH values of which were between 3.17 to 4.52 (168). Based on the Mo depletion model proposed in our study, soluble $MoO_4^{2-}$ in the tested microcosms from the AMD-impacted environment would have been depleted by Fe precipitation that occurred when the pH increased, thus inhibiting nitrate reduction in the AMD-community. The lack of soluble and available Mo may decrease the rate of natural nitrate removal from contaminated groundwater via denitrification, particularly when appropriate electron donors are present. In addition to limiting nitrate reduction by a single organism as shown in this study, a lack of Mo may shift the microbial community structure such that other growth modes are more energetically favorable and become dominant, similar to what was found in estuarine environments (25). It might be expected to take longer to re-establish nitrate to non-contaminant concentrations in these Mo-depleted environments (169).

The depletion of Mo in groundwater and freshwater environments could have additional environmental consequences. For example, Mo depletion in agricultural soils containing nitrate-based fertilizers could decrease denitrification rates compounding nitrate contamination issues (23). In addition, release of nitrate contaminated freshwater into the ocean results in eutrophication of nitrogen-limited estuarine and coastal ecosystems causing the spread of dead zones and hypoxia

at affected river outlets (43, 170). Moreover, limitation of nitrogen fixation by Mo availability could be relevant in areas without nitrate contamination. While environmental acid and metal contamination are clearly critical environmental concerns, it is important to also consider what nutrients are depleted as these contaminants are removed. The depletion of Mo in metal-rich acidic environments may be a key concern that needs to be considered in returning nitrate-contaminated environments to their natural state.

## Experimental Procedures

### Molybdate depletion by iron or aluminum active precipitation

The synthetic groundwater composition was based on the previously published data (130) on the major inorganic ions measured in the highly contaminated well FW-126 (located 11.3 meters down gradient from the S-3 ponds, see Table S2.1). Synthetic groundwater contained $Mg(NO_3)_2$ (8.9 mM), $Na_2SO_4$ (15.2 mM), $NaHCO_3$ (3 mM) and NaCl (10.5 mM). This data was based on the ion concentrations measured from contaminated groundwater (well FW-126; Table S2.1). It is important to note that Mo was not added to any of these solutions. The Mo that was present (up to approximately 50 nM in $Fe(NO_3)_3$ (20mM)) originated as a contaminant in the various chemicals that we added to the solutions. Synthetic groundwater was acidified to pH 2.3, 3.8 or 2.6 by addition of trace metal grade $Fe(NO_3)_3$ (20mM) (99.995% trace metal basis, MilliporeSigma, Missouri, USA), $Al(NO_3)_3$ (20 mM) (99.997% trace metal basis, MilliporeSigma) or a combination of $Fe(NO_3)_3$ (10 mM) and $Al(NO_3)_3$ (10mM), respectively, to give a final concentration of 60 mM nitrate in each case. These acidifications were followed by precipitation of Fe or Al at pH 4.0, which was chosen to mimic the pH of the contaminated groundwater in well FW-126, or pH 6.7, which was used to simulate the neutralization of the contaminated groundwater by mixing with soils and neutral uncontaminated groundwater, induced by the addition of trace grade NaOH (99.99% TraceSELECT, Honeywell Fluka, Michigan, USA) and samples were allowed to settle for 30 min at room temperature. These procedures will be referred to as “Fe treatment”, “Al treatment” or “Fe+Al treatment”. Aliquots were taken prior to and after the pH adjustment, centrifuged (5,000 × *g*, 20 min) and the concentrations of dissolved Fe, Al and Mo before and after Fe treatment, Al treatment and Fe+Al treatment were analyzed by inductively coupled plasma mass spectrometry (ICP-MS) to determine the effect of the treatment on Mo concentrations.

To investigate the effects of different anions on Mo depletion by Fe or Al precipitation, single anions $Na_2SO_4$ (15.2 mM), $NaHCO_3$ (3 mM), $NaH_2PO_4$ (5 mM) or NaCl (10.5 mM) or anion combinations of $Na_2SO_4$ (15.2 mM), $NaHCO_3$ (3 mM) and NaCl (10.5 mM) (SCC) were included exclusively in $Fe(NO_3)_3$ (20 mM) or $Al(NO_3)_3$ (20 mM) solutions with $Mg(NO_3)_2$ (8.9 mM), as $Mg^{2+}$ is the major divalent cation in the ORR monitoring well FW-126 groundwater. Where indicated, molybdate was added as $(NH_4)_2MoO_4$ at final concentrations of 50 nM and 10 nM prior to the Fe or Al treatments, respectively, to provide a Mo concentration where changes could be easily measured. Then different solutions were adjusted to pH 6.7 to induce the precipitation of Fe and Al in 15 ml acid washed falcon tubes. Samples were incubated at room temperature for 30 min. Samples before the treatments and supernatants after treatments were collected for metal analysis by ICP-MS in order to determine the effect of anion interferences on Mo depletion at starting trace levels (pM to nM) of Mo concentration.

**Molybdate adsorption to aluminum or iron precipitates**

$Fe(NO_3)_3$ (20 mM), $Al(NO_3)_3$ (20mM) or a 1:1 ratio thereof (10 mM $Fe(NO_3)_3$ and 10 mM $Al(NO_3)_3$) were added to synthetic groundwater solutions. The pHs of the mixtures were adjusted to either pH 4.0 or pH 6.7 by addition of NaOH (99.99% TraceSELECT). The solutions were then centrifuged at 5,000 × *g* for 20 min to remove the Fe and/or Al precipitates and 10 nM $(NH_4)_2MoO_4$ was added to the supernatant fractions and these were divided into two parts. One was mixed with the precipitate obtained from the prior centrifugation step and the other served as a control (with added Mo but with no precipitate). After equilibration for 16 hours, the solutions were centrifuged at 5,000 × *g* for 20 min, and the supernatants were analyzed by ICP-MS.

**Growth of *Pseudomonas fluorescens* N2A2 in molybdate-depleted media**

The standard growth medium contained 1.3 mM KCl, 2 mM $MgSO_4$, 0.1 mM $CaCl_2$, 0.3 mM NaCl, 30 mM $NaHCO_3$, 5 mM $NaH_2PO_4$ and 20 mM $NaNO_3$ with vitamins and minerals as

described by Widdel and Bak (171) except that molybdenum and tungsten were omitted. Glutamine (20 mM) was used as carbon source. Mo limited media were generated based on the standard medium and by using the Fe- or Al-treatments described above. Glutamine (20 mM), which is neutral, was used as carbon source instead of lactate to avoid interference with Mo depletion. Mo depleted medium solution which contained 1.3 mM KCl, 2 mM $MgSO_4$, 0.1 mM $CaCl_2$, 0.3 mM NaCl and 20 mM glutamine, 10 nM $(NH_4)_2MoO_4$ with vitamins and minerals was mixed with either $Fe(NO_3)_3$ (20 mM) or $Al(NO_3)_3$ (20mM). The solutions were adjusted to pH 6.7 from pH 2.1 for Fe and pH 3.5 for Al to induce their precipitation. Then the supernatants were supplemented with $Fe(NO_3)_3$ (7.4 μM), $Na_2SO_4$ (2 mM), $NaHCO_3$ (30 mM) and $NaH_2PO_4$ (5 mM) which are required for N2A2 growth. $NaNO_3$ (60 mM) was used in untreated media to introduce nitrate. Untreated media, Fe/Al treated media and replete Fe/Al treated media with 10 nM $MoO_4^{2-}$ added back in were inoculated with 1% (vol/vol) of *Pseudomonas fluorescens* N2A2 previously grown anaerobically in medium without added Mo on glutamine at 28 °C. Samples were collected from pre-Fe/Al treatment solutions, post Fe/Al treatment solutions, post Fe/Al treatment solutions with N2A2 cells and post Fe/Al treatment solutions with N2A2 cells and replete Mo for ICP-MS metal analysis. Growth of N2A2 in untreated, Fe- or Al- treated, and Fe- or Al- treated and supplemented with 10 nM $MoO_4^{2-}$ media were compared as indicated. Each growth was performed in triplicate and samples were collected every 5 h for the analyses described below.

**Nitrate and nitrite measurements**

Nitrate and nitrite were measured by the Griess colorimetric assay as previously described (172). Samples were removed from growing cultures, centrifuged in a microcentrifuge to remove cells, and were assayed directly. Typically, 100 μL of diluted samples were mixed with 100 μL Griess reagents (MilliporeSigma) and incubated at 37 °C for 1 h to determine the concentrations of nitrite produced during growth. To reduce the remaining nitrate to nitrite, 50 μL of diluted

samples were mixed with 40 µL saturated $VCl_3$ (400 mg $VCl_3$ in 50 mL 1M HCl). 100 µL of the Griess reagent was added and the mixture was incubated at 37 °C for 4 h before measuring absorption at 540 nm.

**Nitrate reductase activity**

Samples (5 ml) were removed from N2A2 cultures and cells were harvested by centrifugation (10,000 × g for 5 min). The pellet was re-suspended in 100 µL of water and lysed by sonication. The assay mixture (1.0 mL) consisted of 50 mM Tris/HCl buffer, pH 7.5, containing 0.5 mM methyl viologen and 1 mM potassium nitrate in an anaerobic sealed cuvette at 25 °C. Sodium dithionite (4 mg/ml in 50 mM Tris-HCl buffer, pH 7.5) was added until an absorption at 578 nm of approximately 1.5. The reaction was initiated by the addition of the cell-free extract and nitrate reduction was monitored by the oxidation of reduced methyl viologen (173). One unit of total nitrate reductase activity catalyzed the reduction of 1 µmol of nitrate /min.

**Metal analysis**

Synthetic groundwater samples, processed sediment samples or culture samples were vortexed then diluted into 2% (vol/wt) trace-grade nitric acid (VWR, Pennsylvania, USA) in acid-washed polypropylene tubes and stored overnight at 4 °C. Samples were analyzed using an Agilent 7900 ICP-MS fitted with MicroMist nebulizer, UHMI-spray chamber, Pt cones and an Octopole Reaction System (ORS) collision cell (Agilent Technologies, California, USA). The external calibration standards, IV-ICPMS-71A (Inorganic Ventures, Virginia, USA) and IV-ICPMS-71B (Inorganic Ventures, Virginia, USA), were used to create an 11-point curve from 0 – 500 (or 1000) ppb for each element and the internal calibration standard, IV-ICPMS-71D (Inorganic Ventures, Virginia, USA), was added to each sample. The data were collected as a 3-point peak pattern, 3 replicates, 100 sweeps/rep and various integration times (all > 0.3 s) with either no gas or He gas in the ORS collision cell. Data was processed using the nearest internal standard by mass and fitted

to a linear curve though the calibration blank. Where indicated, environmental or biological replicates where averaged and reported with standard deviations (SD). The detection limits (DL) were calculated as three times the standard deviation of the calibration blank. All sediment data are reported in mg/Kg (i.e. ppm) and other data are reported in molar concentrations (i.e. mM - pM).

**ORR sediment coring**

The 800 cm vertical sediment core, EB-106, was located 21.1 m downstream from the southern corner of the S-3 pond, in an extremely contaminated region referred to as Area 3 (174, 175). The contaminated core (EB-106) is located 21.1 meters from the edge of one of the ponds and 10.2 meters from well FW-126. The sediment core spanned the vadose (0-300 cm), capillary fringe (300-350 cm) and saturated (350-800 cm) soil zones. The sediment was cored using a Geoprobe 6610 DT (Geoprobe, Salina, KS) dual tube hydraulic push continuous coring machine. The DT 350 that takes 8.9 cm diameter cores using PVC liners. The filled liners were cut in to ~22 cm segments at the field site and each end was immediately capped.

**Metal extraction from ORR sediment core**

The sediment core was cut into 23 cm sections, the end portion of each 22 cm segment was discarded, and an internal sample was manually homogenized. The moisture content and dry mass of three approximately one gram samples of homogenized sediment were obtained by drying overnight in an oven at 102 ± 2°C. Selected samples were then sequentially extracted for bioavailable metals by the BCR three-step sequential extraction procedure (144), where the soil was sequentially extracted with a weakly acidic (0.11 M acetic acid) solution, a reducing agent (0.5 M hydroxylammonium chloride) and an oxidizing agent (8.8 M hydrogen peroxide at 85°C). The first step involves extraction of the sediment with a weak acid (0.11 M acetic acid), which removes any porewater metals as well as metals that are precipitated with carbonate and are easily

solubilized (176). The second step is the subsequent reductive extraction by incubation with 0.5 M hydroxylammonium chloride, which will release metals bound to metal oxides (176). The third step is oxidative extraction and involves digesting the sediment remaining from the reductive extraction using 8.8 M $H_2O_2$ at 85°C. This extraction also releases metals from organic matter, such as high molecular weight humic compounds (176). Supernatants from the three extraction steps were diluted 1:40 in 2% (vol/vol) nitric acid for ICP-MS analysis. An additional one gram of soil (dry weight) from each segment was microwave digested in 10 mL of concentrated nitric acid as described in EPA protocol 3051A (177) to determine the total metal content of sediment. After microwave digestion, samples were diluted to 100 mL total volume with $ddH_2O$. For ICP-MS analysis, a one mL portion was diluted with 4 mL of $ddH_2O$ resulting in 2% (vol/vol) nitric acid in the samples. These samples were further diluted 1:5 and 1:50 in 2% (vol/vol) nitric acid before being analyzed by ICP-MS.

**Author Contributions**

XG, BV, MT and FP designed this study, performed the experiments, analyzed and interpreted the data and MA directed the research. EM, GZ, KD, AL, JM, CP, and TH contributed to environmental sampling. XG wrote the manuscript and MT, FP, FN, DS, PA, AA, JW, and MA contributed to its revision.

## Tables and Figures

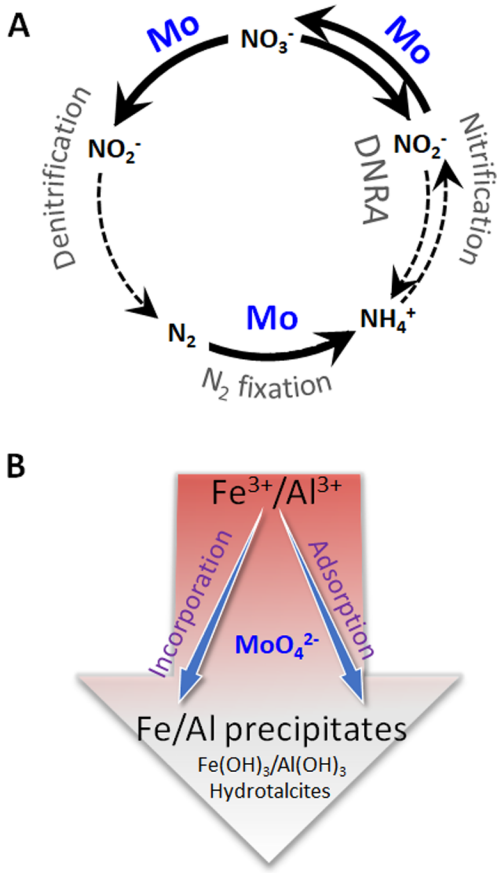


Figure 2.1 Mo in the nitrogen cycle and at ORR. (A) Mo-dependent steps in the nitrogen cycle are indicated by bold black arrows while dashed arrows are independent of Mo (dissimilatory nitrate reduction to ammonium, DNRA). (B) Model of Mo depletion at the ORR contaminated site. The large background arrow indicates pH change of contaminated groundwater from lower pH (red) to higher pH (pink to white). Two mechanisms of Mo depletion by Fe and/or Al precipitates are proposed: incorporation and adsorption as indicated by blue arrows.

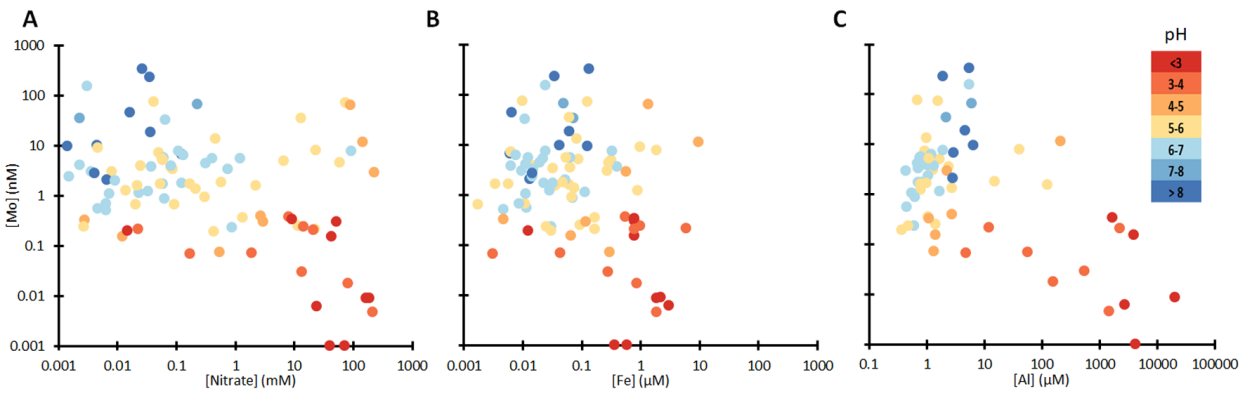


Figure 2.2 Nitrate, Fe, Al and Mo concentrations in ORR groundwater samples at various pH levels. (A) Nitrate and Mo concentrations in groundwater samples from different ORR wells. Each data point represents a groundwater sample from a well. A total of 93 samples were taken from 80 wells. Different colors represent the pH of each well from low (in red) to high (in blue). The X axis indicates the nitrate concentration of each sample in mM, while the Y axis indicates the Mo concentration detected of each sample in nM. The concentrations are plotted on logarithmic scales. Similar plots are drawn to show the relationship between Fe and Mo concentrations (B) as well as Al and Mo concentrations (C) in groundwater from different ORR wells. All samples were measured in duplicate and average values are reported. Wells that are pH>6 and have nitrate concentrations <0.80 mM are considered pristine wells.

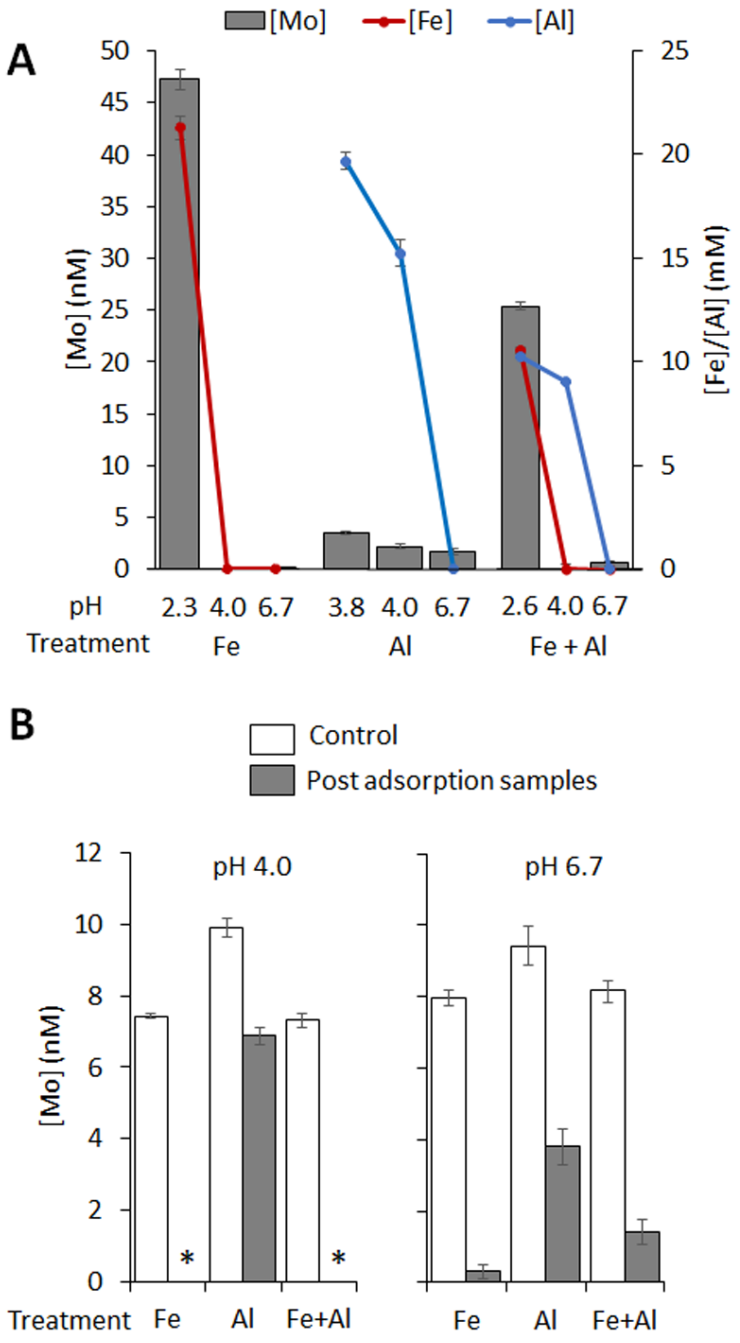


Figure 2.3 Mo depletion in synthetic groundwater. (A) Mo depletion in synthetic groundwater induced by Fe, Al or a combination of Fe and Al precipitation at pH 4.0 and pH 6.7. Mo concentrations of three groups of samples at different pH are indicated by grey bars. The first bars indicate Mo concentrations in synthetic groundwater before pH adjustment with the following bars indicating Mo concentrations after pH adjustment and the pH for each sample is indicated below

each bar. The concentrations of free Fe (red lines) and free Al (blue lines) are also indicated in this figure in mM. (B) Mo adsorption to Fe-, Al- or a Fe+Al-precipitates at pH 4.0 (left) and pH 6.7 (right). Samples were first Mo depleted by the given treatment and pH to generate precipitates. Then half of the supernatant for each sample was removed for the control (white bar), and the remaining supernatant and precipitate was used as the sample (black bar). Additional Mo was added to the control and sample, incubated overnight and then the soluble Mo was measured. *Mo concentrations below the detection limit of ICP-MS

Figure 2.4 Growth and nitrate consumption of ORR isolate N2A2 in Mo depleted and replete media. (A) Growth curves of N2A2 in no treatment media (black line), Mo depleted media resulting from Fe treatment (pink line) or Al treatment (light grey line), and in Mo replete media after Fe treatment (red line) or Al treatment (dark grey line). Mo concentrations in different cultures were measured by ICP-MS and indicated in Table S4.2. (B) Nitrate remaining during the growth of N2A2 in Mo depleted and replete media. (C) Nitrate reductase activity of N2A2 at early log phase (28 h), middle log phase (53 h) and early stationary phase (73 h) under various growth conditions. The total nitrate reductase activity is expressed as units/mg, where 1 unit equals to 1 μmol nitrate reduced/min. The colors of different samples in (B) and (C) are consistent with those in (A). Arrows indicate the time points for enzyme activity assays.

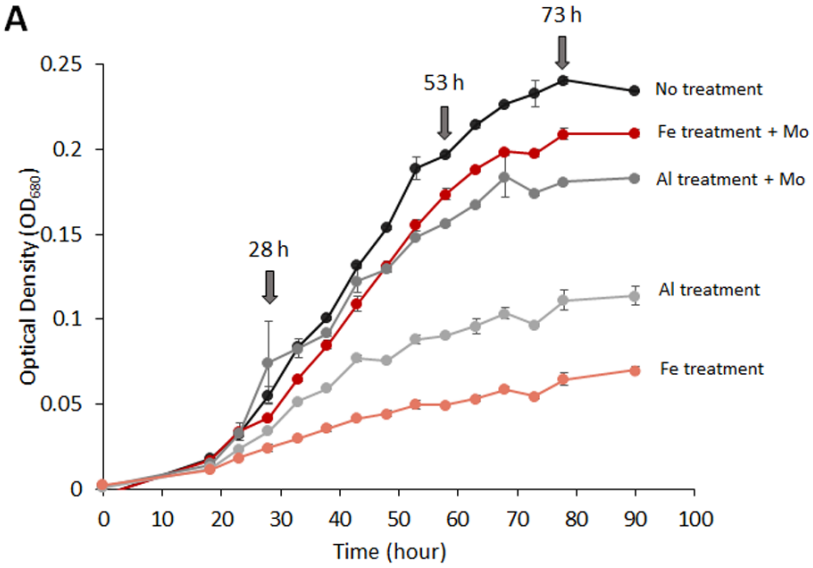
A
73 h
53 h
28 h
No treatment
Fe treatment + Mo
Al treatment + Mo
Al treatment
Fe treatment
Optical Density (OD680)
Time (hour)

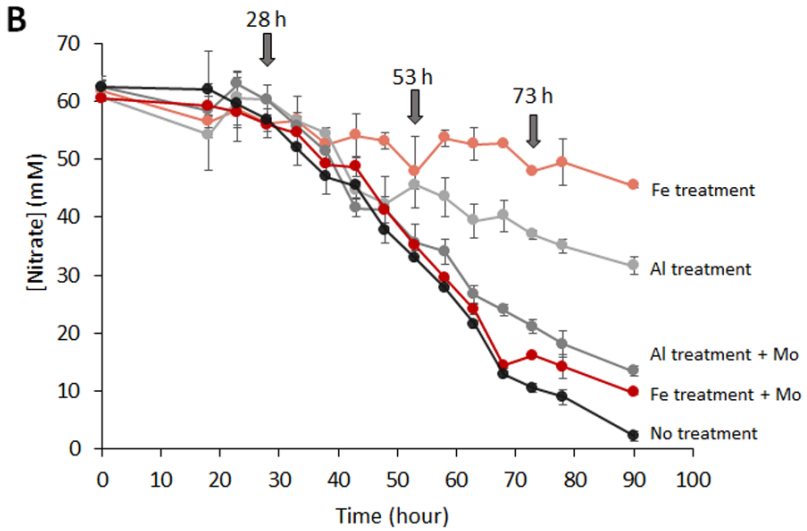
B
28 h
53 h
73 h
Fe treatment
Al treatment
Al treatment + Mo
Fe treatment + Mo
No treatment
[Nitrate] (mM)
Time (hour)

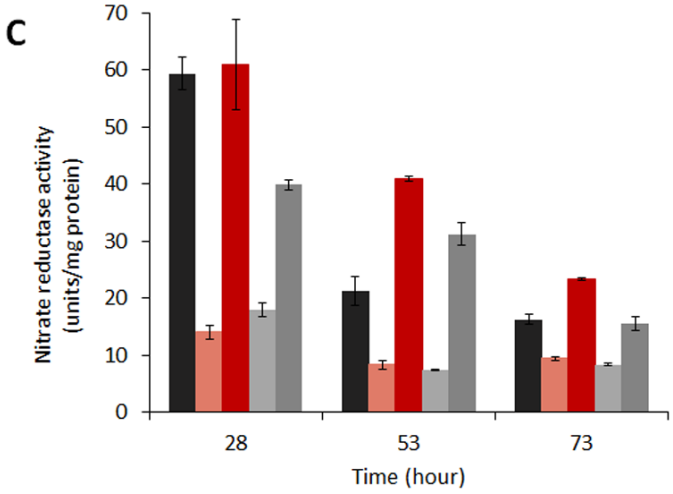
C
Nitrate reductase activity (units/mg protein)
28
53
73
Time (hour)

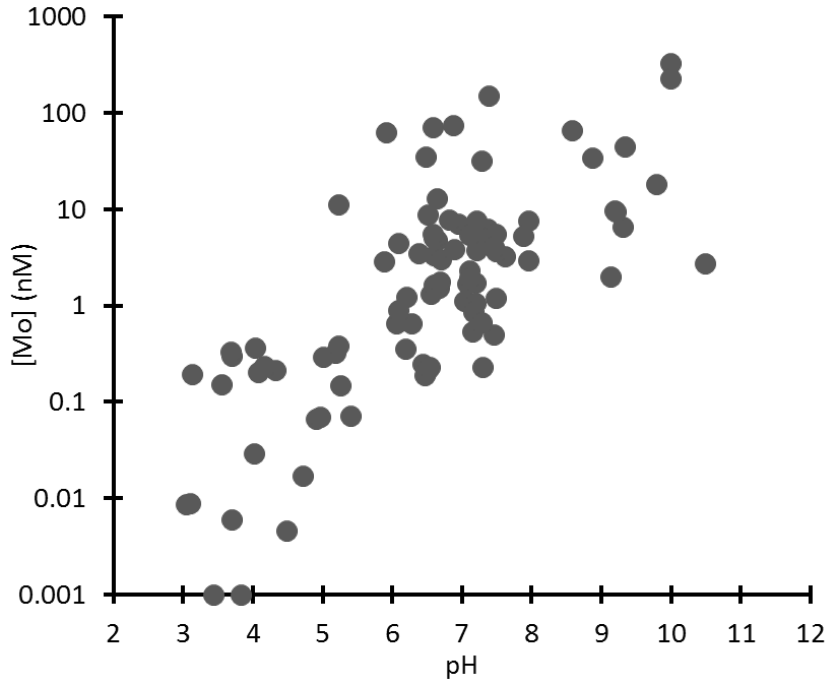


Figure S2.1 pH and dissolved Mo concentrations in groundwater samples from ORR.

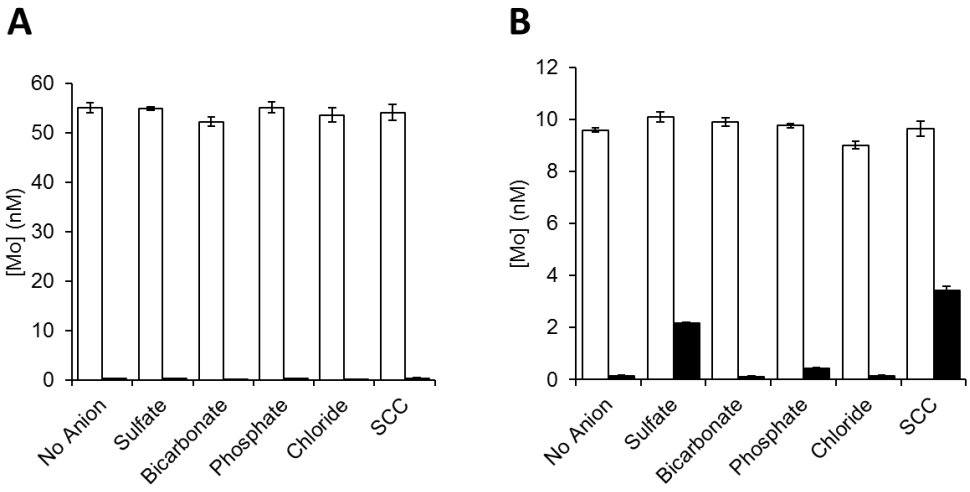


Figure. S2.2. Mo depletion by Fe- and Al-based precipitants with different anions. (A) Removal of soluble Mo by Fe precipitation and inhibition of this process by environmentally relevant anions: sulfate, bicarbonate, phosphate, chloride and a combination of sulfate, bicarbonate and chloride (SCC). pH of the solutions was adjusted from about 2.5 (white bars, before treatment) to 6.7 (black bars, after treatment). (B) Depletion of soluble Mo by Al precipitation and inhibition of this process by environmentally relevant anions: sulfate, bicarbonate, phosphate, chloride and a combination of sulfate, bicarbonate and chloride (SCC). pH of the solutions was adjusted from about 3.5 (white bars, before treatment) to 6.7 (black bars, after treatment).

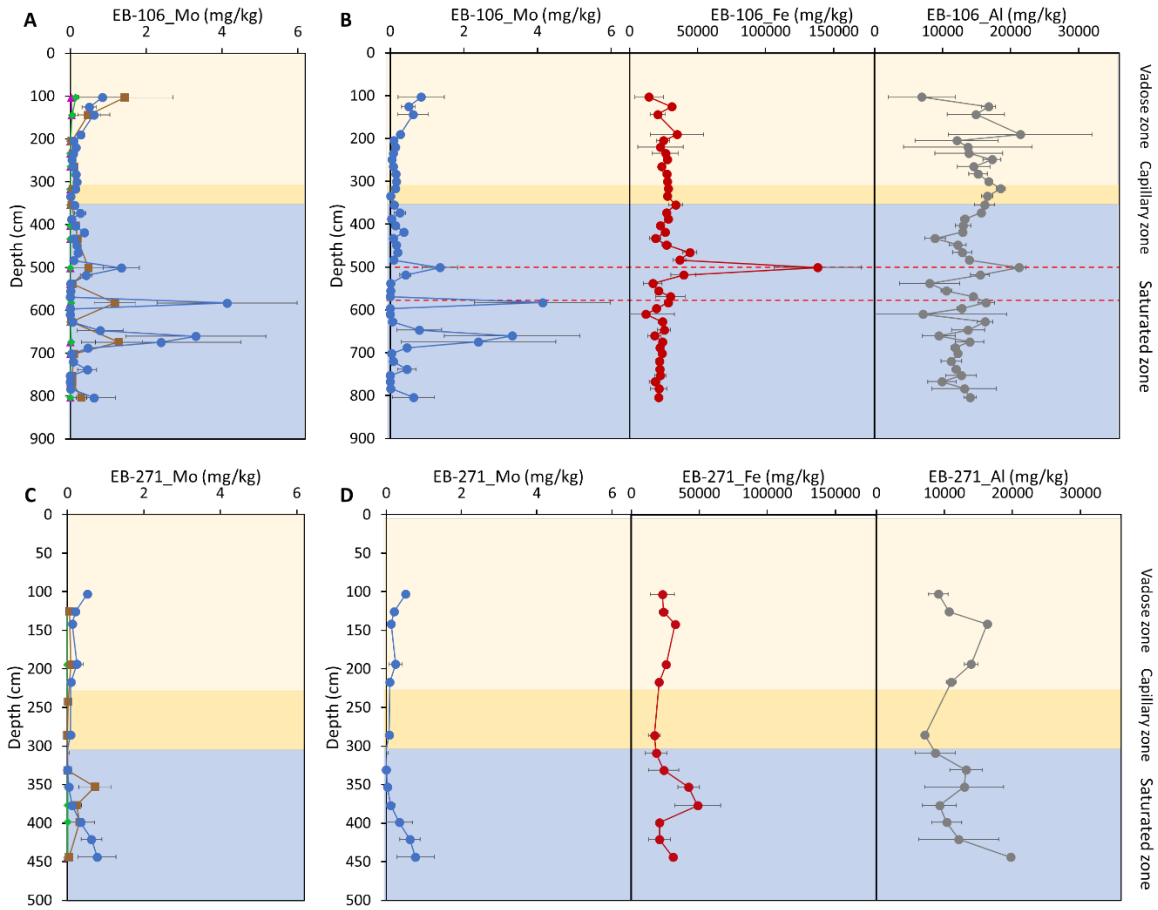


Figure S2.3. Mo, Fe and Al analysis in contaminated ORR sediment. (A)(C) Mo concentrations extracted by different solubilization steps. Soil samples collected from EB-106 (A) and EB-271 (C) covered vadose (pink shading), capillary (light yellow shading) and saturated (blue shading) zones. All extracted samples at various depths were prepared in triplicate and analyzed by ICP-MS. Mo concentrations in acid fractions (pink line with triangles), reducing fractions (green line with diamonds) and oxidizing fractions (tan line with squares) from sequential extraction of every other segment are plotted. Total metal by microwave digestion (blue) is plotted for from every segment. The dotted lines indicate the depths (501 cm and 583 cm) that Mo, Fe and Al peaks overlap. (B)(D) Total Mo, Fe and Al concentrations in contaminated ORR sediment EB-106 (B)

and non-contaminated sediment EB-271 (D). Mo (left, blue), Fe (middle, red) and Al (right, grey) concentrations in total extraction samples from every segment.

Table S2.1 Comparison of ion concentrations. Ions added to the synthetic groundwater used in the abiotic Al or Fe precipitation experiments (left panel). Ions added to standard medium for strain N2A2 growth experiments (right panel).

| **Added Ions (mM)** | **Synthetic Groundwater** | **Added Ions (mM)** | **N2A2 Medium** |
|---|---|---|---|
| $^{*}$**$Al^{3+}$, $Fe^{3+}$or $Al^{3+}$ + $Fe^{3+}$** | 20 | **$Al^{3+}$ or $Fe^{3+}$** | 0 |
| **$Mg^{2+}$** | 8.9 | **$Mg^{2+}$** | 2 |
| **$Cl^{-}$** | 10.5 | **$Cl^{-}$** | 1.7 |
| **$HCO_3^{-}$** | 3 | $^{\dagger}$**$HCO_3^{-}$** | 30 |
| **$PO_4^{3-}$** | 5 | $^{\dagger}$**$PO_4^{3-}$** | 5 |
| **$SO_4^{2-}$** | 15.2 | $^{\dagger}$**$SO_4^{2-}$** | 2 |
| ***$NO_3^{-}$** | 77.8 | **$NO_3^{-}$** | 20 |

*Added to synthetic groundwater as 20 mM $Al(NO_3)_3$, 20 mM $Fe(NO_3)_3$, or 10 mM $Al(NO_3)_3$ plus 10 mM $Al(NO_3)_3$ based on the precipitation experiment. $^{\dagger}$Added post-Al/Fe treatment. $^{\S}$Not detected. All concentrations are indicated in mM.

Table S2.2 Mo concentrations in different media. Mo concentrations in media with no treatment, Fe treatment and Al treatment were analyzed by ICP-MS. $NaNO_3$ was used to supply nitrate to no treatment media, while $Fe(NO_3)_3$/$Al(NO_3)_3$ was used to supply nitrate to Fe/Al treatment media. Samples without treatment or before treatment are named "None" or "Pre", samples after treatment are named "Post". "None + cell" or "Post + cell" represent non-treated medium or Fe/Al-treated medium inoculated with N2A2 cells, and "Post + cell + Mo" samples represent Fe/Al-treated medium inoculated with N2A2 cells plus 20 nM Mo.

| | | Mo [nM ] | Mo [nM] SD |
|---|---|---|---|
| **No treatment** | **None** | 11.7521 | 0.2807 |
| | **None + cell** | 11.9598 | 0.2444 |
| **Fe treatment** | **Pre** | 32.6553 | 0.9035 |
| | **Post** | 0.2730 | 0.0775 |
| | **Post + cell** | 0.3927 | 0.0562 |
| | **Post + cell + Mo** | 19.4673 | 0.5473 |
| **Al treatment** | **Pre** | 13.7253 | 0.6952 |
| | **Post** | 0.6758 | 0.0683 |
| | **Post + cell** | 0.7543 | 0.0859 |
| | **Post + cell + Mo** | 19.3019 | 0.2657 |

# CHAPTER 3

# DRAFT GENOME SEQUENCE OF *BACILLUS SP*. STRAIN EB106-08-02-XG196, ISOLATED FROM HIGH-NITRATE-CONTAMINATED SEDIMENT [2]

[2]Xiaoxuan Ge, Michael P. Thorgersen, Farris L. Poole II, Adam M. Deutschbauer, John-Marc Chandonia, Pavel S. Novichkov, Paul D. Adams, Adam P. Arkin, Terry C. Hazen, and Michael W. W. Adams. (2020). *Microbiology Resource Announcements*, 9:e01149-20.

Reprinted here with permission of the publisher

**Abstract**

*Bacillus sp.* EB106-08-02-XG196 was isolated from a high nitrate- and heavy metal-contaminated site at the Oak Ridge Reservation (ORR). We report the draft genome sequence of this strain to provide insights into the genomic basis for surviving in this unique environment.

The Oak Ridge Reservation (ORR) in Tennessee, USA, contains a site termed the S-3 ponds that has been used for the disposal of waste liquids produced from the Y-12 nuclear plant and is contaminated with nitrate and heavy metals (126). The groundwater at this site has a pH as low as 3.0 and contains up to 230 mM nitrate and high concentrations of over twenty different metals (26, 127, 130). In contrast, the concentration of the metal molybdenum, which is essential for nitrate reduction by microorganisms, is lower in highly contaminated groundwater than it is in the uncontaminated pristine groundwater (142, 178).

Strain EB106-08-02-XG196 (hereafter, referred to as XG196) was isolated from highly contaminated ORR sediment core EB106 located 21 meters downstream of the S-3 ponds (178). It was identified as a *Bacillus sp.* by 16S rRNA gene sequencing. The ORR sediment sample was collected and processed under anaerobic conditions (178). Sediment samples (1 g) were incubated anaerobically in 5 ml of a defined medium described (171). Mixed carbon sources (formate, acetate, ethanol, lactate, succinate and glucose, 2 mM each) and 0.1 g/L yeast extract were used for the enrichment. Cultures were incubated at room temperature for 2 – 7 days and then streaked out on agar plates of defined medium. A single colony of strain XG196 was isolated and cultivated for genomic DNA preparation.

XG196 genomic DNA was prepared using a ZymoBead genomic DNA kit (Zymo Research, CA, USA). The Illumina sequencing library was made by shearing DNA to ~800 bp (Covaris, MA, USA) and the KAPA HyperPrep kit (Roche, Basel, Switzerland) was then used to add Illumina-

compatible adapters to the library. The genome was sequenced using Illumina HiSeq2500 platform. This generated 10,798,254 paired end reads of 151 bp each, totaling 1,630,536,354 bp, with a genome coverage of 215× and an $N_{50}$ value of 283,772 bp. The sequencing reads were trimmed using Trimmomatic 0.36 (179) and assembled de novo using SPAdes v3.12.0 (180). An initial genome annotation was performed using Prokka v1.12 (181) executed using KBase (182). The KBase apps kb_trimmomatic version 1.2.13, kb_SPAdes version 1.1.3, ProkkaAnnotation version 2.0.3 were used for the corresponding steps in the pipeline. Default parameters were used for all software unless otherwise specified. Species trees were built for the XG196 genome using two KBase software packages, GTDB-Tk Classify v1.3.0 and Insert Genome Into Species Tree 2.1.10. Both rely on phylogenetic marker genes other than 16S rRNA and both identified *Bacillus niacini* as having the most similar genome to XG196 (182). Finally, the KBase-derived assembly was deposited into GenBank. Due to compatibility isues, the GenBank PGAP annotation pipeline was re-run on the assembly to produce the final draft genome. We ran the RAST annotation pipeline in KBase (version 0.1.1) on the GenBank-derived genome to classify features. The final draft genome of strain XG196 contained 6,010,169 bp in 55 contigs longer than 500 bp with a 38.35% G+C content. A total of 5721 coding genes and 234 non-coding features were annotated, which included 78 non-coding RNA genes, 42 non-coding regulatory features and 114 other non-coding features.

## Data Availability

This Whole Genome Shotgun project has been deposited in GenBank under the accession number JABWSY000000000 (https://www.ncbi.nlm.nih.gov/nuccore/ JABWSY000000000). The version described in this paper is the first version (JABWSY000000000). The raw sequence reads have been deposited in the SRA database under accession number PRJNA633127 (https://www.ncbi.nlm.nih.gov/sra/PRJNA633127). All KBase analyses and data objects are available in the KBase static narrative https:// kbase.us/n/60201/86.


## Acknowledgments

This material by ENIGMA (Ecosystems and Networks Integrated with Genes and Molecular Assemblies) (http://enigma.lbl.gov), a Scientific Focus Area Program at Lawrence Berkeley National Laboratory, is based upon work supported by the U.S. Department of Energy, Office of Science, Office of Biological and Environmental Research, under contract number DE-AC02-05CH11231. The authors wish to thank Kenneth Lowe and Dominique Joyner for their invaluable help in collecting sediment samples and Astrid Terry for project management.


## Author Contributions

XG isolated the strain and wrote the manuscript. AD, JC and PN carried out the genome sequencing and annotation. TH contributed to environmental sampling. MA directed the research. MT, FP, JC, and MA contributed to its revision.

# CHAPTER 4

# CHARACTERIZATION OF A METAL-RESISTANT *BACILLUS* STRAIN WITH A HIGH MOLYBDATE AFFINITY MODA FROM CONTAMINATED SEDIMENTS AT THE OAK RIDGE RESERVATION[3]

[3]Xiaoxuan Ge, Michael P. Thorgersen, Farris L. Poole II, Adam M. Deutschbauer, John-Marc Chandonia, Pavel S. Novichkov, Paul D. Adams, Adam P. Arkin, Terry C. Hazen and Michael W. W. Adams. (2020). *Frontiers in Microbiology*, 11:2543.

**Abstract**

A nitrate- and metal-contaminated site at the Oak Ridge Reservation (ORR) was previously shown to contain the metal molybdenum (Mo) at picomolar concentrations. This potentially limits microbial nitrate reduction, as Mo is required by the enzyme nitrate reductase, which catalyzes the first step of nitrate removal. Enrichment for anaerobic nitrate-reducing microbes from contaminated sediment at the ORR yielded *Bacillus* strain EB106-08-02-XG196. This bacterium grows in the presence of multiple metals (Cd, Ni, Cu, Co, Mn and U) but also exhibits better growth compared to control strains, including *Pseudomonas fluorescens* N2E2 isolated from a pristine ORR environment under low molybdate concentrations (< 1 nM). Molybdate is taken up by the molybdate binding protein, ModA, of the molybdate ATP-binding cassette transporter. ModA of XG196 is phylogenetically distinct from those of other characterized ModA proteins. The genes encoding ModA from XG196, *P. fluorescens* N2E2 and *Escherichia coli* K12 were expressed in *E. coli* and the recombinant proteins were purified. Isothermal titration calorimetry analysis showed that XG196 ModA has a higher affinity for molybdate than other ModA proteins with a molybdate binding constant ($K_D$) of 2.2 nM, about one order of magnitude lower than those of *P. fluorescens* N2E2 (27.0 nM) and *E. coli* K12 (25.0 nM). XG196 ModA also showed a 5-fold higher affinity for molybdate than for tungstate (11 nM), whereas the ModA proteins from *P. fluorescens* N2E2 ($K_D$ (Mo) 27.0 nM, $K_D$ (W) 26.7 nM) and *E. coli* K12 ($K_D$ (Mo) 25.0 nM, $K_D$ (W) 23.8 nM) had similar affinities for the two oxyanions. We propose that high molybdate affinity coupled with resistance to multiple metals gives strain XG196 a competitive advantage in Mo-limited environments contaminated with high concentrations of metals and nitrate, as found at ORR.

## Introduction

Molybdenum (Mo) is an essential metal for the growth of virtually all known life forms, including humans, plants and microorganisms, as it is required for the function of several key enzymes involved in the cycling of N, C and S (7, 183, 184). Tungsten (W), an antagonist of Mo, is more uncommon in nature but required in some enzymes, most notably in archaea. Physiologically-relevant oxidation states of Mo and W are +4, +5, and +6 (7). There are five distinct enzyme families that use Mo and/or W, represented by nitrogenase (Mo only, although some use vanadium), xanthine oxidase (Mo only), the sulfite oxidase (Mo only), DMSO reductase (most family members use Mo, a few use W) and tungsten-containing oxidoreductase (WOR, W only) (7, 68). In most microorganisms, molybdate is taken up into the cell by the molybdate ATP-binding cassette or Mod transporter (ModABC), which can also take up tungstate (97, 185).

In the nitrogen cycle, Mo is utilized in three key steps, $N_2$-fixation (by nitrogenase), nitrite oxidation (by nitrite oxidoreductase) and nitrate reduction (by nitrate reductase) (20). Hence Mo is required for the biological removal of nitrate from contaminated environments as the reductase is a key enzyme in both the denitrification (yielding $N_2$) and dissimilatory nitrate reduction to ammonium (DNRA) pathways (20). Consequently, in natural environments, the availability of Mo can limit nitrate removal (23, 24). Mo limitation can also negatively impact nitrate removal in contaminated environments, which can be caused by the extensive use of nitrate-containing fertilizers, the release of nitrate-containing industrial wastes, as well as mining and other anthropogenic activities leading to problems for human health and natural environments (18, 26, 35, 43, 47, 186, 187).

The Oak Ridge Reservation (ORR) in Tennessee, USA contains a nitrate-contaminated waste site - the S-3 ponds. These are four adjacent (~9.5 million liters each) earthen reservoirs used for the disposal of waste liquids that had been produced from the Y-12 nuclear plant for more

than 30 years (126). The waste liquids contained high, and potentially toxic, concentrations of nitrate (up to 1.2 M) and a wide variety of metals, such as iron (up to 21 mM), aluminium (up to 180 mM), magnesium (up to 28 mM), and uranium (up 1.3 mM) (126). In 1983, the waste liquids in the S-3 ponds were adjusted to about pH 9, and the precipitates formed were allowed to settle before the liquid was removed (126, 127). In 1988, the S-3 ponds were filled and capped and now serve as a parking lot (127). However, the area is still heavily contaminated and groundwater in the contamination plume emanating from the former S-3 ponds is at low pH (as low as 3.0) and contains high concentrations of nitrate (up to 230 mM), much higher than the surrounding pristine groundwater (less than 32 μM) (39, 178). In addition, the contaminating plume has elevated concentrations of over 20 metals, including uranium (up to 580 μM) (26, 130). In stark contrast, extremely low concentrations of Mo (in the picomolar range) were measured in this highly contaminated groundwater. It was demonstrated experimentally that the pM concentrations of Mo in ORR contaminated groundwater were likely a result of molybdate adsorption and incorporation into Fe- and Al-based minerals that are formed as the groundwater from the highly contaminated area (pH < 1) mixes with the surrounding groundwater (142, 178).

Hence, a fundamental question is whether microorganisms that thrive in the unique ORR environment contaminated with high concentrations of metals and nitrate, yet containing only picomolar levels of Mo, have unique features that enhance Mo utilization. Herein, we describe the characterization of a novel nitrate-reducing *Bacillus,* designated strain EB106-08-02-XG196 (hereafter XG196), that was isolated from a sample of nitrate- and metal-contaminated ORR sediment (EB-106) located 21 meters downstream of the S-3 ponds area (178). XG196 is resistant to high concentrations of a metal mixture that was designed to mimic the ORR contaminated groundwater. More importantly, it is also much less sensitive to Mo-limitation than other ORR isolates, including four other EB-106 strains and a microbe obtained from a non-contaminated

ORR environment. The molecular basis for the ability of XG196 to thrive under Mo-limited conditions was investigated.

## Methods and Materials

### Sampling and isolation of strains

An 8-meter-deep borehole of 8.9 cm diameter (designated EB-106) located 21.1 meters downstream from the S-3 ponds area was drilled at ORR. The sediment was collected and cut into 22 cm segments under anaerobic conditions, as reported elsewhere (178, 188). For microbial enrichment, sediment samples (1 g) were incubated anaerobically in 5 ml of a defined medium (pH 7.0) containing 1.3 mM KCl, 2 mM $MgSO_4$, 0.1 mM $CaCl_2$, 0.3 mM NaCl, 30 mM $NaHCO_3$, 5 mM $NaH_2PO_4$ and 20 mM $NaNO_3$, with added vitamins and minerals as described (171). A mixture of 2 mM of different carbon sources (formate, acetate, ethanol, lactate, succinate and glucose) and 0.1 g/L yeast extract was used as carbon sources. Metal mix (MM) was used to mimic the metal contamination in the groundwater near the ORR S-3 ponds. MM (1x) resulted in final concentrations in the media of 5 µM cadmium acetate ($Cd(CH_3COO)_2 \cdot 2H_2O$), 100 µM manganous chloride ($MnCl_2 \cdot 2H_2O$), 30 µM cobalt chloride ($CoCl_2 \cdot 6H_2O$), 100 µM nickel chloride ($NiCl_2 \cdot 6H_2O$), 10 µM cupric chloride ($CuCl_2 \cdot 2H_2O$), 10 µM ferrous ammonium sulfate ($Fe(NH_4)_2(SO_4)_2 \cdot 6H_2O$) and 100 µM uranyl acetate ($UO_2(CH_3COO)_2 \cdot 2H_2O$) (Table S4.1). For enrichment, all cultures were incubated anaerobically in anaerobic chamber (filled with 95% argon and 5% hydrogen) at room temperature for 2 to 7 days in media containing either 1×, 0.5× or no MM of final concentrations. Cultures with turbidity were streaked out on plates (1.5% agar) using the same medium and were incubated at room temperature for single colony isolation. For purified microbial strains, the sequences of their 16S rRNA genes were determined as described below and compared with those in the BLASTN suite (https://blast.ncbi.nlm.nih.gov) using default parameters (189).

**Nitrate reductase activity**

Nitrate reductase activities of the EB-106 isolates were determined using whole cell suspensions (190). Strains were grown anaerobically in Hungate tubes and cells were collected at mid-log phase and early stationary phase, then 15 µL of 5 mg/ml chloramphenicol was added to 1.5 ml of culture to inhibit protein synthesis. Cells were washed twice and re-suspended in buffer (50 mM phosphate buffer, pH 7.2) and the $OD_{660}$ was determined. 200 µL of cells were mixed with 25 µL of methyl viologen (0.5 mg/ml) in an anaerobic sealed cuvette at 25 °C. 100 µL of reaction solution (4 mg/ml $Na_2S_2O_4$, 4 mg/ml $NaHCO_3$ and 100 mM $KNO_3$) was added to start the reaction. In control reaction buffer, $Na_2S_2O_4$ was replaced with water. After incubation at room temperature for 5 min, the mixtures were vortexed in air to stop the reaction by oxidizing the electron donors ($Na_2S_2O_4$ and reduced methyl viologen). The amount of nitrite produced was measured by adding 100 µL of sulfanilic acid (1% w/v in 20% HCl) to 30 µL of each reaction mixture followed by 100 µL of N-(1-naphthyl)ethylenediamine-HCl (1.3 mg/ml). The $OD_{540}$ of each sample supernatant was measured and the amount of nitrite was calculated according to nitrite standards. The $OD_{420}$ of the samples was also measured to account for light scattering by residual cells and cell fragments. Nitrate reductase specific activity is expressed as units/$OD_{660}$, in which units are calculated using the formula $100 \times [OD_{540} - (0.72 \times OD_{420})]/(T \times V)$, T is time in minutes and V is reaction volume in milliliters (141, 190).

**Carbon sources utilization for anaerobic growth analysis**

Growth on various carbon sources was determined at 25 ℃ under anaerobic conditions using the standard medium lacking yeast extract and the organic mixture but containing either formate, acetate, ethanol, lactate, succinic acid, fumarate, xylose, xylitol, glucose, fructose, maltose, sodium benzoate, sodium 4-hydroxybenzoate, potassium sodium tartrate, proline, phenylalanine, arginine, threonine, leucine, glutamate or glutamine (all at 2 mM) with and without nitrate ($KNO_3$, 20 mM).

Growth was measured in 400 µl wells on a 100-well plate (Bioscreen sterile plates HONEYCOMB, Thermo Fisher Scientific, Massachusetts, USA) using a Bioscreen C (Thermo Labsystems, Thermo Fisher Scientific, Massachusetts, USA) placed in a PLAS LABS anaerobic chamber under a 5% $H_2$ and 95% Ar atmosphere. Optical density ($OD_{600}$) of cultures in each well were measured every 5 mins, after the plate was shaken using the Bioscreen C to resuspend cells.

**Mo accumulation analysis**

EB-106 isolates were grown in 500 ml of defined media with 1 µM Mo ($(NH_4)_2MoO_4$) and harvested at mid log phase, washed three times with 10 ml of Tris buffer (Tris 50 mM, pH 8.0, containing 100 mM NaCl) and then resuspended in Tris buffer. Cells were lysed by sonication, then were spun down at 10,000×G for 15 min and the supernatants were used for further centrifugation. The cytoplasmic extract (S100) was obtained after centrifugation at 100,000 × G for 1 hour in a Beckman Coulter Optima L-90 ultracentrifuge. The membrane fraction was resuspended in 2 ml of Tris buffer. Both S100 and membrane fractions were diluted (1:40) with trace grade 2% nitric acid (VWR, Pennsylvania, USA) and incubated overnight prior to analysis by inductively coupled plasma mass spectrometry (ICP-MS) analysis to quantify Mo (191, 192). Protein concentrations were measured using the Bradford assay (Bio-Rad protein assay kit, Bio-Rad, California, USA). The amount of Mo accumulated is expressed as nmoles per gram of protein (nmol/g).

**Molybdenum-limited growth**

For the Mo-depleted medium, a solution was prepared that contained 1.3 mM KCl, 2 mM $MgSO_4$, 0.1 mM $CaCl_2$ and 0.3 mM NaCl together with the vitamins and minerals described above except that molybdenum and tungsten were not added (171). $Fe(NO_3)_3$ (20 mM) was then added, which acidifies the solution to pH ~ 2.5. The pH was then adjusted to pH 6.7 using trace grade NaOH (2 M) to induce precipitation of ferric hydroxide. As previously described (178), the Fe precipitates

any contaminating Mo present in the medium components. The Mo-depleted growth medium was prepared by adding trace grade $Fe(NO_3)_3$ (7.4 μM), $Na_2SO_4$ (2 mM), $NaHCO_3$ (30 mM) and $NaH_2PO_4$ (5 mM) and inoculated with 1% (vol/vol) washed XG77, XG146, XG95, XG201 or XG196 cells grown in media with no Mo added. Growth in this medium with and without added Mo (0.1 nM, 0.5 nM, 1 nM, 5nM, 10 nM, 50 nM or 500 nM $Na_2MoO_4$) was measured in quadruplet using the Bioscreen C described above. Mo and W competition analysis of XG196 and *P. fluorescens* N2E2 under nitrate reducing conditions were performed using the same media with added Mo (0 nM, 5 nM, 50 nM, 500 nM, 5000 nM or 50000 nM $Na_2MoO_4$) and added W (0 nM, 50 nM, 5 μM or 500 μM $Na_2WO_4$).

**Metal tolerance assay**

Each EB-106 isolate (XG77, XG146, XG95, XG201 and XG196) was incubated with individual metals at multiple concentrations, including manganous chloride ($MnCl_2 \cdot 2H_2O$, 0 ~ 6 mM), cobalt chloride ($CoCl_2 \cdot 6H_2O$, 0 ~ 600 μM), nickel chloride ($NiCl_2 \cdot 6H_2O$, 0 ~ 250 μM), cupric chloride ($CuCl_2 \cdot 2H_2O$, 0 ~ 250 μM), cadmium acetate $Cd(CH_3COO)_2 \cdot 2H_2O$, 0 ~ 200 μM) or uranyl acetate ($UO_2(CH_3COO)_2 \cdot 2H_2O$, 0 ~ 2 mM), or with the MM (0 ~ 2 ×) described above (Table S4.1). Cultures were grown in defined medium described above containing 0.1 g/L yeast extract using the Bioscreen C described above and growth data were analyzed using R with Grofit package (193). The average half maximal inhibitory concentration ($IC_{50}$) was used to reflect the tolerance of each EB-106 isolate to each individual metal and the MM.

**Genome sequencing**

The ZymoBead Genomic DNA kit was used to extract genomic DNA from strain XG196 and XG77. More than 1 μg of purified gnomic DNA from each strain was used for Illumina sequencing. The Illumina sequencing reads were trimmed using Trimmomatic 0.36, with parameters "-phred33 LEADING:3 TRAILING:3 SLIDINGWINDOW:4:15 MINLEN:36

ILLUMINACLIP:TruSeq3-PE.fa" (179). The trimmed reads were assembled de novo using SPAdes v3.12.0 with parameters "-k 21,33,55,77" (180). Genes were identified using Prokka v1.12, with default parameters (181). This pipeline was executed using the Department of Energy KnowledgeBase software platform (KBase; http://www.kbase.us, (182)). The genome of XG196 was submitted to GenBank (accession number: JABWSY000000000).

**16S rDNA sequencing and phylogenetic analysis**

The 16S rDNA of isolate XG196 was amplified by PCR using universal bacterial primers 27F (5'-AGA GTT TGA TCC TGG CTC AG-3') and 1492R (5'-ACG GCT ACC TTG TTA CGA CTT-3') from Integrated DNA Technologies, IA, USA. DNA sequencing was carried out by GENEWIZ, NJ, USA. The sequence was first analyzed by BLAST (https://blast.ncbi.nlm.nih.gov/Blast.cgi) (189), which indicated that XG196 is a *Bacillus* strain. The sequence was uploaded to the Ribosomal Database Project (RDP; http://rdp.cme.msu.edu/) (194). The RDP tool Seqmatch was run to find the closest relatives of isolate XG196 and the *Bacillus* type strains with high quality 16S rDNA sequences (>1200 bp). The two closest relatives of XG196 and a total of 187 *Bacillus* type strains with one out group strain were selected to build the 16S rRNA phylogenetic tree by IQ-TREE using maximum likelihood (http://www.iqtree.org/; (195)). GTR+F+R6 model was selected by ModelFinder (196) and 1000 times of bootstrapping was run using UFBoot (197).

**Phylogenetic analysis of molybdate and tungstate binding proteins**

Accession numbers of ModA (family IPR005950) and WtpA (family IPR022498) were downloaded from the InterPro database (https://www.ebi.ac.uk/interpro/) (198). Information, such as sequence, mass, protein name, gene name, taxonomic lineage, cross-reference in PDB, cross-reference in KEGG, PubMed ID, etc. were all downloaded together. Proteins with candidadus/candidate organisms, uncultured organisms, fragment proteins, wrong/poorly-labelled

organisms, and duplicates were removed from the list. Two lists (A and B) of strains were selected from downloaded candidates for ModA phylogenetic analysis. List A uses strains with ATCC (American Type Culture Collection) or DSM (Deutsche Sammlung von Mikroorganismen und Zellkulturen GmbH) reference IDs. For list B, all downloaded protein sequences were clustered by CD-HIT (http://weizhongli-lab.org/cd-hit/) at 60% sequence identity (199). In both lists, all archaea, eukaryote sequences and sequences with KEGG cross-reference or 3D structures were kept. Several *Bacillus* type-strains and the top two closest isolate XG196 ModA relatives and ORR isolate *Pseudomonas fluorescens* N2E2 from non-contaminated area were also kept. ModA/WtpA sequences from list A (617 sequences, supplemental material list A) and B (4623 sequences, supplemental material list B) were all used for tree building. Multiple sequence alignment was done by Clustal Omega (https://www.ebi.ac.uk/Tools/msa/clustalo/) (200). IQ-tree were used to build the phylogenetic tree by maximum likelihood (195). LG+F+R10 model and WAG+R9 model were selected for list A and B ModA tree building by ModelFinder (196). 2000 and 3000 times of bootstrapping was run for list A and B ModA tree using UFBoot (197). Signal peptide prediction analysis was performed for all list A sequences by SignalP5.0 (http://www.cbs.dtu.dk/services/SignalP/) (201).

**Multi-alignment and structural modeling analysis of ModA**

Multiple sequence alignments of XG196 ModA and selected proteins were first run by Clustal Omega (https://www.ebi.ac.uk/Tools/msa/clustalo/) (200) and further analyzed with selected ModA proteins with structural data from the PDB (https://www.rcsb.org/) using ESPript 3.0 (http://espript.ibcp.fr/ESPript/ESPript/) (202). The structures of the ModA proteins from *Pyrococcus furiosus* ATCC 43587 ModA (PDB: 3CG1) and *Escherichia coli* K12 ModA (PDB: 1AMF) were used for comparison with XG196 ModA. Mean identity and mean similarity of protein sequences were also calculated by ESPript 3.0. SWISS-MODEL

(https://swissmodel.expasy.org/) (126) was used to predict the model of XG196 using template ModA (PDB: 2H5Y) from *X. axonopodis pv. citri* 306. UCSF Chimera (http://www.cgl.ucsf.edu/chimera) (203) was used to visualise the model.

**Expression and purification of recombinant ModA proteins**

ModA genes were amplified by PCR from the genomes of XG196, *P. fluorescens* N2E2 and *E. coli* K12. The primers are listed in Table S4.2. The forward primer for the ModA gene of XG196 was designed to omit the N-terminal 20 amino acids, which include a signal peptide and a putative lipoprotein-attachment sight (Cys20). The forward primers for ModA genes of *P. fluorescens* N2E2 and *E. coli* K12 were designed to omit the N-terminal signal peptides, the first 23 and 25 amino acids, respectively. Signal sequences and lipoprotein-attachment site were predicted by SignalP-5.0 (http://www.cbs.dtu.dk/services/SignalP-5.0/) (201). The PCR amplicons were cloned into the pET24a (+) plasmid (Novagen). ModA proteins were expressed in *E. coli* Rosetta 2 (DE3)pLysS (Novagen) cells in LB media supplemented with kanamycin (50 µg/ml). Recombinant gene expression was induced at an $OD_{600}$ ~ 0.6 with 0.5 mM IPTG and the growth temperature was reduced from 37 to 25 °C. Cells were harvested after 16 hours and resuspended in start buffer (Tris 20 mM, pH 7.6, 100 mM NaCl, 5 mM imidazole). Cells were lysed by sonication and centrifuged to remove unlysed cells. The supernatant fractions were loaded onto a HisTrap FF crude column (GE health care) pre-equilibrated with start buffer and washed with two column volumes of wash buffer (Tris 20 mM, pH 7.6, 100 mM NaCl, 30 mM imidazole) and the recombinant ModA proteins were then eluted with elution buffer (Tris 20 mM, pH 7.6, 100 mM NaCl, 300 mM imidazole). ModA proteins were further purified by gel filtration using a Superdex 200 HiLoad 16/60 prep grade column (GE health care) equilibrated with Tris 20 mM, pH 7.6, containing 250 mM NaCl. Fractions containing the purified ModA protein as determined by SDS-PAGE were buffer exchanged to a low salt buffer (Tris 20 mM, pH 7.6, 90 mM NaCl) using an

Amicon Ultra-15 10K centrifugal filter device at 4 °C for 16 hr for further ITC analysis. Mo in 40 μM of protein samples before and after dialysis were measured by ICP-MS. Trace grade of Tris (MilliporeSigma, Missouri, USA) and NaCl (MilliporeSigma, Missouri, USA) were used in protein purification and dialysis.

**Isothermal titration calorimetry (ITC) analysis**

Molybdate (100 mM $Na_2MoO_4$) and tungstate (100 mM $Na_2WO_4$) stock solutions were prepared in trace grade ITC buffer (Tris 20 mM, pH 7.6, 90 mM NaCl) and then diluted to a final concentration of 0.3 or 0.4 mM using ITC buffer. ITC analysis was performed using a Malvern MicroCal PEAQ-ITC (Malvern Panalytical, Malvern, UK) at 25 °C. Molybdate or tungstate were injected into the sample chamber (300 μL) containing 30 μM or 40 μM ModA to give a final molar ratio of oxyanion to ModA of 2:1. Displacement titrations were carried out by titrating molybdate or tungstate with chromate-saturated ModA (containing 2-fold of chromate from $Na_2CrO_4$) (204). Data were analyzed by Malvern MicroCal PEAQ-ITC analysis software (Malvern Panalytical, Malvern, UK). Each test was done twice and the average data were used.

**ICP-MS analysis**

Samples were vortexed and then diluted (at various concentrations depending on sample type) into 2% (vol/wt) trace-grade nitric acid (VWR, Pennsylvania, USA) in acid-washed 15 mL polypropylene tubes. Samples were analyzed by an Agilent 7900 ICP-MS fitted with MicroMist nebulizer, UHMI-spray chamber, Pt cones, x-lens and an Octopole Reaction System (ORS) collision cell with He-mode (Agilent Technologies, California, USA) as described in (178).

**Metagenome annotation and analysis of nitrate-reducing bacteria in ORR**

Previously published metagenome sequence reads of samples from ORR groundwater were obtained from the NCBI database under BioProject PRJNA513876 (205). Metagenomic reads were preprocessed using BBtools version 38.60 (no references known, https://jgi.doe.gov/data-

and-tools/bbtools/) to remove Illumina adapters, perform quality filtering and trimming, and remove PhiX174 spike-ins. The script bbduk.sh was run with parameters *ktrim=r k=23 mink=11 hdist=1 ref=adapters.fa tbo tpe 2* to remove any remaining standard Illumina adapters given in adapters.fa. The script was run again with parameters *bf1 k=27 hdist=1 qtrim=rl trimq=17 cardinality=t ref=phix174_Illumina.fa* to perform quality filtering and trimming, and to remove Illumina PhiX174 spike ins given in the file phix174_Illumina.fa. We assembled the reads using SPAdes version 3.13.0 (180) with parameters --*meta -k 21,33,55,77,99,127*. We predicted protein-coding genes using Prodigal v 2.6.3 (206) with parameters -*n -p single*.Predicted protein-coding genes were annotated on the contigs using eggNOG mapper (v2) with default parameters (207). The number of predicted genes for each protein of interest was normalized by the number of raw reads obtained from metagenome sequencing.

## Results

### Isolation and physiological characterization of *Bacillus* strain XG196

In order to isolate nitrate-reducing microbes with a high affinity for molybdate from the metal- and nitrate-contaminated ORR site, sediments from the contaminated EB-106 vertical core were used for enrichment and isolation. This 8-meter core, taken about 21 meters downstream of the contamination source (the S-3 ponds), was cut into 22 cm segments under anaerobic conditions (178, 188). The EB-106 core covered the vadose zone (0–300 cm, the area between the land surface and water table), the capillary fringe (300–350 cm, the subsurface layer between vadose zone and the water table), and saturated zone (350–800 cm, the region below the water table) of the soil (Figure 4.1A). The groundwater passing through the saturated zone of the EB-106 core flows from the contamination site and is considered to be highly contaminated. A total of 88 unique nitrate-reducing bacteria were isolated from EB-106 sediment samples under nitrate-reducing conditions in a medium containing a combination of carbon sources (2 mM of formate, acetate, ethanol, lactate, succinate and glucose, together with 0.1g/L yeast extract) and various levels of metal contaminants (no, 0.5 × or 1.0 × MM). Five strains, XG77, XG95, XG146, XG196 and XG201, were selected for further characterization based on their ability to grow anaerobically on nitrate, their nitrate reductase activities and metal resistance properties. XG77, XG95 and XG196 were identified as *Bacillus* strains, while XG146 and XG201 were identified as *Ensifer* and *Enterobacter* strains, respectively, by 16S rDNA sequences (Figure 4.1B). All five were isolated from the contaminated saturated zone (below 350 cm) (Figure 4.1A and 1B).

As shown in Table S4.3, all five isolates use various carbon sources (2 mM) for nitrate-reducing growth. Isolate XG196 exhibited more robust growth on maltose ($OD_{600max}$ = 0.95), glucose (0.63), xylose (0.48), fructose (0.48), proline (0.47), glutamate (0.47), lactate (0.33), arginine (0.29) and fumarate (0.25), than other tested carbon sources (formate, acetate, ethanol,

succinic acid, xylitol, benzoate, 4-hydeoxybenzoate, tartrate, phenylalanine, threonine, leucine and glutamine, $OD_{600max} \leq 0.11$). Xylose, glucose, fructose, maltose, proline and glutamine also support the growth of isolate XG196 by fermentation. Lactate was selected as the carbon source for further characterization of strain XG196, as it supported robust nitrate-reducing growth and did not support fermentative growth. Xylose was selected for the other four EB-106 isolates as they exhibited good growth (XG77, $OD_{600max}$ 0.22; XG95, 0.22; XG146, 0.20; and XG201, 0.18) on xylose under nitrate-reducing conditions but did not use xylose for fermentation. Higher biomass yields were obtained with 20 mM of the preferred carbon source (lactate for isolate XG196 or xylose for strains XG146, XG201, XG95 and XG77). The maximum $OD_{600}$ values for XG146, XG201, XG95 and XG77 increased from 0.20, 0.18, 0.22 and 0.22 to 0.5, 0.7, 0.25, and 0.4 respectively. XG196 reached the highest cell density under nitrate-reducing conditions, with $OD_{600}$ reaching 1.5 when lactate was increased to 20 mM (Figure 4.1B). Nitrate reductase activities of XG146, XG201, XG95, XG77 and XG196 were determined using whole cell suspensions from cultures collected under anaerobic nitrate-reducing conditions using 20 mM nitrate (190, 208). Strains XG77 and XG196 showed higher nitrate reductase activities than the other three isolates (Figure S4.1).

Growth of the EB-106 isolates was determined under nitrate-reducing growth conditions in the presence of increasing concentrations of a single metal (Cd, Ni, Cu, Co, Mn or U) or the MM metal mixture containing all six metals, which mimics the concentrations of metals found in the ORR contaminated groundwater (Table S4.1). The effects of the metals on growth was determined by calculating the $IC_{50}$ values. Generally, strain XG196 had the highest metal tolerance of the five stains to the metal contaminants in the EB-106 sediments. Specifically, isolate XG196 had the highest $IC_{50}$ values when grown with $Ni^{2+}$ (119 μM), $Co^{2+}$ (220 μM), $Mn^{2+}$ (> 900 μM), $U^{6+}$ (2,000 μM) and the metal mixture (1.2 ×) and the second highest $IC_{50}$ value when grown with

$Cu^{2+}$ (94 μM) (Figure S4.2). Strain XG196 also grew in the presence of very high concentrations of nitrate and nitrite, with $IC_{50}$ values of 299 mM and 99 mM, respectively (Figure S4.2).

To analyze the dependence of growth under nitrate-reducing conditions on Mo, the five EB-106 strains and one strain previously isolated from non-contaminated ORR groundwater (*Pseudomonas fluorescens* N2E2) were grown with increasing concentrations of molybdate in Mo depleted media prepared with trace metal grade chemicals in order to lower the amount of contaminating Mo to picomolar concentrations in cultures (~ 400 pM, (178)). As shown in Figure 4.2A, strain XG196 showed the highest percentage of maximum growth (84% of highest $OD_{600}$) even when no Mo was added to the medium, while the other EB-106 sediment strains tested required at least 1 nM Mo to reach ≥ 74% of maximum growth. *P. fluorescens* N2E2, which has been used as a reference strain in other ORR contamination studies (26, 178), had the lowest percentage (as low as 43%) of maximum growth when less than 1 nM Mo was added.

Tungstate is a competitive inhibitor of molybdate transport (97, 100, 185). A Mo/W competitive growth analysis of isolate XG196 and *P. fluorescens* N2E2 under nitrate reducing conditions showed that low concentrations of W (up to 50 nM) do not affect the nitrate-dependent growth of XG196 but limits the growth of *P. fluorescens* N2E2 to only 20% of the maximum (Figure 4.2B). At higher W concentrations, W inhibits nitrate-dependent growth of both isolate XG196 and *P. fluorescens* N2E2. However, strain XG196 requires the addition of less Mo to resume maximal growth. For example, when 5 μM W was added to their media, XG196 only required 50 nM Mo to reach maximum growth, but *P. fluorescens* N2E2 required at least two orders of magnitude more Mo (5,000 nM; Figure 4.2B). Our hypothesis is that XG196 has a much higher affinity for molybdate than the other strains tested, especially that of strain N2E2. The environment from which strain N2E2 was isolated has much higher molybdate concentrations (approx. 10 nM) than the contaminated groundwater (Mo < 1 nM) (26, 130). A higher affinity for

molybdate could give a growth advantage to XG196 by nitrate reduction under Mo-limited conditions.

**Genomic and 16S rDNA analysis of XG196**

The draft genome of strain XG196 contained 6,010,169 bp in 55 contigs longer than 500 bp with a 38.35% G+C content. A total of 5721 coding sequences were predicted. The genome sequencing information from strain XG196 was submitted to the National Center for Biotechnology Information (NCBI) genome database and the accession number is JABWSY000000000. Nitrate reduction-related genes were annotated in the XG196 genome, including for nitrate reductase (*napA* and *napB*), copper-containing nitrite reductase (*aniA*) and nitrous-oxide reductase (*nosZ*), while the gene encoding nitric oxide reductase (*nor*) was missing. Some assimilatory nitrate reduction-related genes (*nasC*, *nasD* and *nasE*) were also present in the genome. Genes encoding the molybdate ABC transport system (*modA* and *modB*) were also identified. The 16S rDNA sequence (1487 bp) of strain XG196 identified the organism as a member of the *Bacillus* genus. In order to characterize it at the species level, a total of 190 16S rDNA sequences, which include those of two XG196 close relatives, 186 *Bacillus* type strains and one out group strain, were used to build a phylogenetic tree using maximum likelihood by IQ-TREE (Figure S4.3). Strain XG196 is closely related to *B. niacini* RB-113 (non-type, 99.176%), *B. sp.* LMG20241 (non-type, 99.663%), *B. niacini* IFO15566 (type, 99.193%) and *B. drentensis* LMG 21831 (type, 99.084%).

**Phylogenetic analysis of the molybdate binding protein (ModA) of XG196**

ModA is the molybdate-binding protein component of the molybdate ModABC transporter. We hypothesize that the ability of XG196 to grow by nitrate reduction using an extremely low concentration of Mo (< 1 nM in contaminated groundwater close to S3 ponds area (178)) is because its ModA has an unusually high affinity for molybdate. Phylogenetic analysis of

XG196 ModA based on protein sequences of about 600 ATCC and DSM strains, including those from Archaea, Bacteria and Eukaryota, showed that it is, indeed, distinct from those of the ORR isolate *P. fluorescens* N2E2 (N2E2) and of *E. coli* K12 (Figure 4.3). The same conclusion was reached by a similar analysis using over 4,000 strains (Figure S4.4). Most ModA proteins in proximity to XG196 ModA on the phylogenetic tree originate from other *Bacillus* strains, most of which were also isolated from soil, but their sequence identities are only about 50% (Table S4.4). The two closest relatives of XG196 ModA are from *Rhodococcus qingshengii* (entry: A0A4R6A6K9, 85.9% identity) and *Bacillus sp*. 7884-1 (entry: A0A268JZS1, 85.9% identity) by UniProt BLAST (Figure 4.4 and Table S4.4).

The structures of the ModA proteins of *Peptoclostridium difficile* 630, also known as *Clostridium difficile* 630 (PDB: 4KD5), *Xanthomonas axonopodis pv. citri* 306 (PDB: 2H5Y, $MoO_4^{2-}$), *E. coli* K12 (PDB: 1AMF, $MoO_4^{2-}$), *Vibrio cholerae* serotype O1 ATCC 39315 (PDB:4RXL, $WO_4^{2-}$) and *Azotobacter vinelandii* (PDB: 1ATG, $WO_4^{2-}$) have been determined (Figure 4.3 and 3.5) (100-102). Each binds a single molybdate (or tungstate) ion. In addition, some archaea are able to utilize tungsten, a metal seldom used in biology, in their pyranopterin-containing enzymes (other than Mo-dependent nitrate reductase) (108, 209). These tungsten-utilizing microorganisms take up tungstate using a transporter (WtpA) that is highly homologous to ModA (Figure S4.5), and the structures of WtpA from *Methanosarcina acetivorans* ATCC 35395 (PDB: 3CFX, $WO_4^{2-}$), *Methanocaldococcus jannaschii* ATCC 43067 (PDB: 3CFZ, $WO_4^{2-}$), *Pyrococcus furiosus* ATCC 43587 (PDB: 3CG1, $WO_4^{2-}$), *Archaeoglobus fulgidus* ATCC 49558 (PDB: 3CIJ, $WO_4^{2-}$) and *P. horikoshii* ATCC 700860 (PDB: 3CG3, $WO_4^{2-}$) are known, all of which bind one tungstate ion (Figure S4.5) (103).

XG196 ModA was modeled using ModA (PDB: 2H5Y) from *X. axonopodis pv. citri* 306 as the template, which has 37% sequence identity with XG196 ModA and contains molybdate as

the ligand in the crystal structure. Based on the residues invoved in molybdate binding in *X. axonopodis pv. citri* 306 ModA, Ser36, Ser63, Ala149, Val176 and Tyr194 of XG196 ModA are predicted to directly bind molybdate via hydrogen bonds (Figures 4.5 and S4.6). However, from the modeling it is not clear why the XG196 protein has increased affinity for the metal. Although archaeal and bacterial WtpA/ModA proteins are evolutionally distant, the residues involved in metal binding are partially conserved, suggesting a similar ligand binding mechanism (Figures 4.3 and S4.5). Multi-alignment analysis of the ModA proteins from *E. coli* K12, XG196, two close relatives of XG196 ModA (from *Rhodococcus qingshengii* and *Bacillus sp.* 7884-1), other *Bacillus* ModA proteins from phylogenetic analysis (Figure 4.3 and Table S4.4) and of EB-106 isolate XG77, isolated from sediments of similar depth with isolate XG196 (Figure 4.1A and 4.1B), are shown in Figure S4.7. The mean sequence identity and similarity of these ModA sequences is about 12.2% and 65.4%, respectively. The sizes of these ModA proteins are similar (about 250 residues) and their sequences are conserved at 11 out of 12 the molybdate binding residues found in *E. coli* K12 ModA (Ala34, Ala35, Ser36, Ser63, Ala82, Val147, Pro148, Ala149, Asp175, Val176 and Tyr/Phe194), the exception being position Ser/Gly/Ala62. It seems that ModA proteins are quite similar, particularly XG196 ModA and other *Bacillus* ModA proteins, and novel attributes of the XG196 protein are not obvious, especially in the deduced oxyanion binding site.

**ITC analysis of ModA proteins**

To determine their molybdate-binding properties, the genes encoding the ModA proteins from XG196, N2E2 and *E. coli* were expressed in, and the recombinant proteins were purified from, *E. coli*. ICP-MS analysis showed that XG196 ModA (40 μM) can naturally bind about 67 nM of Mo even when trace grade chemicals were used, higher than what N2E2 ModA (15 nM) and *E. coli* ModA (9 nM) can bind (Figure S4.8). After dialysis in low salt ITC buffer, all ModA proteins can pick up a little bit more Mo from the ITC buffer (XG196 ModA to 82 nM, N2E2

ModA 19 nM and *E. coli* ModA 10 nM). On average, XG196 ModA, N2E2 ModA and E. coli ModA bound 0.002, 0.0005 and 0.0003 of molybdate per protein, respectively, which are far away from being saturated. ITC analysis showed that these proteins contain a single binding site for molybdate (values were 1.10 ± 0.01, 0.95 ± 0.08 and 0.92 ± 0.01, respectively). However, the molybdate binding curves showed that XG196 ModA had a $K_D$ value for molybdate of 2.21 ± 1.03 nM, which is about one order of magnitude lower than those of N2E2 (27.0 ± 6.2 nM) and *E. coli* (25.01 ± 3.7 nM) ModA (Table 4.1, Figure S4.9). Hence, XG196 ModA has a much higher affinity for molybdate, consistent with results from the physiological study showing that XG196 is able to grow by nitrate reduction using Mo concentrations (< 1 nM) that limit the growth of other bacteria, including N2E2. The tungstate-binding affinity of XG196 ModA was about five-fold higher than that for molybdate ($K_D$ 11.15 ± 1.34 nM), and about half of the tungstate dissociation constent values for the ModA proteins of N2E2 and *E. coli* (26.6 ± 2.0 nM and 23.7 ± 0.6 nM, respectively; see Table 4.1, Figure S4.9). The stoichiometry of tungstate binding to each of these proteins was also 1:1, as found for molybdate. Hence, the lower binding affinity for molybdate than tungstate of XG196 ModA is consistent with the better growth of the organism under nitrate-reducing conditions than N2E2 when tungstate is present (Figure 4.2B).

The $K_D$ value of XG196 ModA for molybdate was extremely low (≤ 2 nM), which is only just within the confidence range of the direct ITC approach. Hence, another approach known as displacement titration analysis was used (204, 210). Chromate ($CrO_4^{2-}$) was use as the weak binding ligand. ITC analysis of XG196 ModA binding chromate gave the following results: $K_D$ = 1.56 μM ± 0.05 μM, N = 0.83 ± 0.09, and ΔH = -1.71 ± 0.26 kcal/mol. XG196 ModA saturated with chromate was then titrated with molybdate or tungstate. The results for molybdate ($K_D$ = 2.04 ± 0.19, N = 0.84 ± 0.02, ΔH = -3.76 ± 0.49 kcal/mol) and tungstate ($K_D$ = 10.6 ± 2.6, N = 0.87 ±

0.02, ΔH = -4.01 ± 0.49 kcal/mol), are similar to those obtained using ITC analysis of direct molybdate or tungstate titrations (Table 4.1).

**Gene abundance of Mo-related proteins in ORR groundwater**

To better understand the utilization of Mo in the ORR environment, the abundances of ModA genes and genes encoding representative proteins from the four families of Mo proteins were analyzed in ORR groundwater samples from both contaminated and background wells. As shown in Table 4.2, the abundance of Mo-related genes are generally higher in ORR contaminated groundwater samples. In particular, the abundance of *modA* (encoding ModA) and *napA*/*narG* (encoding dissimilatory nitrate reductase Mo-containing subunit) are significantly higher in contaminated well FW021, FW104 and FW106 (*modA* 27 to 39.9 copies per $10^8$ reads, *napA* 11.2 to 32.5 copies per $10^8$ reads and *narG* 26.4 to 42.6 copies per $10^8$ reads) than in background well FW300, FW301 and FW305 (*modA* 4.1 to 27 copies per $10^8$ reads, *napA* 1.6 to 8.9 copies per $10^8$ reads and *narG* 1.8 to 10.5 copies per $10^8$ reads). In contrast, the abundance of *nasA* (encoding assimilatory nitrate reductase Mo-containing subunit), *dmsA* (encoding DMSO reductase Mo-containing subunit), *xdhB* (xanthine oxidase/dehydrogenase) and *sorA* (encoding sulfite oxidoreductase Mo-containing subunit) were only slightly higher in contaminated wells, while the abundance of *nifK* (encoding nitrogenase) is similar in both contaminated and background wells (Table 4.2). The higher abundance of *modA*, *napA* and *narG* relative to other Mo-related protein genes in the contaminated wells is likely an adaptive advantage given the high nitrate concentrations (0.02 – 13.3 mM), which are about 1000-fold higher than in the background wells (0.1 – 1.8 μM).

## Discussion

The ORR S-3 ponds contamination plume is unique as it contains high concentrations of nitrate (up to 230 mM in groundwater) and various metals (Cd, Ni, Cu, Co, Mn, U, etc.) at low pH (~3) (126, 127). Yet, we previously showed that in this unique environment, Mo is generally limiting for microbial nitrate reduction (26). Previous studies have revealed that complex microbial communities survive in this contaminated site (211, 212). The overall goal of this research was to elucidate the molecular mechanisms that give certain microorganisms competitive advantages in these extreme habitats. *Bacillus* strain XG196 was isolated from contaminated core EB-106 that was drilled adjacent to the origin of the contamination (the S-3 ponds). XG196 was shown to grow by nitrate reduction in the presence of an exceedingly low concentration of Mo that contaminated its defined medium from the inoculum and the chemicals that make the media (to which no Mo was added). The ability to grow with limited Mo appears to be due to its molybdate-binding protein, ModA, which has a very high affinity for molybdate ($K_D$ ~ 2 nM). This is the lowest $K_D$ value yet reported for any ModA to date and it is also the first ModA characterized from a *Bacillus* strain. Previous studies have typically reported molybdate affinities with ModA proteins that are more than an order of magnitude lower (105, 108, 213, 214). A similarly high affinity but for tungstate was reported for the Wtp protein of W-dependent *P. furiosus,* a member of the archaea domain. Its binding affinity of molybdate is about five-fold lower ($K_D$ = 11 ± 5 nM) than that found here for XG196 ModA (108).

The molybdate binding affinity of *E. coli* ModA measured in this study (~25 nM) is consistent with what has been reported by others ($K_D$ = 20 - 26 nM; (104, 213)). The $K_D$ value for molybdate of N2E2 ModA is about 27 nM, consistent with the poor nitrate-reducing growth observed in Mo-limited media compared to XG196. In addition, the ModA proteins of *E. coli* and N2E2 have very similar $K_D$ values for both molybdate and tungstate, hence, neither protein is able

to distinguish between these two oxyanions, consistent with what has been reported for *E coli* ModA (104, 215). In contrast, XG196 ModA has a five-fold higher affinity for molybdate compared to tungstate, which could give the organism a selective advantage in scavenging molybdate for growth in the presence of tungstate as seen in the Mo/W competition growth studies herein (Figure 4.2).

Phylogenetic analysis showed that XG196 ModA is distinct from previously described ModA proteins, including that of *E. coli* K12 (105, 213), the WtpA/ModA proteins from the bacterium *Azotobacter vinelandii* (102), and the archaea *P. horikoshii* (103) and *P. furiosus* (108). Multi-alignment analysis indicates that XG196 ModA is quite similar to those of other *Bacillus* species based on their sequence (65.4% mean similarity) and their deduced oxyanion binding sites (Figure S4.7). However, it is hard to conclude that all of these *Bacillus* ModA proteins have molybdate affinities as high as that of XG196 ModA since the molybdate-binding residues are highly conserved. Unfortunately, modeling of XG196 ModA (Figure S4.6) did not shed light on why it has a much higher affinity for molybdate than structurally-characterized proteins. ModA proteins contain a signal peptide at the N terminus that enables the protein to be transported across the membrane. ModA signal peptides fall into one of four different groups: Sec/SPI, Sec/SPII, Tat/SPI and other (216). Surprisingly, the ModA from XG196 grouped with the ModA proteins from archaea, and these are all predicted to be lipopeptides and belong to the Sec/SPII group, while N2E2 and *E. coli* ModA proteins belong to the Sec/SPI group with non-lipopeptides (Figure 4.3). Substrate-binding lipoproteins are widely observed in gram-positive bacteria (217, 218). It is believed that the lipopeptides can tether substrate-binding proteins in order to prevent their loss into the growth environment because of the absence of the retentive outer membrane in gram-positive bacteria (217). At present, not enough information is available to distinguish “high” affinity molybdate transporters (like XG196 ModA) from “low” affinity ones (like those of N2E2

and *E. coli* ModA) based only on sequence similarity or the deduced molybdate-binding residues. Structural determinations of high affinity ModA proteins in addition to that of XG196 will be required to elucidate the molecular basis as to why these particular proteins bind molybdate so tightly.

Strain XG196 exhibited higher nitrate reductase specific activity than the other EB-106 strains XG95, XG146 and XG201 (Figure S4.1) and accumulated more Mo in its cytoplasm than XG77, XG95, XG146 and XG201 (Figure S4.10). This could be the result of the higher molybdate affinity of its ModA, which must provide more than sufficient Mo for the biosynthesis of functional pyranopterin cofactor in nitrate reductase (219) when Mo is limited in the environment. XG196 also accumulated the second highest concentration of Mo in the membrane fractions compared to the other EB-106 strains, which might be the result of a high nitrate reductase concentration in the membrane because of more than sufficient Mo taken up from environment. However, these results might not be directly related to the high affinity of ModA for molybdate. Nitrate reductases with high specific activities or high affinity molybdate storage proteins described in previous studies (185, 220) could also contribute to XG196 being able to grow robustly under nitrate reducing conditions with limited Mo. Further study is required to clarify this issue.

Mo is removed from groundwater in the ORR contaminated area but not from the non-contaminated area as a result of Fe and Al precipitation (178). The low Mo concentrations (picomolar range) in the ORR contaminated environment is unusual but not unique. Low Mo concentrations (5 - 70 nM) occur in naturally-acidic groundwater (pH 2.4 to 2.9) (164), in an acid mine drainage (< 10 nM) (165), in harbors (< 20 nM) as a result of sedimentary processes (161), and in various aquifers, including the Yorkshire Chalk aquifer (<10 nM) due to co-precipitation with or adsorption to sulfide minerals under strong reducing conditions (221). These environments have significantly lower Mo concentrations than most freshwater and open seawater systems,

which are typically > 300 nM (65). Limiting Mo concentrations in natural water systems could lead to other environmental problems, for example, by affecting critical steps in the nitrogen cycle, such as nitrate reduction, leading to nitrate accumulation or to slowing down of nitrate removal from contaminated water or soil systems.

There are several factors that affect nitrate reduction in the ORR contaminated environment besides lack of the essential metal Mo. These include the acidic conditions, high nitrate concentrations, the presence of heavy metal contaminants, and limited availability of carbon sources to serve as electron donors for nitrate reduction (26, 130, 178). Other factors, such as $O_2$ concentrations in the soil and groundwater (146, 154), temperature and denitrifier community composition (222), can also affect the efficiency of nitrate reduction. Meanwhile, the higher abundance of genes encoding the molybdate transport protein (modA) and assimilatory nitrate reductase Mo-containing subunits (*napA*/*narG*) in nitrate-contaminated wells indicates enhanced nitrate reduction in the ORR contaminated groundwater. The high abundance of *modA* could result in a greater uptake of molybdate into cells for the biosynthesis of dissimilatory nitrate reductase, enabling microorganisms to survive in the nitrate-contaminated and Mo-limited ORR environment. These numerous complex environmental factors make it difficult to study the relationships between nitrate reduction and natural microbial communities. There are therefore many unanswered questions at present that can be addressed in part by characterizing novel microbial stains with unique molecular mechanisms, as reported here for XG196 and its ModA protein. Such microorganisms could also be instrumental in developing novel methods to remove contaminating nitrate in complex waste environments.

**Conflict of Interest**

The authors declare no conflict of interest.

**Author Contributions**

XG, MT and FP designed this study, performed the experiments, analyzed and interpreted the data and MA directed the research. AD, JC and PN carried out the genome sequencing. SGD, LL, and TN performed ORR metagenome annotation and analysis. TH contributed to environmental sampling. XG wrote the manuscript and MT, FP, AD, JC, PN, SGD, PA, AA, TH and MA contributed to its revision.

**Funding**

This material by ENIGMA (Ecosystems and Networks Integrated with Genes and Molecular Assemblies) (http://enigma.lbl.gov), a Scientific Focus Area Program at Lawrence Berkeley National Laboratory, is based upon work supported by the U.S. Department of Energy, Office of Science, Office of Biological and Environmental Research, under contract number DE-AC02-05CH11231.

**Acknowledgement**

The authors wish to thank Kenneth Lowe and Dominique Joyner for their invaluable help in collecting sediment samples, John Rose for protein modeling analysis, Astrid Terry for project management and Scott Pegan and Brendan Freitas for their assistance in ITC analysis.

## Tables and Figures

A

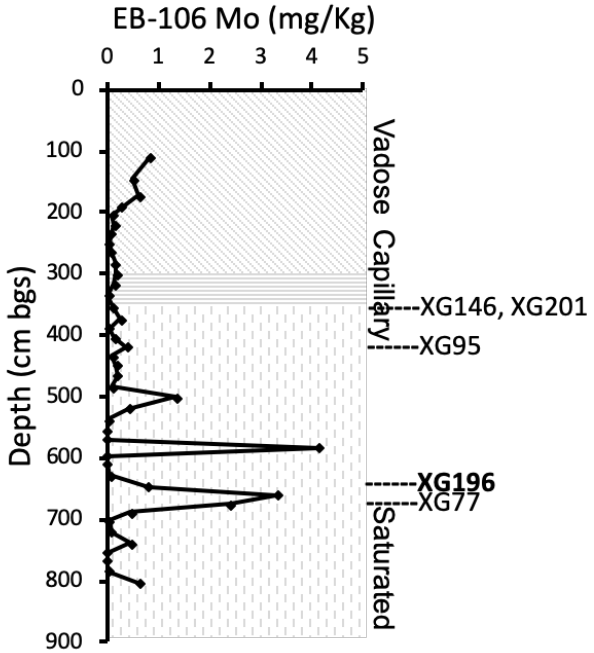


B

| Strain | Depth (cm) | Closest 16S Relative | Max $OD_{600}$ |
|---|---|---|---|
| XG146 | 373 | *Ensifer adhaerens* strain WJB133 | 0.5 |
| XG201 | 373 | *Enterobacter amnigenus* strain PY23 | 0.7 |
| XG95 | 433 | *Bacillus sp.* strain F-10 | 0.3 |
| XG196 | 661 | *Bacillus sp.* strain 30.1 | 1.5 |
| XG77 | 674 | *Bacillus cereus* strain ES103 | 0.4 |

Figure 4.1. Five EB-106 sediment isolates used in this study. (A) Sketch of core EB-106. Subsurface layers: vadose zone (diagonal), capillary zone (horizontal) and saturated zone (vertical). Each point represents average Mo concentration at different depths. Depths of EB-106 sediments where XG146, XG201, XG95, XG196 and XG77 were isolated are indicated. (B) Properties of the ORR strains. Max $OD_{600}$ was determined under nitrate reducing conditions with 20 mM carbon sources (lactate for XG196 and xylose for the other strains).

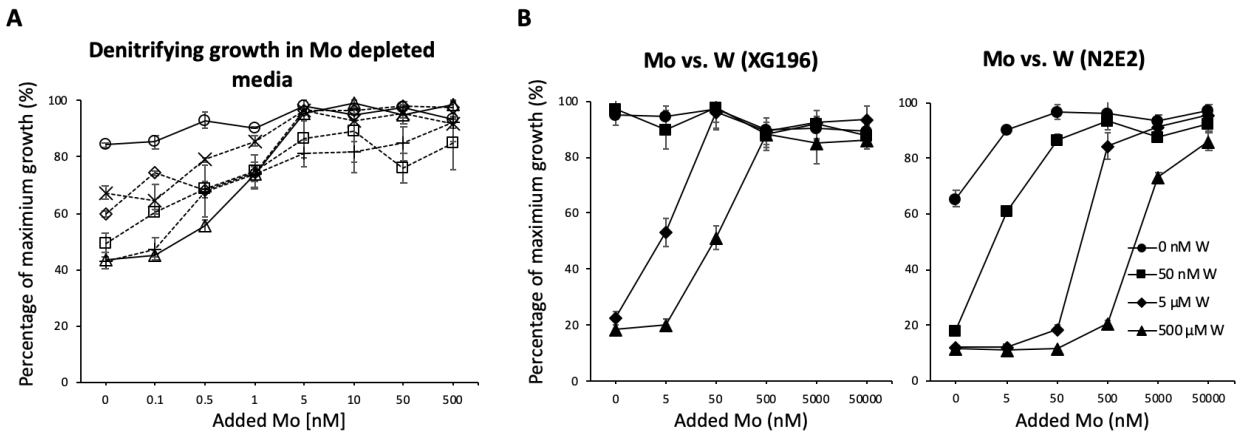


Figure 4.2. Strain XG196 is resistant to Mo limiting growth conditions. (A) Percentage of maximum growth ($OD_{600}$) of ORR strains XG196 (*Bacillus*, circle), XG77 (*Bacillus*, cross), XG201 (*Enterobacter*, diamond), XG95 (*Bacillus*, square), XG146 (*Ensifer*, plus sign) and *Pseudomonas fluorescens* N2E2 (triangle) under nitrate-reducing conditions in Mo depleted media with the indicated concentration of added Mo. (B) Percentage of maximum growth of XG196 (left) and *P. fluorescens* N2E2 (right) under nitrate reducing conditions with tungstate at the indicated concentration competing with molybdate.

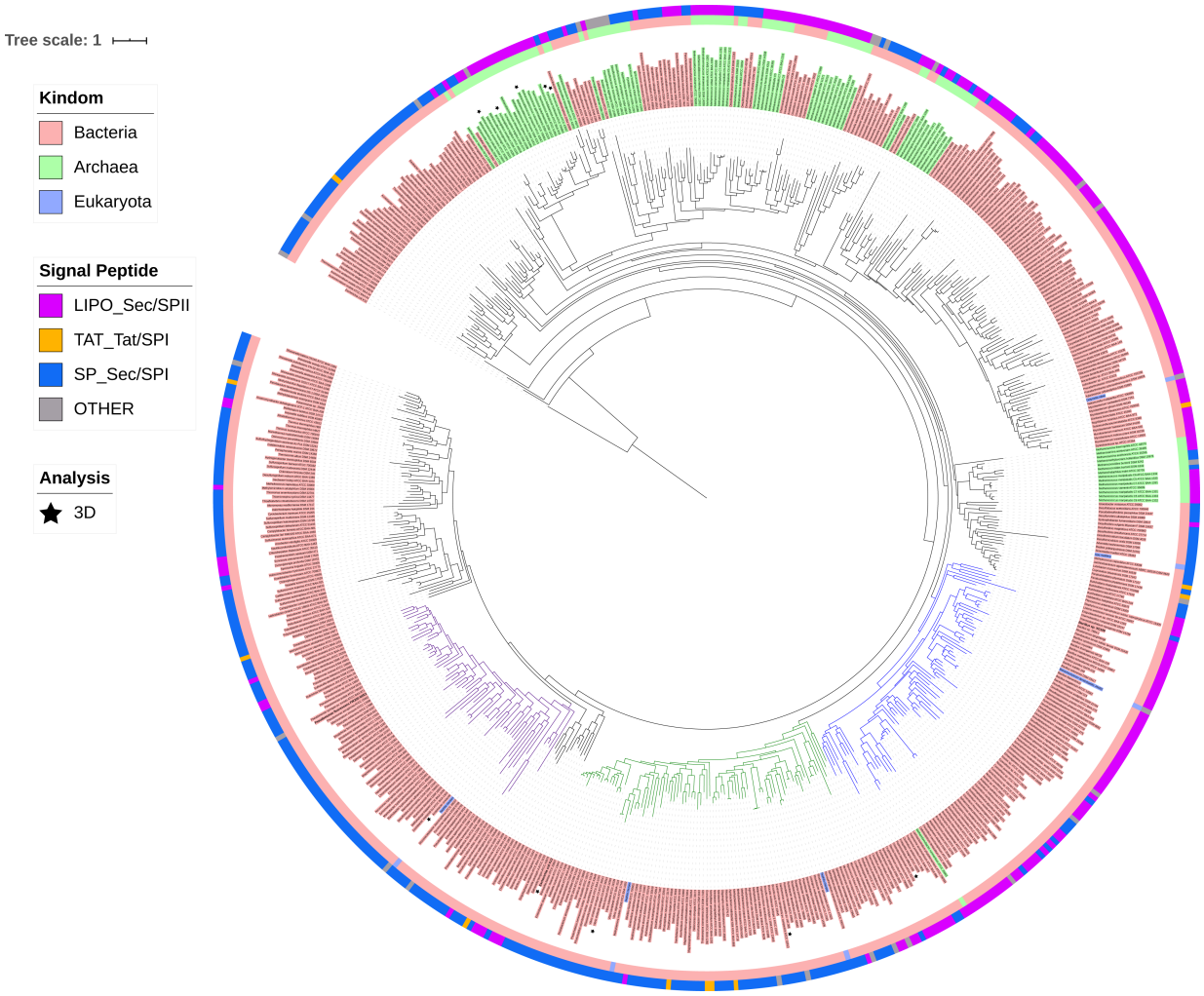


Figure 4.3. Phylogenetic analysis of ModA. Rooted phylogenetic tree of ModA and WtpA from Bacteria (pink, inner circle), Archaea (green, inner circle) and Eukaryota (blue, inner circle). Outer circle indicates different signal peptide type (LIPO_Sec/SPII in purple, TAT-Tat/SPI in yellow, SP_Sec/SPI in blue and other in grey). ModA proteins with PDB 3D structure data were indicated as black stars. Clades where XG196 ModA (blue clade), N2E2 ModA (purple clade) and Ecoli ModA (green clade) belong to were also labeled in different colors.

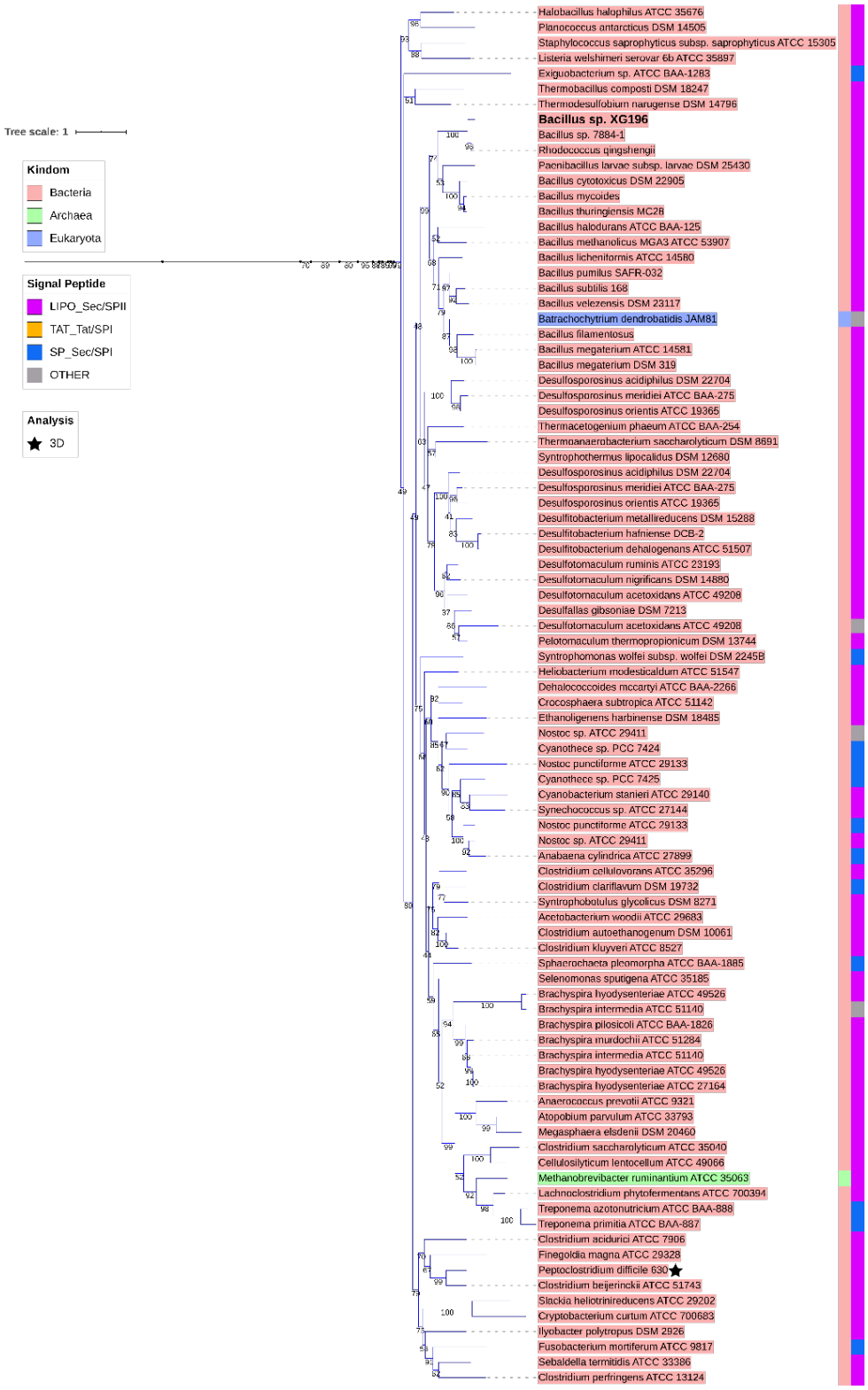


Figure 4.4. Zoomed-in clade of XG196 ModA and its close relatives. Bootstrap data are shown in the middle of each branch.

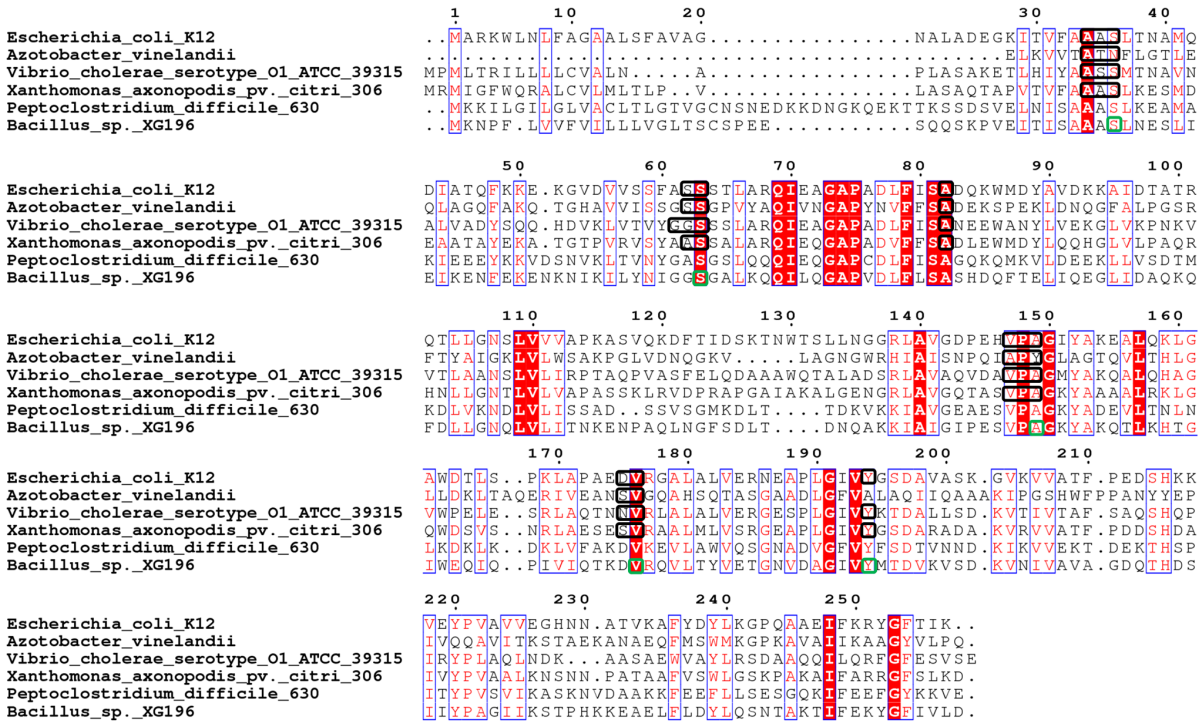


Figure 4.5. Multi-alignment analysis of ModA proteins with crystal structures. Proteins are from *Peptoclostridium difficile* 630 (ModA, UniProt Entry: Q18A64, PDB: 4KD5), *Xanthomonas axonopodis pv. citri* 306 (ModA, UniProt Entry: Q8PHA1, PDB: 2H5Y, $MoO_4^{2-}$), *Escherichia coli* K12 (ModA, UniProt Entry: P37329, PDB: 1AMF, $MoO_4^{2-}$), *Vibrio cholerae* serotype O1 ATCC 39315 (ModA, UniProt Entry: Q9KLL7, PDB:4RXL, $WO_4^{2-}$), *Azotobacter vinelandii* (ModA, UniProt Entry: Q7SIH2, PDB: 1ATG, $WO_4^{2-}$) and *Bacillus sp.* XG196. Identical residues are in white and boxed in red, while similar residues are in red and boxed in blue. Molybdate/tungstate binding residues of ModA proteins resolved by crystal structures were indicated in black squares. Molybdate binding residues of XG196 ModA identified by protein modeling using *X. axonopodis pv. citri* 306 ModA (PDB: 2H5Y) are indicated in green squares.

Table 4.1. Molybdate and tungstate binding properties of ModA proteins determined by isothermal titration calorimetry and displacement titration.

| ModA | Molybdate | | | Tungstate | | |
|---|---|---|---|---|---|---|
| | **$K_D$ (nM)** | **N[a]** | **ΔH (kcal/mol)** | **$K_D$ (nM)** | **N** | **ΔH (kcal/mol)** |
| **XG196** | 2.2±1.0 | 1.1±0.0 | -4.0±0.3 | 11.2±1.3 | 1.1±0.1 | -4.2±0.3 |
| | 2.0±0.2[b] | 0.8±0.0[b] | -3.8±0.5[b] | 10.6±2.7[b] | 0.9±0.0[b] | -4.0±0.1[b] |
| **N2E2** | 27.0±6.2 | 1.0±0.1 | -5.0±0.3 | 26.7±2.1 | 0.9±0.1 | -4.4±0.3 |
| ***E. coli*** | 25.0±3.7 | 0.9±0.0 | -5.9±0.0 | 23.8±0.6 | 0.9±0.0 | -4.9±0.2 |

[a]N=measured stoichiometry (oxyanion per protein)

[b]Data obtained by displacement titration using chromate ($CrO_4^{2-}$) as the weak binding ligand.

Table 4.2. Gene abundance of Mo-related proteins in ORR groundwater. The values represent gene copies per $10^8$ reads in samples from contaminated wells (orange) and background wells (blue). The pH and nitrate concentration of each sample is also indicated. The higher values for gene abundance and nitrate are indicated in red.

| Well | Mo Transport | DMSO Reductase Family | | | | Xanthine Oxidase Family | Sulfite Oxidase Family | Nitrogenase | pH | Nitrate (mM) |
|---|---|---|---|---|---|---|---|---|---|---|
| | *modA* | *napA* | *narG* | *nasA* | *dmsA* | *xdhB* | *sorA* | *nifK* | | |
| **DP16D** | 27 | 27 | 26.5 | 20.5 | 9.3 | 6 | 13.5 | 10.2 | 6.67 | 0.02 |
| **FW215** | 39.9 | 32.5 | 42.6 | 25.5 | 13.3 | 16.5 | 12.2 | 6.4 | 6.6 | 0.06 |
| **FW602** | 38.8 | 11.2 | 26.4 | 20 | 9.4 | 21.7 | 5.3 | 1.8 | 6.48 | 13.26 |
| **FW300** | 27 | 8.9 | 10.5 | 25.3 | 5.3 | 13.8 | 6.9 | 11.2 | 6.59 | 0.0001 |
| **FW301** | 4.1 | 1.6 | 1.8 | 4 | 0.9 | 2.4 | 0.9 | 1.6 | 6.08 | 0.0018 |
| **FW303** | 19 | 5.6 | 6.7 | 19.6 | 1.1 | 15.1 | 2.2 | 2.2 | 7.28 | 0.0015 |

**Supplemental Materials**

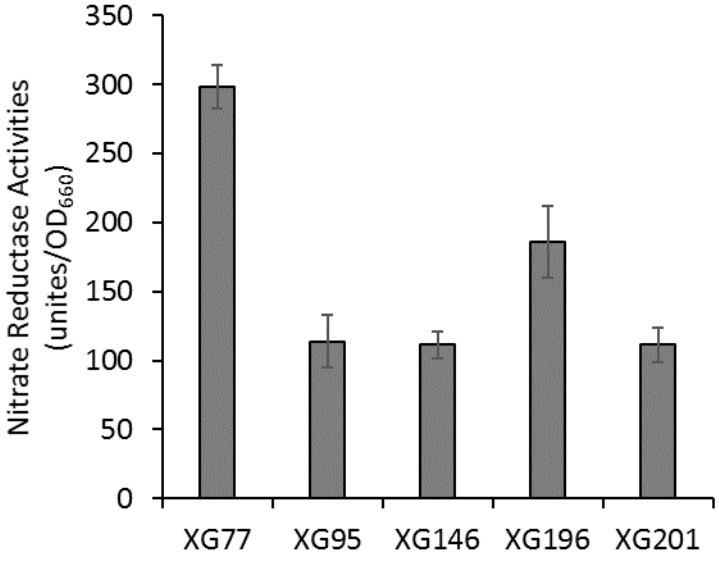


Figure S4.1. Nitrate reductase activities of EB-106 isolates.

| Strain | $Cd^{2+}$ (µM) | $Ni^{2+}$ (µM) | $Cu^{2+}$ (µM) | $Co^{2+}$ (µM) | $Mn^{2+}$ (µM) | $U^{6+}$ (µM) | Metal Mix (X) | Nitrate (mM) | Nitrite (mM) |
|---|---|---|---|---|---|---|---|---|---|
| XG77 | 43.33 | 58.14 | 70.82 | 63.72 | 99.55 | >2000 | 0.69 | 413.34 | 167.92 |
| XG146 | 27.48 | 69.53 | 3.94 | 50.55 | >900 | >2000 | 0.422 | 197.99 | 71.62 |
| XG95 | 145.72 | 74.41 | 100.35 | 52.49 | >200 | >2000 | 0.39 | 1326.13 | 354.02 |
| XG201 | 50.69 | 75.62 | 54.93 | 129.88 | >900 | >2000 | 0.59 | 478.66 | 39.84 |
| XG196 | 23.10 | 119.45 | 94.49 | 220.29 | >900 | >2000 | 1.16 | 299.15 | 99.01 |

Figure S4.2. $IC_{50}$ values for individual metals, Metal Mix, nitrate and nitrite for EB-106 strains. Gradient colors from red to green represent lower to higher values.

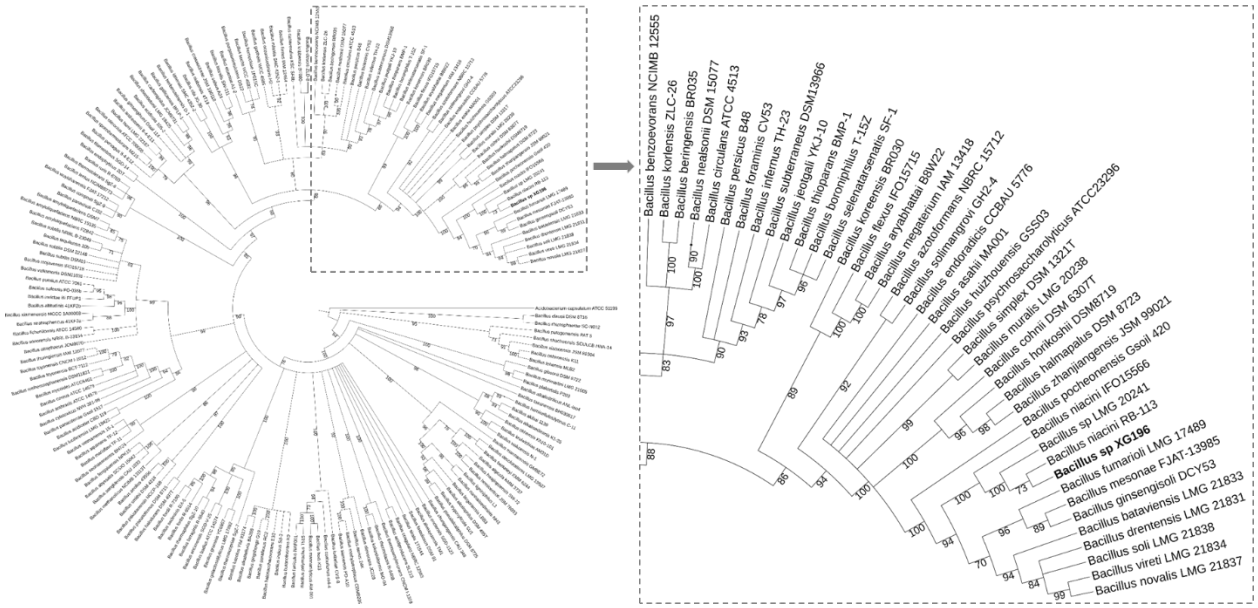


Figure S4.3. Rooted phylogenetic tree of 16S rRNA gene sequences from *Bacillus sp.* XG196 and other type *Bacillus* strains. Bootstrap data were labelled at the middle of each branch. Zoomed-in figure shows the close relatives of XG196.

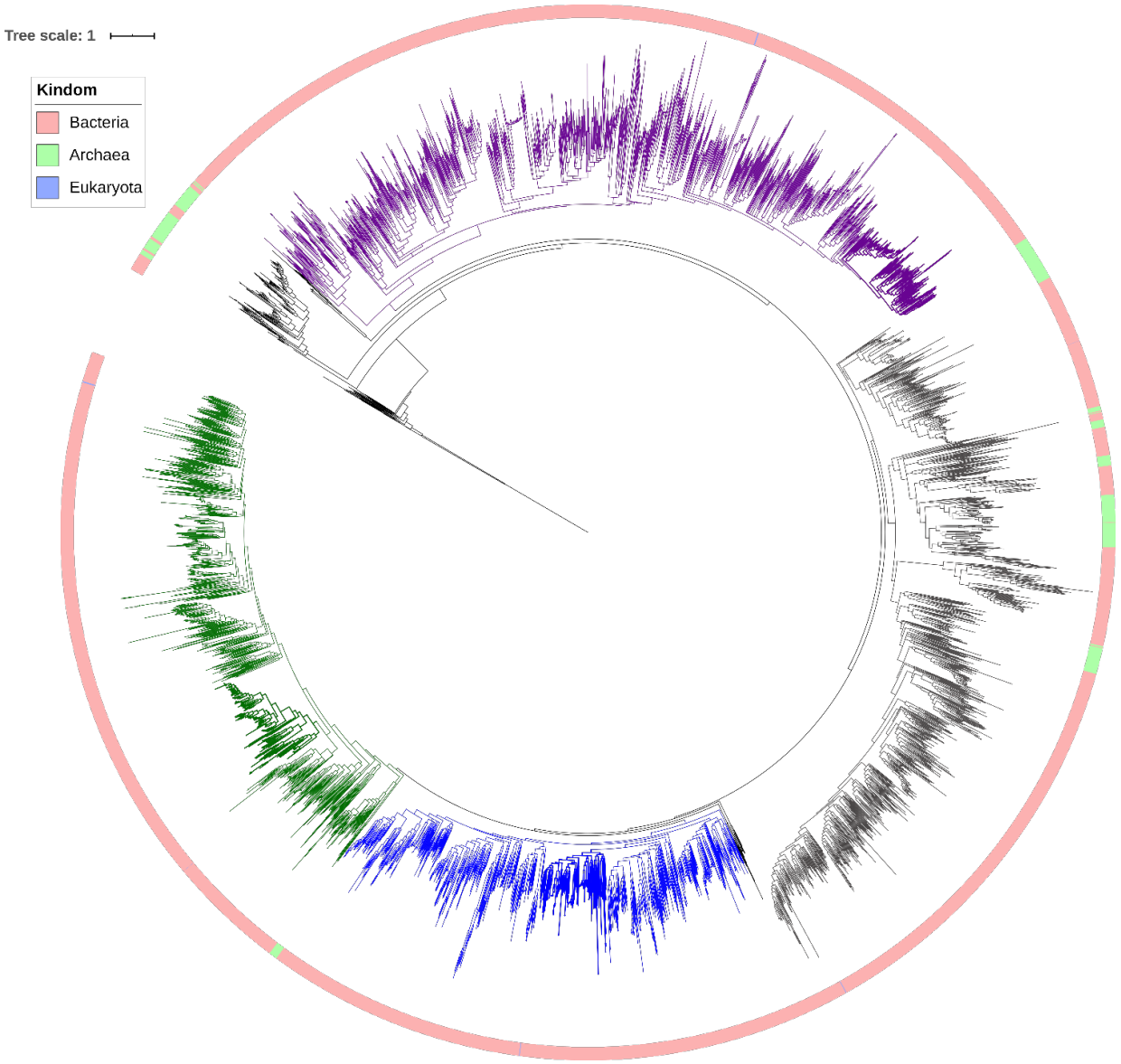


Figure S4.4. Rooted phylogenetic tree of ModA and WtpA. Proteins are from Bacteria (pink part of circle), Archaea (green part of circle) and Eukaryota (blue part of circle). Clades to which XG196 ModA (blue clade), N2E2 ModA (purple clade) and Ecoli ModA (green clade) belong are labeled in different colors.

Figure S4.5. Multi-alignment analysis of WtpA/ModA proteins with crystal structures. Proteins are from *Methanosarcina acetivorans* ATCC 35395 (WtpA/ModA, UniProt Entry: Q8TTZ5, PDB: 3CFX, $WO_4^{2-}$), *Methanocaldococcus jannaschii* ATCC 43067 (WtpA/ModA, UniProt Entry: Q58586, PDB: 3CFZ, $WO_4^{2-}$), *Pyrococcus furiosus* ATCC 43587 (WtpA/ModA, UniProt Entry: Q8U4K5, PDB: 3CG1, $WO_4^{2-}$), *Archaeoglobus fulgidus* ATCC 49558 (WtpA/ModA, UniProt Entry: O30142, PDB: 3CIJ, $WO_4^{2-}$), *Pyrococcus horikoshii* ATCC 700860 (WtpA/ModA, UniProt Entry: O57890, PDB: 3CG3), *Peptoclostridium difficile* 630 (ModA, UniProt Entry: Q18A64, PDB: 4KD5), *Xanthomonas axonopodis pv. citri* 306 (ModA, UniProt Entry: Q8PHA1, PDB: 2H5Y, $MoO_4^{2-}$), *Escherichia coli* K12 (ModA, UniProt Entry: P37329, PDB: 1AMF, $MoO_4^{2-}$), *Vibrio cholerae* serotype O1 ATCC 39315 (ModA, UniProt Entry: Q9KLL7, PDB:4RXL, $WO_4^{2-}$), *Azotobacter vinelandii* (ModA, UniProt Entry: Q7SIH2, PDB: 1ATG, $WO_4^{2-}$) and *Bacillus sp.* XG196. Secondary structure of *Pyrococcus furiosus* ATCC 43587 WtpA/ModA (UniProt Entry: Q8U4K5, PDB: 3CG1, $WO_4^{2-}$) was listed on top. Identical residues are in white and boxed in red, while similar residues are in red and boxed in blue. α- and η-helixes are displayed as squiggles, β-strands are displayed as arrows, strict β-turns are indicated by TT letters. Molybdate/tungstate binding residues of ModA/WtpA proteins resolved by crystal structures were indicated in black squares.

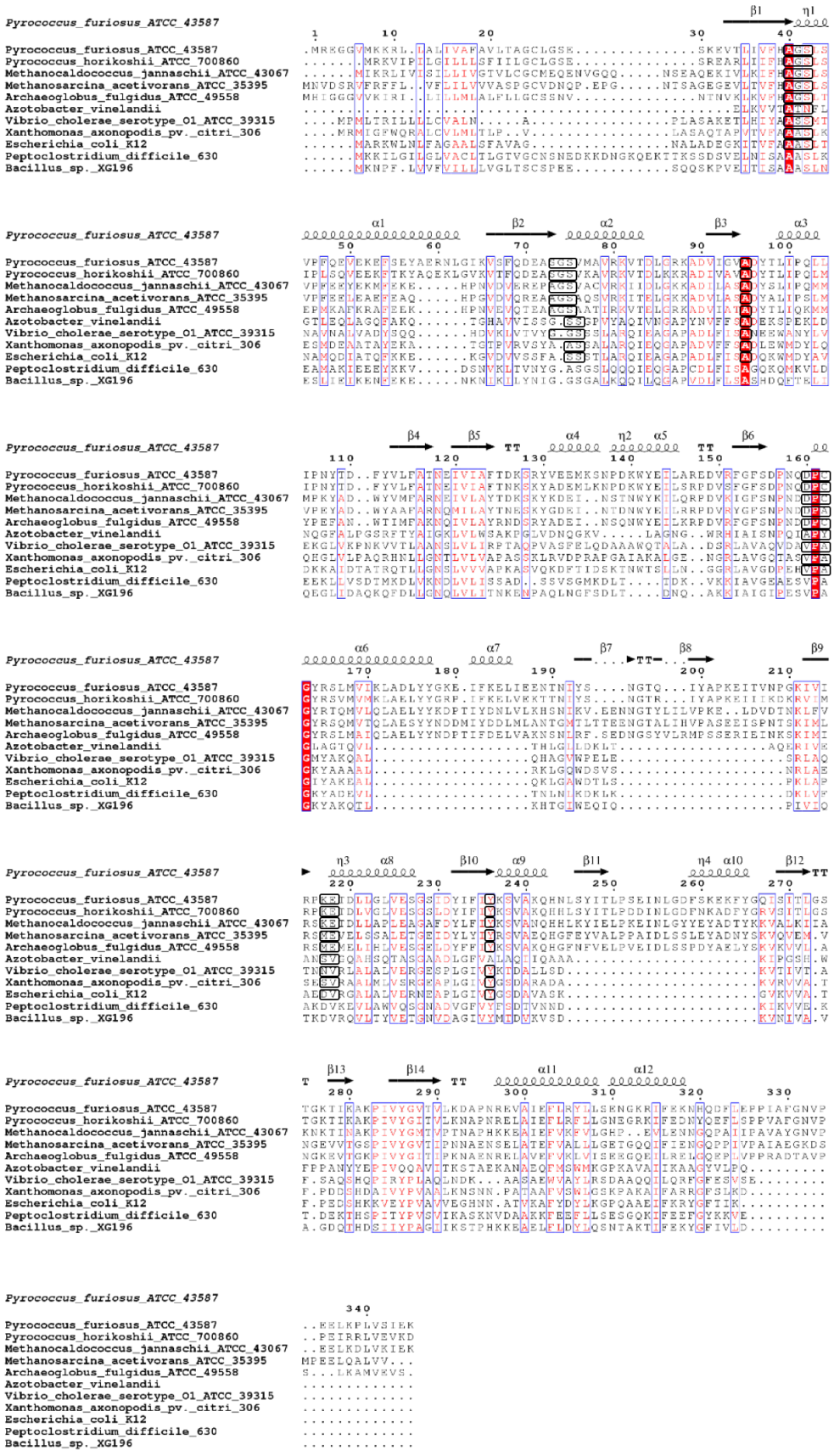
Pyrococcus_furiosus_ATCC_43587
Pyrococcus_horikoshii_ATCC_700860
Methanocaldococcus_jannaschii_ATCC_43067
Methanosarcina_acetivorans_ATCC_35395
Archaeoglobus_fulgidus_ATCC_49558
Azotobacter_vinelandii
Vibrio_cholerae_serotype_O1_ATCC_39315
Xanthomonas_axonopodis_pv._citri_306
Escherichia_coli_K12
Peptoclostridium_difficile_630
Bacillus_sp._XG196

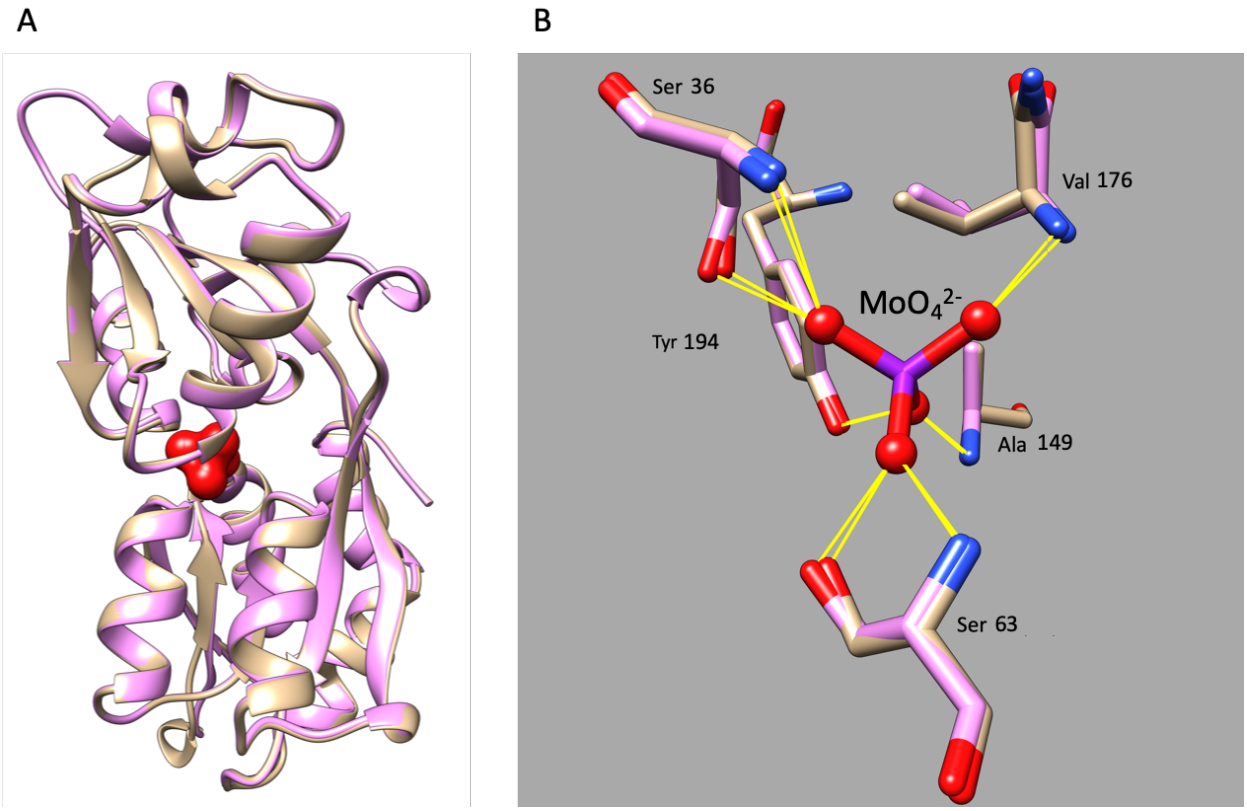


Figure S4.6. The 3D structure of XG196 ModA modelled from the Swiss Model server. Template ModA (PDB: 2H5Y) from *X. axonopodis pv. citri* 306 has a sequence identity of 36.96% with XG196 ModA. (A) The overlap of template (PDB: 2H5Y, pink) and XG196 ModA model (tan). Molybdate is labelled in red. (B) Predicted molybdate binding residues in XG196 ModA model overlapped with template ModA (PDB: 2H5Y) molybdate binding residues. XG196 ModA model residue numbers match the multi-alignment result in Figure 4.5. Predicted hydrogen bonds were indicated in yellow lines.

Figure S4.7. Multi-alignment analysis of ModA proteins from *Escherichia coli* K12, *Bacillus sp.* XG196, close relatives and selected *Bacillus* strains. Proteins are from *Escherichia coli* K12 (ModA, UniProt Entry: P37329, PDB: 1AMF, $MoO_4^{2-}$), EB-106 isolates *Bacillus sp.* XG196 and *Bacillus sp.* XG77 (genome accessible on KBase https://narrative.kbase.us/narrative/61518), two close relatives (*Rhodococcus qingshengii* and *Bacillus sp*. 7884-1) and other *Bacillus* strains from phylogenetic analysis (Figure 4.3) and listed in Table S4.4. Secondary structure of *E. coli* K12 ModA was listed on top. Identical residues are in white and boxed in red, while similar residues are in red and boxed in blue. α- and η-helixes are displayed as squiggles, β-strands are displayed as arrows, strict β-turns are indicated by TT letters. Molybdate binding residues of *E. coli* K12 ModA were indicated in black squares.

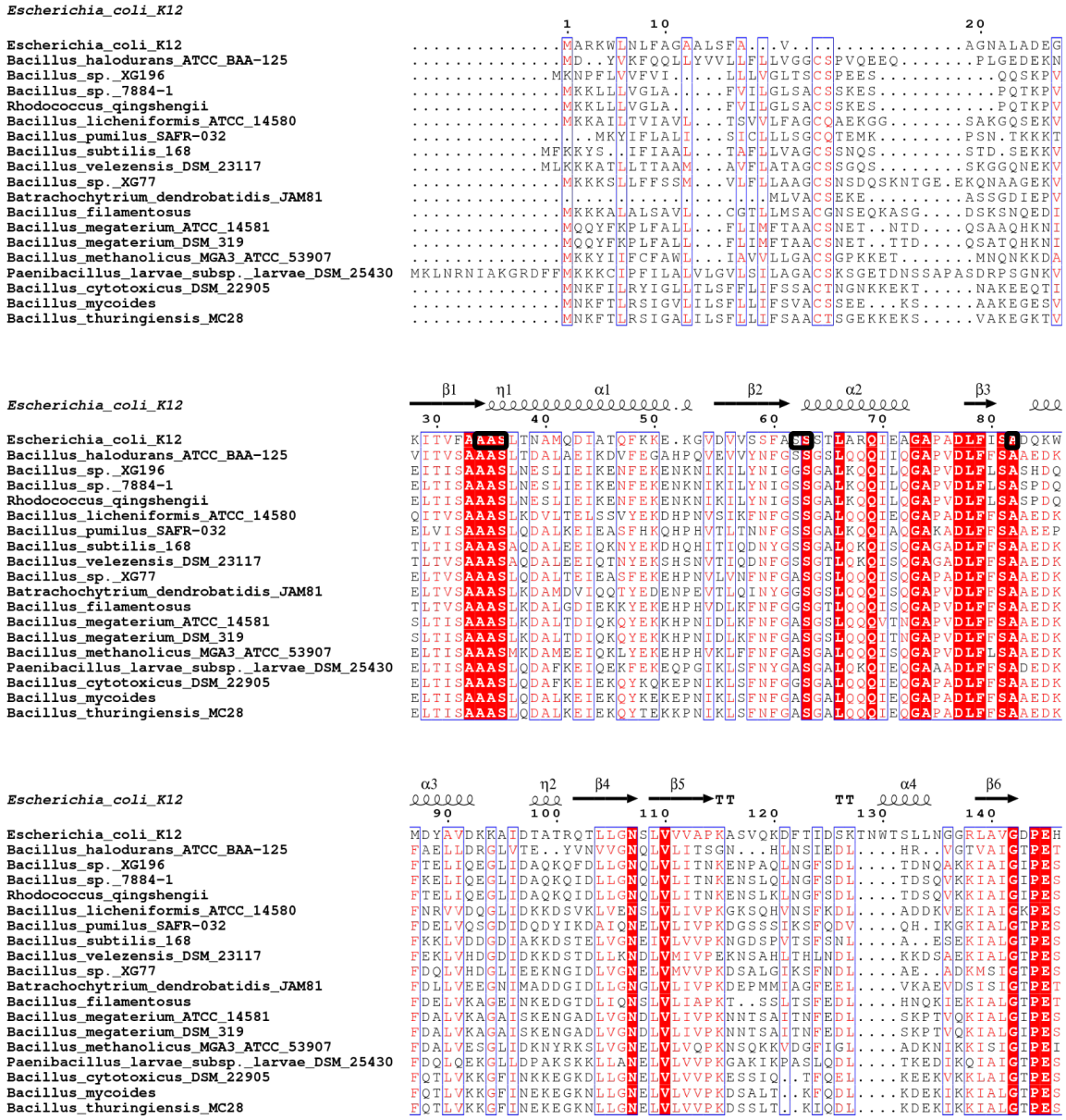
Escherichia_coli_K12
Escherichia_coli_K12
Bacillus_halodurans_ATCC_BAA-125
Bacillus_sp._XG196
Bacillus_sp._7884-1
Rhodococcus_qingshengii
Bacillus_licheniformis_ATCC_14580
Bacillus_pumilus_SAFR-032
Bacillus_subtilis_168
Bacillus_velezensis_DSM_23117
Bacillus_sp._XG77
Batrachochytrium_dendrobatidis_JAM81
Bacillus_filamentosus
Bacillus_megaterium_ATCC_14581
Bacillus_megaterium_DSM_319
Bacillus_methanolicus_MGA3_ATCC_53907
Paenibacillus_larvae_subsp._larvae_DSM_25430
Bacillus_cytotoxicus_DSM_22905
Bacillus_mycoides
Bacillus_thuringiensis_MC28
Escherichia_coli_K12
Escherichia_coli_K12
Bacillus_halodurans_ATCC_BAA-125
Bacillus_sp._XG196
Bacillus_sp._7884-1
Rhodococcus_qingshengii
Bacillus_licheniformis_ATCC_14580
Bacillus_pumilus_SAFR-032
Bacillus_subtilis_168
Bacillus_velezensis_DSM_23117
Bacillus_sp._XG77
Batrachochytrium_dendrobatidis_JAM81
Bacillus_filamentosus
Bacillus_megaterium_ATCC_14581
Bacillus_megaterium_DSM_319
Bacillus_methanolicus_MGA3_ATCC_53907
Paenibacillus_larvae_subsp._larvae_DSM_25430
Bacillus_cytotoxicus_DSM_22905
Bacillus_mycoides
Bacillus_thuringiensis_MC28
Escherichia_coli_K12
Escherichia_coli_K12
Bacillus_halodurans_ATCC_BAA-125
Bacillus_sp._XG196
Bacillus_sp._7884-1
Rhodococcus_qingshengii
Bacillus_licheniformis_ATCC_14580
Bacillus_pumilus_SAFR-032
Bacillus_subtilis_168
Bacillus_velezensis_DSM_23117
Bacillus_sp._XG77
Batrachochytrium_dendrobatidis_JAM81
Bacillus_filamentosus
Bacillus_megaterium_ATCC_14581
Bacillus_megaterium_DSM_319
Bacillus_methanolicus_MGA3_ATCC_53907
Paenibacillus_larvae_subsp._larvae_DSM_25430
Bacillus_cytotoxicus_DSM_22905
Bacillus_mycoides
Bacillus_thuringiensis_MC28

Figure S4.7. Continued

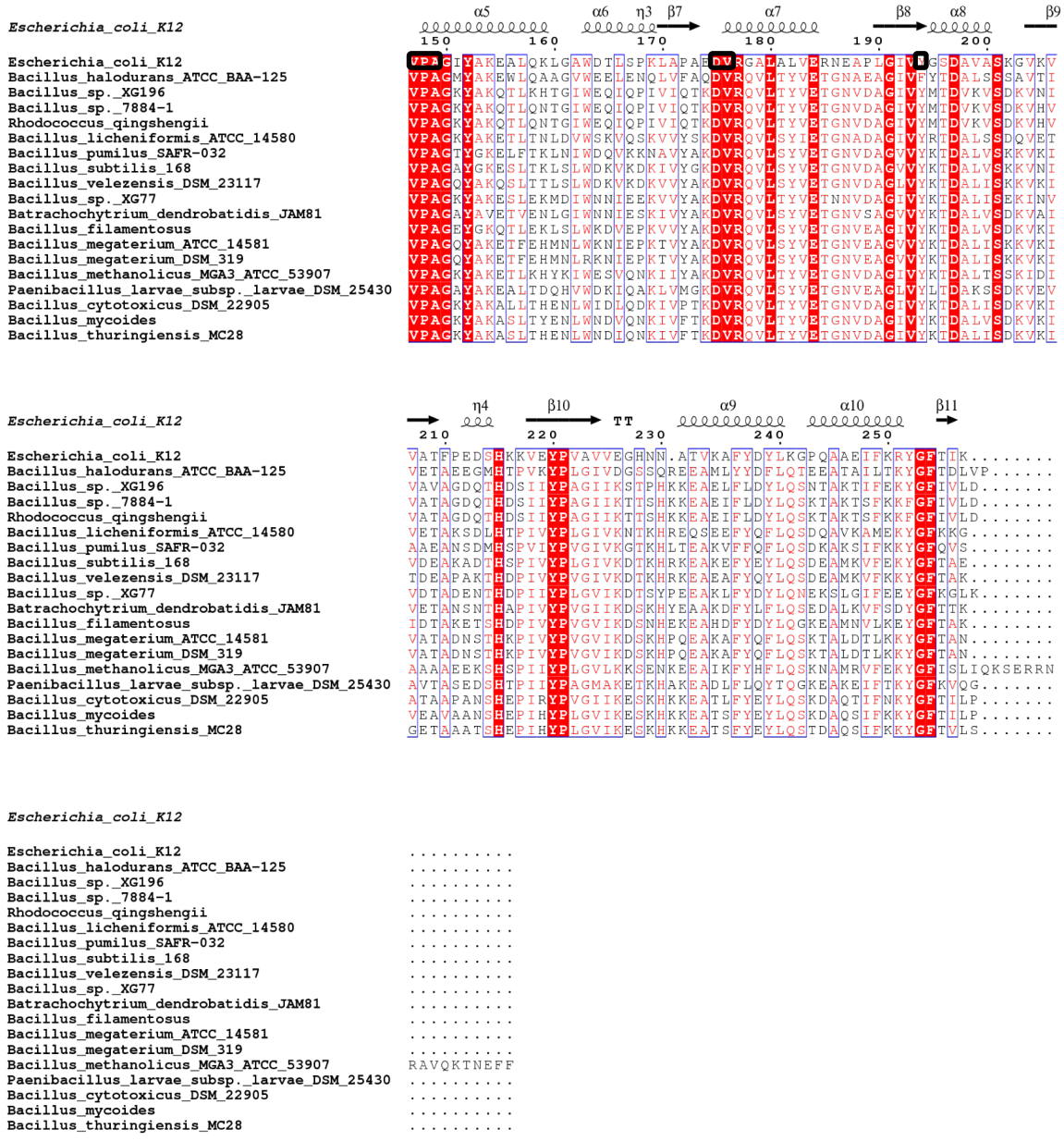

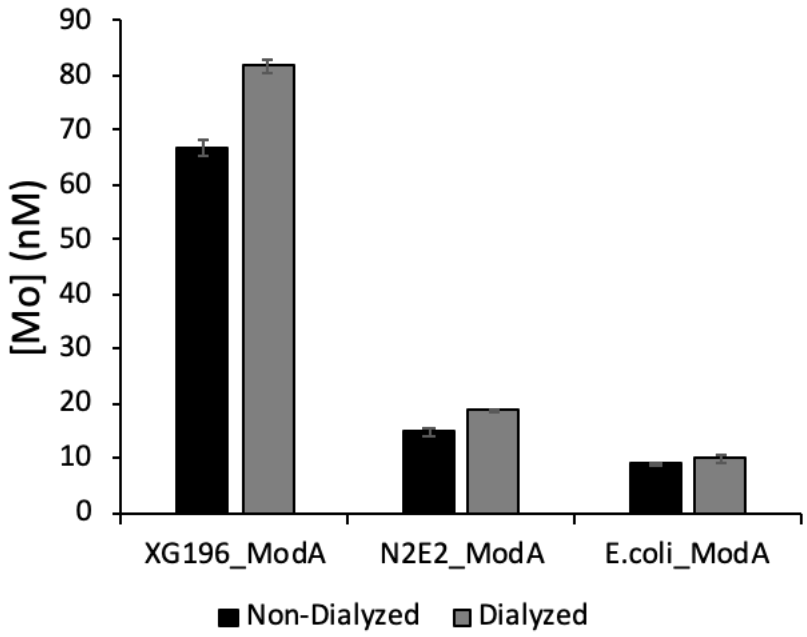


Figure S4.8. Mo accumulation in 40 μM of XG196 ModA, N2E2 ModA or *E. coli* ModA before and after dialysis.

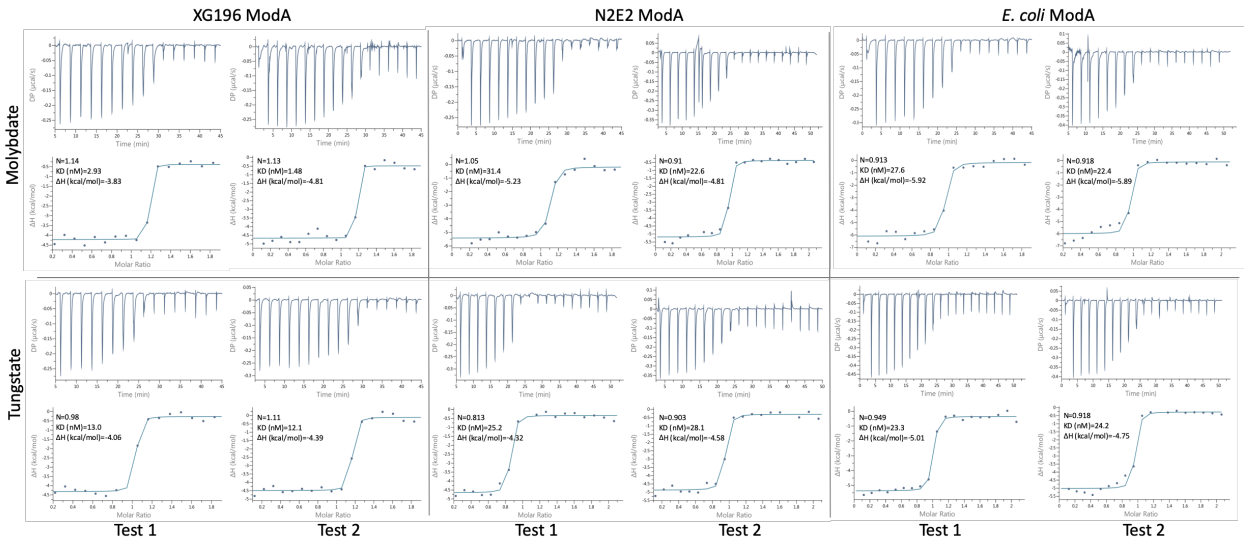


Figure S4.9. ITC profiles for the binding of molybdate or tungstate of XG196 ModA, N2E2 ModA and *E. coli* ModA.

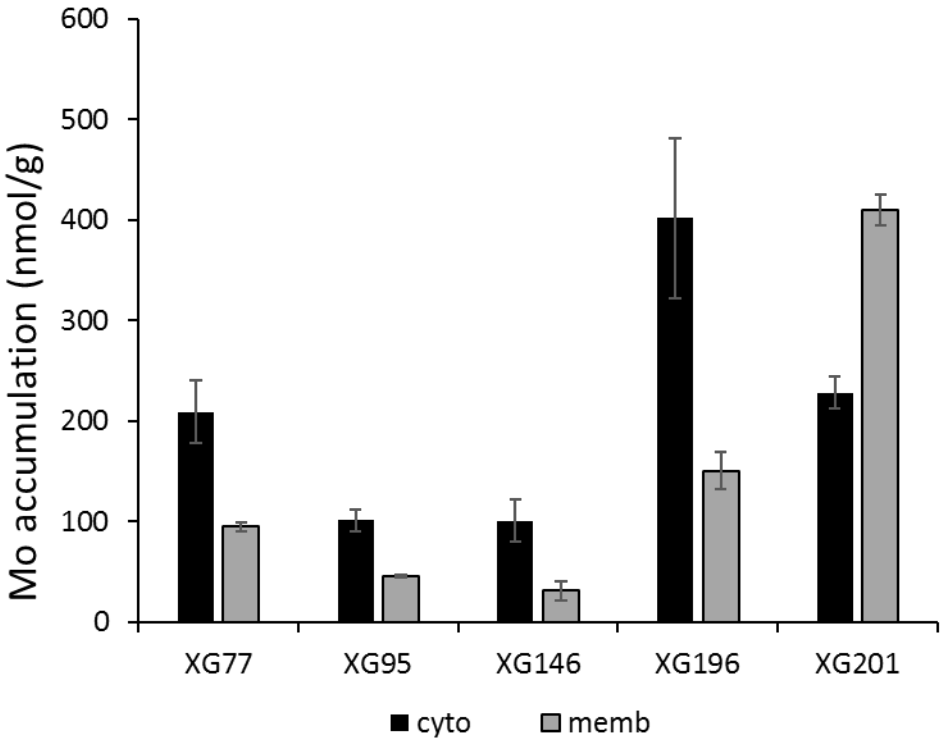


Figure S4.10. Mo accumulation in ORR isolates under anaerobic nitrate reducing growth using 1 µM molybdate.

Table S4.1. Metals used to mimic ORR contamination.

| **Metal (1×)** | **Compound added** | **Final Conc. (μM)** |
|---|---|---|
| $Mn^{2+}$ | $MnCl_2 \cdot 2H_2O$ | 100 |
| $Fe^{2+}$ | $Fe(NH_4)_2(SO_4)_2 \cdot 6H_2O$ | 10 |
| $Co^{2+}$ | $CoCl_2 \cdot 6H_2O$ | 30 |
| $Ni^{2+}$ | $NiCl_2 \cdot 6H_2O$ | 150 |
| $Cu^{2+}$ | $CuCl_2 \cdot 2H_2O$ | 10 |
| $Cd^{2+}$ | $Cd(CH_3COO)_2 \cdot 2H_2O$ | 5 |
| $U^{6+}$ | $UO_2(CH_3COO)_2 \cdot 2H_2O$ | 100 |

Table S4.2. Primers for *modA* amplification.

| Primer ID | Primer Sequence | Restriction Enzyme Site |
|---|---|---|
| XG196-modA-F | GGAATTC**CATATG**CACCACCACCACCACCACTCGCCCGAAGAATCACAAC | NdeI |
| XG196-modA-R | CAG**CTCGAG**TCAATCCAATACTATAAAGCC | XhoI |
| N2E2-modA-F | GGAATTC**CATATG**CACCACCACCACCACCACGAGGTGCAGGTGGCGGTC | NdeI |
| N2E2-modA-R | GTAT**GGATCC**TTAGCGTTGGTAACCGTAGGCTTGG | BamHI |
| Ecoli-modA-F | GGAATTC**CATATG**CACCACCACCACCACCACGAAGGGAAAATCACGGTGTTCG | NdeI |
| Ecoli-modA-R | CAG**CTCGAG**TTACTTGATTGTAAATCCGTAACGTTTAAAG | XhoI |

Table S4.3. Maximum $OD_{600}$ of EB-106 isolates grown under different conditions. Isolates were grown with 2 mM of each carbon source anaerobically with or without nitrate (20 mM).

| Carbon sources | Metabolite class | Growth of XG196 | | Growth of XG146 | | Growth of XG201 | | Growth of XG77 | | Growth of XG95 | |
|---|---|---|---|---|---|---|---|---|---|---|---|
| | | + nitrate | - nitrate | + nitrate | - nitrate | + nitrate | - nitrate | + nitrate | - nitrate | + nitrate | - nitrate |
| Formate | organic acid | - | - | - | - | - | - | - | - | - | - |
| Acetate | organic acid | 0.11 | - | 0.11 | - | - | - | - | - | - | - |
| Ethanol | alcohol | - | - | 0.1 | - | - | - | - | - | - | - |
| Lactate | organic acid | 0.33 | - | 0.17 | - | - | - | 0.15 | - | - | - |
| Succinic acid | organic acid | - | - | 0.17 | - | - | - | 0.10 | - | 0.09 | - |
| Fumarate | organic acid | 0.25 | - | 0.17 | - | - | - | 0.12 | - | 0.13 | - |
| Xylose | pentose | 0.48 | 0.13 | 0.20 | - | 0.18 | - | 0.22 | - | 0.22 | - |
| Xylitol | sugar alcohol | - | - | 0.27 | - | - | - | - | - | - | - |
| Glucose | hexose | 0.63 | 0.29 | 0.27 | - | 0.23 | 0.13 | 0.28 | - | 0.27 | - |
| Fructose | hexose | 0.48 | 0.22 | 0.25 | - | 0.23 | 0.12 | 0.25 | - | 0.27 | - |
| Maltose | dihexose | 0.95 | 0.15 | 0.37 | - | 0.38 | 0.11 | 0.20 | - | 0.18 | - |
| Benzoate | aromatic compounds | - | - | - | - | - | - | - | - | - | - |
| 4-hydroxybenzoate | aromatic compounds | - | - | - | - | - | - | - | - | - | - |
| Tartrate | aromatic compounds | - | - | 0.15 | - | - | - | - | - | - | - |
| Proline | amino acid | 0.47 | 0.08 | 0.19 | - | - | - | 0.10 | - | 0.14 | - |
| Phenylalanine | amino acid | - | - | - | - | - | - | - | - | - | - |
| Arginine | amino acid | 0.29 | - | 0.19 | - | - | - | - | - | 0.14 | - |
| Threonine | amino acid | - | - | 0.15 | - | - | - | - | - | - | - |
| Leucine | amino acid | - | - | - | - | - | - | - | - | - | - |
| Glutamate | amino acid | 0.47 | 0.11 | 0.19 | - | - | - | 0.09 | - | 0.08 | - |
| Glutamine | amino acid | 0.08 | - | 0.2 | - | - | - | 0.09 | - | 0.15 | - |

* -, no growth ($OD_{600max} \leq 0.07$)

Table S4.4. ModA proteins in ModA tree closely related to XG196 ModA.

| UniProt Entry | ModA Origin Strain | % Identity | Alignment Length | E Value | Bit Score | % positives | Origin/type* |
|---|---|---|---|---|---|---|---|
| A0A4R6A6K9 | *Rhodococcus qingshengii* | 85.938 | 256 | 3.92E-164 | 446 | 93.75 | Soil* |
| A0A268JZS1 | *Bacillus sp.* 7884-1 | 85.938 | 256 | 8.91E-164 | 444 | 93.36 | Unknown |
| I3E8R5 | *Bacillus methanolicus* MGA3 ATCC 53907 | 52.652 | 264 | 1.74E-94 | 270 | 71.21 | Soil (223) |
| C2PQ60 | *Bacillus mycoides* | 52.344 | 256 | 5.41E-93 | 265 | 71.88 | Soil** |
| A7GKA9 | *Bacillus cytotoxicus* DSM22905 | 50.373 | 268 | 9.43E-92 | 263 | 69.4 | Food-borne pathogen (224) |
| K0FWH0 | *Bacillus thuringiensis* MC28 | 51.55 | 258 | 4.89E-91 | 261 | 70.16 | Forest (225) |
| A0A0B6AUR2 | *Bacillus megaterium* ATCC14581 | 48.473 | 262 | 6.41E-90 | 258 | 67.94 | Soil ** |
| D5DNA1 | *Bacillus megaterium* DSM319 | 48.473 | 262 | 3.04E-88 | 253 | 67.56 | Soil*** |
| V9W849 | *Paenibacillus larvae subsp. larvae* DSM25430 | 50.936 | 267 | 9.43E-88 | 253 | 64.04 | Honey bee pathogen (226) |
| A7Z8Q5 | *Bacillus velezensis* DSM23117 | 50.202 | 247 | 1.01E-87 | 252 | 68.42 | Soil* |
| Q65LK2 | *Bacillus licheniformis* ATCC14580 | 49.042 | 261 | 4.54E-87 | 250 | 65.52 | Soil* |
| A0A1X7EDU8 | *Bacillus filamentosus* | 46.591 | 264 | 2.55E-84 | 243 | 67.42 | Sediment* |
| O32208 | *Bacillus subtilis* 168 | 48.016 | 252 | 6.04E-84 | 242 | 68.25 | Lab mutant(227, 228) |
| F4PF01 | *Batrachochytrium dendrobatidis* JAM81 | 50.413 | 242 | 6.34E-84 | 242 | 67.36 | Frog**** |
| A8FHD9 | *Bacillus pumilus* SAFR-032 | 48.846 | 260 | 1.42E-80 | 234 | 63.46 | Spacecraft assembly clean room (229) |
| Q9K7N2 | *Bacillus halodurans* ATCCBAA-125 | 47.107 | 242 | 6.80E-74 | 217 | 66.94 | Soil* |

*Information from https://bacdive.dsmz.de/
** Information from https://microbewiki.kenyon.edu/index.php/MicrobeWiki
*** Information from http://bacmap.wishartlab.com/organisms/1082
**** Eukaryota, information from https://mycocosm.jgi.doe.gov/Batde5/Batde5.home.html

Table S4.5. Properties of characterized ModA proteins.

| **Proteins** | **AA (Putative signal peptide removed)** | **MW (Da) with $His_6$** | **Putative lipoprotein-attachment site** |
|---|---|---|---|
| XG196 ModA | 21-260 (240 AA) | 27233.86 | Cys20 |
| N2E2 ModA | 24-250 (227 AA) | 24890.04 | none |
| *E. coli* ModA | 26-257 (232 AA) | 25624.07 | none |

# CHAPTER 5

## EFFECTS OF ESSENTIAL AND TOXIC METALS ON NITRATE AND NITROUS OXIDE METABOLISM BY KEY ORR STRAINS[4]

[4]Xiaoxuan Ge, Michael P. Thorgersen, Farris L. Poole II, James Wilson, Jake Valenzuela, Nitin Baliga, Adam P. Arkin, and Michael W. W. Adams. To be submitted to *Applied and Environmental Microbiology*.

**Abstract**

Nitrous oxide ($N_2O$) is an important greenhouse gas that can be produced by biotic (nitrification, denitrification) and abiotic (chemodenitrification) mechanisms in nature. Anthropogenic activities such as fertilizer usage in agriculture as well as nitrate contamination contribute largely to $N_2O$ emissions. $N_2O$ has been detected in the contaminated area at ORR, which is an acidic area containing high levels of nitrate and various types of metals. In order to investigate the effects of essential (molybdenum, Mo) and toxic metals (Cu, Ni, Co, Cd and U) on nitrate and nitrous oxide metabolism in complex ORR microbial communities, ORR isolates *Rhodanobacter* R12 and *Acidovorax* 3H11 were selected to form a synthetic nitrate-reducing community. The co-culture can decrease the amounts of both nitrite and $N_2O$ that accumulate compared with a culture of either R12 or 3H11 alone. Mo addition did not show any significant effects on the nitrate-reducing growth of R12, 3H11 or the co-culture as more than sufficient Mo was present in the growth media as a contaminant. A mixture of metals at concentrations that mimic the ORR contaminated environment inhibit the growth of R12 and of the co-culture under nitrate reducing conditions, although 3H11 was unaffected. Ni is proposed to play the most important role in growth inhibition as its determined inhibition constant value ($IC_{50}$) was comparable to environmental concentrations whereas the values for other metals (Cu, Cd, Co and U) were much higher than the concentrations found in contaminated groundwater.

## Introduction

Nitrous oxide ($N_2O$) is a greenhouse gas, the global warming potential is about 300 times higher than carbon dioxide over a 100 year time period (132, 133). $N_2O$ also contributes to stratospheric ozone destruction (132, 133). Figure 5.1 shows the main pathways of $N_2O$ production: nitrification, denitrification and chemodenitrification (230, 231). $N_2O$ is produced by reduction of nitrite under anoxic conditions by denitrification or by nitrification in presence of $O_2$ when $NH_4^+$ present (134, 135). In chemodenitrification, reactive N intermediates like $NH_2OH$ and $NO_2^-$ produced in nitrogen cycle pathways may engage in direct chemical reactions that yield $N_2O$, especially in the presence of $Fe^{2+}/Fe^{3+}$, $Cu^{2+}$, $Mn^{2+}$, organic matter or at acidic pH ($\leq 5$) (134, 136, 137). However, it was estimated that abiotic $N_2O$ production contributes less than 3% of total $N_2O$ production, while biotic $N_2O$ production contributes about 97% to total $N_2O$ emissions in typical nitration reactor systems (pH 6.5 to 8) (134). Other side pathways like the DNRA pathway that produce nitrite and $NH_3/NH_4^+$, can also contribute to $N_2O$ production (231). About 50% of global anthropogenic $N_2O$ emissions is from the microbial processes of nitrification and denitrification in agriculture (132).

Nitrate is a main contaminant (up to 230 mM) in the acidic contaminated area at ORR. This area is also contaminated by various metals, including uranium (up to 580 μM), aluminum (up to 20709 μM), manganese (up to 3150 μM), nickel (up to 157 μM), cobalt (up to 30 μM), cadmium (up to 10 μM), copper (up to 15 μM), chromium (up to 11 μM), lead (up to 0.5 μM) and thorium (up to 8 μM) (26, 130). The emission of $N_2O$ was measured in the contaminated area at ORR (as high as 1.2 mg/L) (131).

In this work, ORR strains *Rhodanobacter* R12 and *Acidovorax* 3H11 were selected to generate a synthetic nitrate-reducing community in order to investigate the effects of ORR-related metals on nitrate-reducing growth and $N_2O$ production. *Rhodanobacter* was the most abundant

genus in ORR environment and can reduce nitrate at low pH (< 4) (232) while *Acidovorax* was found in all contaminated sites, and was one of the dominant species in high nitrate sites in ORR (150). The genes encoding nitrous oxide reductase (NosZ) and nitrite reductase (NirK/NirS) were not found in the draft genomes of ORR strains R12 and 3H11, respectively (Figure 5.2), and whether they are present in the complete genomes is not known. We investigated the effects of the ORR-related metals Mo, U, Cd, Mn, Co and Cu on microbial $N_2O$ production. Mo is essential for environmental nitrate reduction as it is a cofactor for nitrate reductase (68) while U, Cd, Mn, Co, Cu are present in unusually high concentrations in the ORR contaminated area (26). The following questions were addressed in this study: 1) Does increased Mo availability increase $NO_2^-$ and $N_2O$ production by R12? 2) Do environmentally-relevant concentrations of toxic metals inhibit nitrate-reducing growth of R12, 3H11, and R12/3H11 co-cultures? 3) Do environmentally-relevant concentrations of toxic metals inhibit biotic $N_2O$ production and consumption by R12, 3H11, and R12/3H11 co-cultures?

## Results

### Effects of Mo and toxic ORR metals on the nitrate reducing growth of R12, 3H11 and R12/3H11 co-culture

In order to investigate the effects of Mo on the nitrate reducing growth of *Rhodanobacter* R12, *Acidovorax* 3H11 and R12/3H11 co-culture, all strains were inoculated in the medium described by Widdel and Bak (171) except that Mo was omitted. In this medium, acetate is the carbon source and energy is obtained by nitrate reduction. As shown in Figure 5.3, the growth of R12, 3H11 and the co-culture did not show significant differences if Mo was added or not. This indicates that more than sufficient Mo is already present in the media as a contaminating metal to support nitrate reduction as carried out by the nitrate reductases in these two organisms, which use Mo as cofactor.

Potentially toxic metals were also tested on the growth of R12, 3H11 and the co-culture under nitrate reducing conditions. As shown in Figure 5.4, the ORR metal mixture (MM) contains $Cu^{2+}$ (10 μM), $Cd^{2+}$ (5 μM), $Co^{2+}$ (30 μM), $Ni^{2+}$ (150 μM), $U^{6+}$ (100 μM), $Fe^{2+}$ (10 μM) and $Mn^{2+}$ (100 μM) at concentrations found in the most contaminated ORR well FW126 (Table S4.1, (26)) can inhibit the nitrate reducing growth of R12, 3H11 and R12/3H11 co-culture as shown in Figure 5.4 with $IC_{50}$ values of 0.4×, 0.6× and 0.5×, respectively (Table 5.1). 0.25× of MM can inhibit R12 growth by about 60%. MM can extend the log phase of 3H11 growth under lab conditions but did not affect the final cell density significantly. MM can affect the nitrate reducing growth of R12/3H11 co-culture growth significantly; 0.5× MM inhibits the co-culture growth by about 38% while 1× MM inhibits its growth by about 57%.

$Cu^{2+}$, $Cd^{2+}$, $Co^{2+}$ and $Ni^{2+}$ inhibited the nitrate-reducing growth of the R12/3H11 cocultures, affecting both growth rates and final cell densities, as shown in Figure 5.5. The $IC_{50}$ values were 47.0 μM, 37.8 μM, 72.3 μM and 67.6 μM, respectively (Table 5.1). $U^{6+}$ did not show

inhibition ($IC_{50}$ > 500 μM). $Cd^{2+}$ has the lowest $IC_{50}$ of 18.4 μM for the R12/3H11 co-culture, which compares with only 5 μM $Cd^{2+}$ detected in the ORR environment (well FW126) so growth inhibition is minimal at these concentrations. ORR environmental concentrations of $Cu^{2+}$ (10 μM) and $Co^{2+}$ (30 μM) do not inhibit the nitrate-reducing growth of the co-culture but $Ni^{2+}$ is present in the ORR contaminated well FW126 at 125 μM and this inhibits growth of the co-culture by about 45%.

$Cu^{2+}$, $Cd^{2+}$ and $Ni^{2+}$ inhibited R12 growth in terms of growth rate and final cell density with $IC_{50}$ values of 75.8 μM, 16.9 μM and 114.9 μM, respectively (Table 5.1), while $Co^{2+}$ ($IC_{50}$ > 200 μM) and $U^{6+}$ ($IC_{50}$ > 500 μM) did not inhibit growth of R12 at tested concentrations. $Cd^{2+}$ has the lowest $IC_{50}$ (16.9 μM) and is the most toxic among these five metals tested. However, the highest concentration of $Cd^{2+}$ detected in the most contaminated well (FW126) in ORR is about 5 μM, which inhibited the growth of R12 by only about 12% under lab conditions (Figure 5.6A). The highest concentrations of $Cu^{2+}$ and $Ni^{2+}$ detected in well FW126 are about 10 μM and 150 μM, respectively, which inhibited R12 growth by about 26% and 100%, respectively (Table S4.1 and Figure 5.6A). Therefore, ORR environmental levels of $Cu^{2+}$ and $Ni^{2+}$ may play a major role in inhibiting the growth of the nitrate reducing bacterium R12 in the contaminated area at ORR.

$Cu^{2+}$, $Cd^{2+}$, $Co^{2+}$ and $Ni^{2+}$ also inhibited the nitrate-dependent growth in terms of growth rates and maximum cell densities of *Acidovorax* 3H11with $IC_{50}$ values of 77.2 μM, 18.4 μM, 53.7 μM and 26.3 μM, respectively (Figure 5.7 and Table 5.1). However, $U^{6+}$ ($IC_{50}$>500 μM) did not show significant inhibition on 3H11. $Cd^{2+}$ is the most toxic metal among these five metals for 3H11 with the lowest $IC_{50}$ (18.4 μM). Under environmental concentrations of $Cd^{2+}$, $Cu^{2+}$, $Ni^{2+}$ and $Co^{2+}$ as detected in the highly contaminated well FW126 (26), the growth of 3H11 was inhibited 23%, 6%, 23% and 11%, respectively (Table S4.1 and Figure 5.7A). ORR environmental concentrations of $Cd^{2+}$ and $Ni^{2+}$ therefore inhibit the nitrate reducing growth of 3H11 significantly.

**Effects of toxic ORR metals on nitrate consumption and nitrite and $N_2O$ production of R12, 3H11 and the co-culture**

To investigate the effects of ORR metals on the nitrate reduction, nitrite and $N_2O$ production by R12, 3H11 and the R12/3H11 co-culture, nitrate, nitrite and $N_2O$ were quantified at the end point (240 h) of cell growth. In terms of a combination of metals as the ORR MM, as shown in Figure 5.4, when R12 was grown with increasing concentrations, higher concentrations of nitrate and decreased amounts of $N_2O$ were detected. 30 to 45 μmoles of nitrogen was mainly detected as nitrate or $N_2O$, 15 to 30 μmoles of nitrogen was not recovered and must be released as another product (NO or $N_2$, as described above). Increased concentrations of MM didn't affect nitrite or $N_2O$ production of 3H11. About 50 μmoles of nitrate nitrogen was reduced to nitrite nitrogen and about 10 μmoles was detected as $N_2O$ in 3H11 with MM. Co-culture reduced nitrate and nitrite more efficiently than R12 or 3H11 single cultures. Less than 10 μmoles of nitrogen were detected in the form of nitrate, nitrite or $N_2O$ when up to 0.25× MM was added to the co-culture, about 50 μmoles of nitrogen were detected mainly in form of nitrite, with some $N_2O$ as well, when the co-culture grew with between 0.5× to 1.2× MM. No nitrite detected in R12 cultures meanwhile no nitrate remained in 3H11 cultures, indicating R12 and 3H11 have high-efficient nitrite reductase and nitrate reductase, respectively, which contribute to the efficient nitrate and nitrite reduction in R12/3H11 co-culture.

Low concentrations of nitrate, nitrite or $N_2O$ were detected in R12/3H11 cocultures when grown with no ORR metals, low concentrations of $Cu^{2+}$ (5 and 10 μM), $Cd^{2+}$ (5, 20 and 40 μM), $Co^{2+}$ (30 μM), $Ni^{2+}$ (25 and 50 μM) or $U^{6+}$ (as high as 1000 μM). High concentrations of $Cu^{2+}$ (50, 100 and 150 μM), $Co^{2+}$ (60, 100, 150 and 200 μM) inhibited nitrate reduction significantly, indicating their repression on nitrate reductases of R12 and 3H11. High levels of $Cd^{2+}$ (60 and 100 μM), $Ni^{2+}$ (100, 125 and 150 μM) inhibited nitrite reduction significantly, indicating they may

inhibit the nitrite reductase activities of R12 and/or 3H11. However, various concentrations of five tested metals did not have any effect on low $N_2O$ accumulation of co-culture (Figure 5.5).

As shown in Figure 5.6B, 40 μmoles out of 60 μmoles of nitrogen were recovered when R12 was inoculated with no metal, where 30 μmoles were reduced to $N_2O$, about 10 μmoles remained as nitrate, while no nitrite was detected. Concentrations of $Cu^{2+}$ above 5 μM inhibited nitrate reduction in R12 significantly and also reduced $N_2O$ production. $Cd^{2+}$ (above 5 μM) inhibits nitrate reduction of R12 but did not affect $N_2O$ production. $Co^{2+}$ (above 30 μM) did not have much effect on nitrate reduction of R12 but there was an accumulation of about 10 μmoles of nitrogen (from 60 μmoles of nitrate) as $N_2O$ compared with the no metal added control. High concentrations of $Ni^{2+}$ (more than 100 μM) inhibited nitrate reduction significantly, while Ni increased nitrate reduction at low concentration (25 μM). 30 μmoles of nitrogen was detected as nitrite (from 60 μmoles of nitrate) when R12 was incubated with 100 μM $Ni^{2+}$, indicating more than 100 μM $Ni^{2+}$ can inhibit nitrite reductase activity of R12. $U^{6+}$ at the concentrations used (up to 0.1 mM) did not have much effect on nitrate reductions or $N_2O$ accumulation by R12. Between 5 and 30 μmoles of nitrogen was missing in R12 cultures depending on the concentration of the ORR metal that was present. This might be released as $N_2$ or as NO by an uncharacterized nitrous oxide reductase (NosZ). Neither of these compounds were measured in these experiments.

As shown in Figure 5.7B, 60 μmoles of nitrate nitrogen was reduced to 30 μmoles of nitrogen as nitrite and about 30 μmoles of nitrogen as $N_2O$ when 3H11 was inoculated with no ORR metals. Increased concentrations of $Cu^{2+}$ (between 5 to 50 μM) resulted in higher accumulation of nitrite and lower production of $N_2O$, which could be the result of $Cu^{2+}$ inhibition of the nitrite reductase activities of 3H11. Higher concentrations of $Cu^{2+}$ (above 100 μM) interfered with nitrate reduction. This is the result of $Cu^{2+}$ toxicity on 3H11 biomass and possibly on the activity of 3H11 nitrate reductase. The majority of nitrate was reduced to nitrite in 3H11 cultures

in the presence of $Cd^{2+}$, $Co^{2+}$ and $Ni^{2+}$, which instead affected nitrite consumption compared with no metal added. About 50 μmoles of nitrogen existed as nitrite and 10 μmoles as $N_2O$ in cultures with $Cd^{2+}$ and $Ni^{2+}$. About 50 μmoles of nitrogen existed as nitrite and 10 μmoles as $N_2O$ when 3H11 grew with higher than 60 μM of $Co^{2+}$. U has no influence on nitrate reduction of 3H11.

## Discussion

The greenhouse gas $N_2O$ is detected in the ORR contaminated area (131). It is assumed to be the result of denitrification by nitrate-reducing microbial communities. The ORR contaminated area is a complex environment which is not only acidic and Mo-limited but also contaminated by high nitrate and various metals (26, 130). To investigate the effects of ORR related metals (Mo, U, Cd, Mn, Co, Cu) on $N_2O$ production at ORR, ORR strains *Rhodanobacter* R12 and *Acidovorax* 3H11 were selected and co-cultured as an artificial nitrate-reducing community. The nitrate-reducing growth, nitrate consumption, and nitrite and $N_2O$ production with environmentally-relevant concentrations of ORR metals were studied. Increased Mo availability did not significantly increase nitrate reducing growth of R12, 3H11 or the R12/3H11 co-culture. But Cu, Co, Cd and Ni inhibited nitrate-reducing growth of R12, 3H11, and the R12/3H11 co-culture very significantly. Meanwhile, nitrate consumption, and nitrite and $N_2O$ production by R12, 3H11 and the co-culture were also inhibited by these four metals.

Mo did not have much effect on nitrate reducing growth of the ORR strains likely because of the presence of 1 to 2 nM of Mo in the growth media as contamination without any added Mo. This low concentration of Mo appears to be more than sufficient for nitrate-reducing growth of these strains. Mo is essential as it is a cofactor of the enzyme nitrate reductase. In future work, the media could be specifically depleted of Mo to the picomolar level by $Fe^{3+}$ precipitation (178). This would simulate the Mo limited conditions that naturally occur in the ORR contaminated area where the Mo concentration is in the pM range as a result of depletion by $Fe^{3+}/Al^{3+}$ precipitation when the pH of the acidic groundwater increases as it mixes with neutral groundwater (178).

In R12 cultures, generally not much nitrite was produced from nitrate while with 3H11 cultures most of the nitrate was reduced to nitrite and this was released into the medium (Figure 5.6 and 5.7). This indicates that R12 can reduce nitrite efficiently and 3H11 can reduce nitrate

efficiently. In the R12/3H11 co-culture, nitrate, nitrite and $N_2O$ were barely detectable in the presence of low concentrations of ORR metals, indicating that the two organisms worked well together and removed nitrate more efficiently and decreased the accumulation the greenhouse gas $N_2O$ under lab conditions. This could be of significance if the same occurs in the contaminated ORR environment, although this a much more complex system and has other potential inhibition factors, such as low pH, limiting carbon sources and fluctuating temperatures.

The ORR metal mixture (MM) inhibited nitrate reducing growth and nitrate consumption of R12 very significantly. Metal mix as high as 1.2× affected the growth rate of 3H11 but not the final cell density. The inhibition by ORR metal mix on the co-culture should be the result of growth inhibition of R12 as the growth curve with 1.2× MM matched the growth curve of 3H11 with 1.2× MM. Even though Cu, Cd, Co and Ni inhibited the denitrifying growth of R12, 3H11 and the co-culture, Ni should have the most effect of the ORR metals as it is at a high concentration (150 μM) in the metal mix and showed significant inhibition to the growth of both R12 and the co-culture. This indicates that Ni should be the main toxic metal that limits the nitrate removal and might affect nitrite and $N_2O$ levels in the ORR environment.

The inhibition by metals of nitrate, nitrite or $N_2O$ production by R12, 3H11 or the co-cultures could be due to several reasons. First, the metals could directly inhibit denitrification enzymes (nitrate reductase, nitrite reductase, nitric oxide reductase, and nitrous oxide reductase). For example, high nitrate concentration remained when R12 was incubated with high $Cu^{2+}$ and $Ni^{2+}$ and when 3H11 was incubated with high $Cu^{2+}$, suggesting that their nitrate reductases were inhibited. R12 accumulated about 30 μmoles of nitrite when 100 μM $Ni^{2+}$ was added, which indicates that $Ni^{2+}$inhibited the nitrite reductase activity of R12. Second, metals could affect the activities of enzymes in other essential pathways that are not directly related to denitrification but could result in growth inhibition, thus inhibiting nitrate or nitrite reduction indirectly. Third, nitrite

is also toxic, and so the accumulation of nitrite in cultures could also play a role in inhibiting its nitrate-reducing growth. Further biochemical analysis of the enzyme activities of the denitrification pathways of R12 and 3H11 should be performed to address which is the dominant process by which the ORR-relevant metals affect their metabolisms.

$N_2O$ emissions in the high nitrate and low pH environment of the Oak Ridge Reservation can be very complex. Biotic (nitrate reducing community components, nitrate reducing enzyme activities, bacteria interactions, etc.) and abiotic aspects (pH, carbon source availability, temperature, metals, etc.) could independently perturb emissions. In order to investigate $N_2O$ emissions at ORR, we are collaborating with other researchers on the ENIGMA project (Ecosystems and Networks Integrated with Genes and Molecular Assemblies, https://enigma.lbl.gov/) and try to answer the following questions: 1) How does low pH affect the nitrous oxide reductase (NosZ) activity of denitrifying microbes that have all of the enzymes of the denitrification pathway? 2) How does the low pH affect organisms that don't have the full denitrifying pathway but have NosZ? 3) How do Fe, Mn, and organic compounds affect the abiotic production of $N_2O$ by abiotic chemodenitrification? These questions will be addressed using selected ORR isolates and/or artificial microbial communities from ORR isolates to develop quantitative and predictive models for gene regulatory and metabolic networks related to $N_2O$ production. The models can then be used to explain or predict ORR field-observed phenomena related with $N_2O$ emissions, such as the effects of rainfall on $N_2O$ production at ORR.

## Experimental Procedures

### Growth and culture conditions

ORR strains *Rhodanobacter* R12 and *Acidovorax* 3H11 were first cultured aerobically in R2A media at 30 °C until their cell density (OD680) reached 0.8 to 1.0. Cultures were normalized to the same cell density and 0.12 ml of each or 0.06 ml of each for the co-culture were transferred to Hungate tubes (average volume 16.6 ml). All cultures were grown in the standard medium which contained 1.3 mM KCl, 2 mM $MgSO_4$, 0.1 mM $CaCl_2$, 0.3 mM NaCl, 30 mM $NaHCO_3$, 5 mM $NaH_2PO_4$, 0.1g/L YE, and 10 mM $NaNO_3$ with vitamins and minerals as described by Widdel and Bak (171). Molybdenum and tungsten were omitted in Mo-related experiments. Acetate (20 mM) was used as carbon source, the gas phase was $N_2/CO_2$ (80/20%, v/v) and cultures were incubated at 30 °C in triplicate. Mo as $Na_2MoO_4$, Cu as $CuCl_2 \cdot 2H_2O$, Cd as $Cd(CH_3COO)_2 \cdot 2H_2O$, Co as $CoCl_2 \cdot 6H_2O$, Ni as $NiCl_2 \cdot 6H_2O$ and U as $UO_2(CH_3COO)_2 \cdot 2H_2O$, and metal mix (MM) as described in Table S4.1, were added to cultures as indicated and the cell density (OD680) was measured over time. Spent media at the end time point (240 hours) were collected and used for nitrate and nitrite measurements, and the gas phase in the Hungate tubes were used for $N_2O$ measurements.

### Nitrate and nitrite measurement

Nitrate and nitrite were measured by the Griess colorimetric assay (172). 100 µL of diluted samples were mixed with 100 µL the Griess reagent (MilliporeSigma) and incubated at 37 °C for 1 h to determine the concentrations of nitrite produced during growth (data A). To reduce the remaining nitrate to nitrite, 50 µL of diluted samples were mixed with 40 µL saturated $VCl_3$ (400 mg $VCl_3$ in 50 mL 1M HCl). 100 µL of the Griess reagent was added and the mixture was incubated at 37 °C for 4 h before measuring absorption at 540 nm, which measures nitrite of original nitrite and nitrite reduced by $VCl_3$ from nitrate in samples (data B). Nitrite concentrations were calculated

based on standards using data A and nitrite+nitrate concentration based on standards using data B. Subtracting nitrite concentration from nitrite+nitrate data gives nitrate concentration in tested sample.

**$N_2O$ measurement by Gas Chromatography**

A gas chromatograph (GC, Agilent Technologies 7890A GC system, Santa Clara, CA, USA) equipped with an electron capture detector (GC-ECD) was used to quantify $N_2O$ in the gas phase of R2A, 3H11 or the co-culture in Hungate tubes. $N_2O$ standards (5, 10, 20, 30, 50 μmoles) were prepared in duplicate using the same Hungate tubes containing 6 ml of medium described above and filled with $N_2/CO_2$ (80%/20%, v/v), 100 μl of gas phase in each tube was transferred to a Hungate tube with 6 ml of fresh media and filled with $N_2/CO_2$ (80%/20%, v/v) to dilute the gas. 100 μl of diluted gas was injected into GC to quantify $N_2O$ production of each sample.

**Tables and Figures**

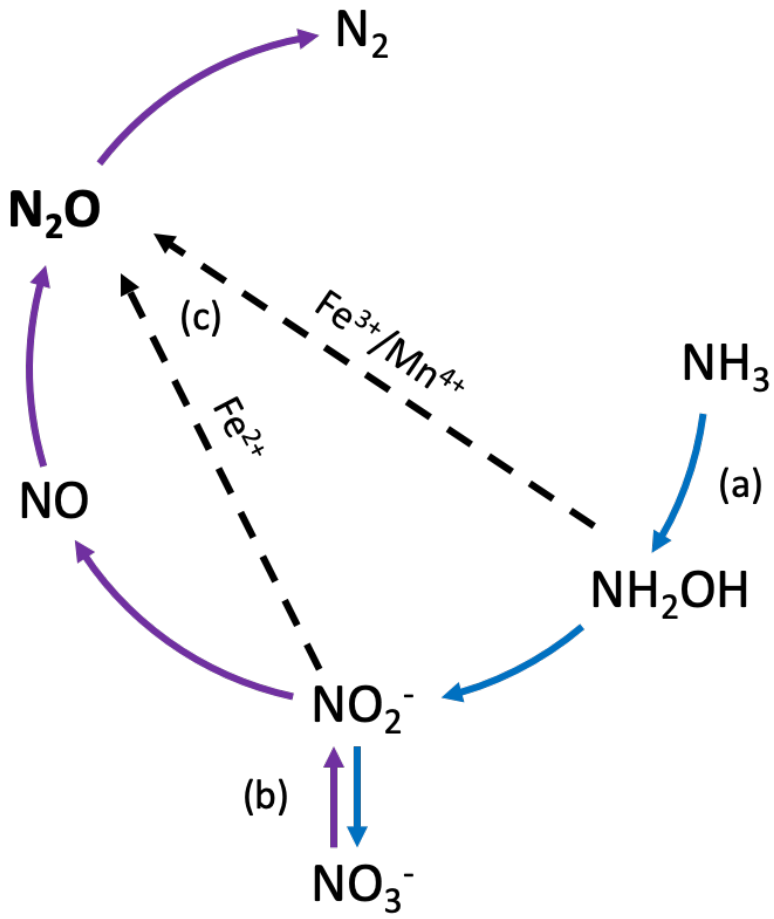


Figure 5.1 Main pathways of $N_2O$ production. (a) nitrification (from $NH_3$); (b) denitrification (from $NO_3^-$); (c) chemodenitrification (directly from $NO_2^-$ or $NH_2OH$).

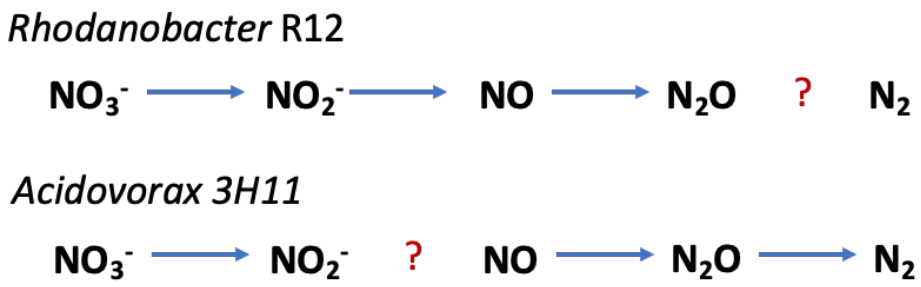


Figure 5.2 Denitrification pathways predicted from draft genome sequences in ORR strains *Rhodanobacter* R12 and *Acidovorax* 3H11.

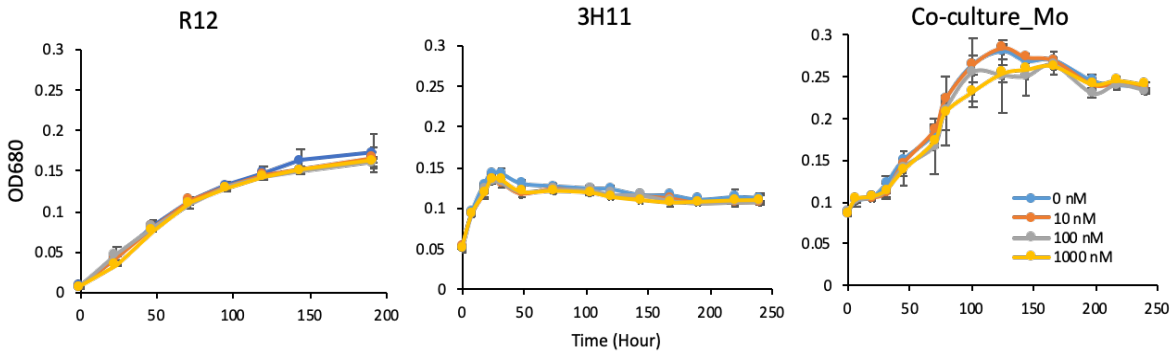


Figure 5.3 Nitrate-reducing growth of *Rhodanobacter* R12, *Acidovorax* 3H11 and the R12/3H11 co-culture with added Mo.

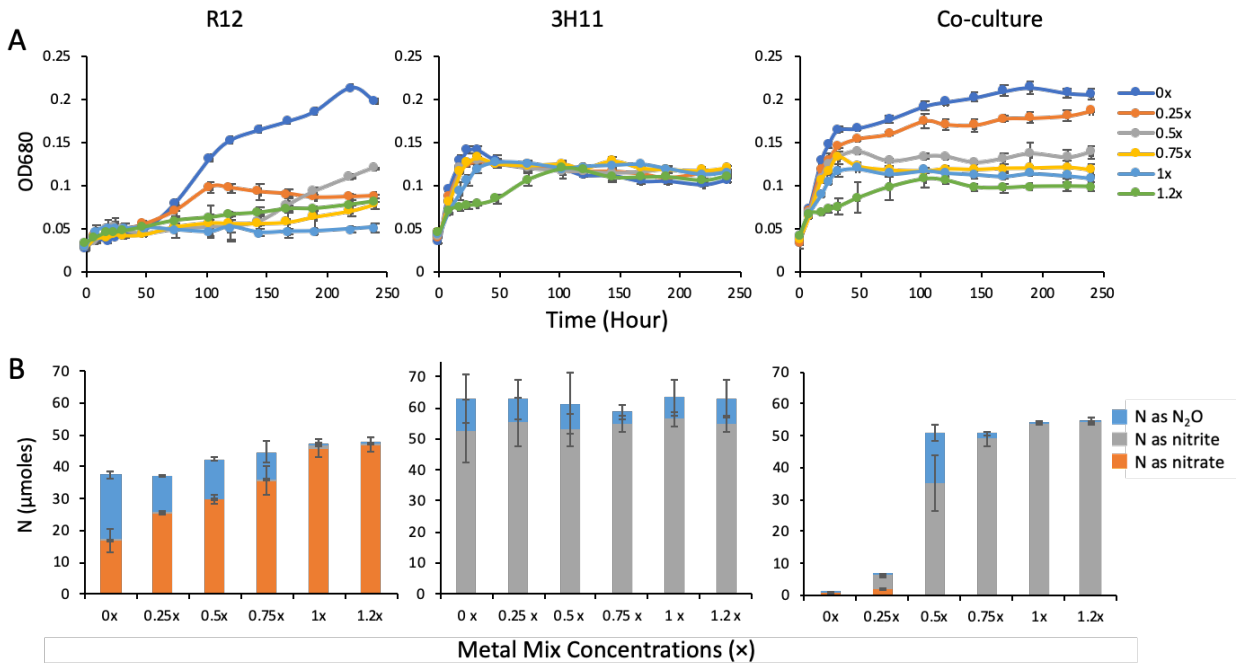


Figure 5.4 Nitrate reducing growth of *Rhodanobacter* R12, *Acidovorax* 3H11 and R12/3H11 co-culture with metal mix. (A) Growth curves of R12 with increasing concentrations of Cu, Cd, Co, Ni and U, (B) nitrate, nitrite and $N_2O$ measured in spent media or in the gas phase of R12 cultures in Hungate tubes. The amounts of nitrate (orange bars), nitrite (grey bars) and $N_2O$ (blue bars) are given in terms of µmoles of N.

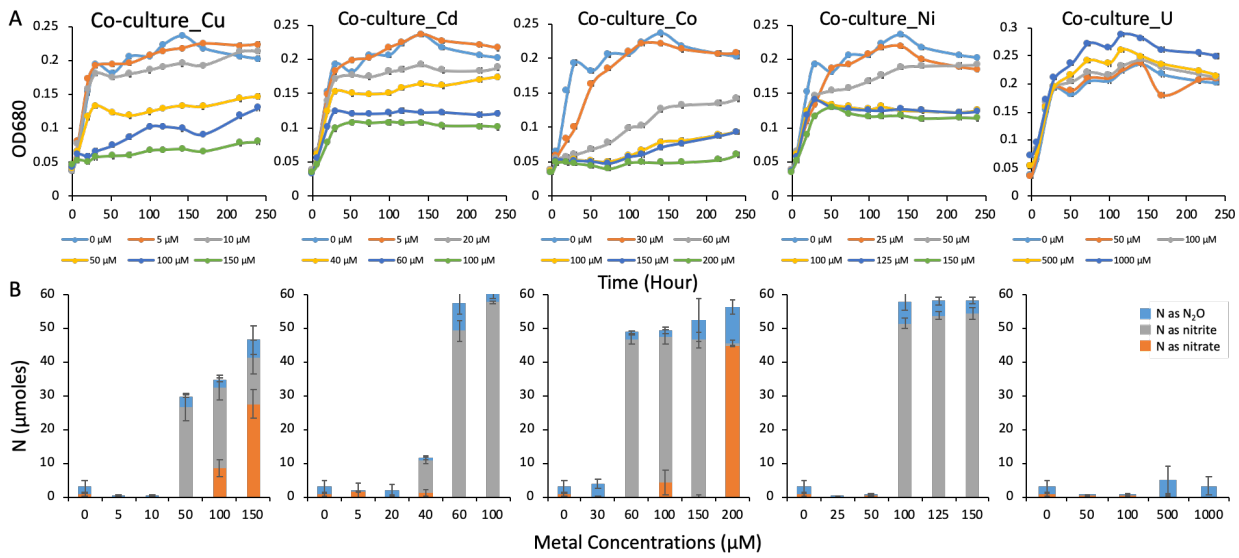


Figure 5.5 Nitrate reducing growth of *Rhodanobacter* R12 and *Acidovorax* 3H11 co-culture with Cu, Cd, Co, Ni and U. (A) Growth curves of Co-cultures with increasing concentrations of Cu, Cd, Co, Ni and U, (B) nitrate, nitrite and $N_2O$ measured in spent media or in the gas phase of Co-cultures in Hungate tubes. The amounts of nitrate (orange bars), nitrite (grey bars) and $N_2O$ (blue bars) are given in terms of µmoles of N.

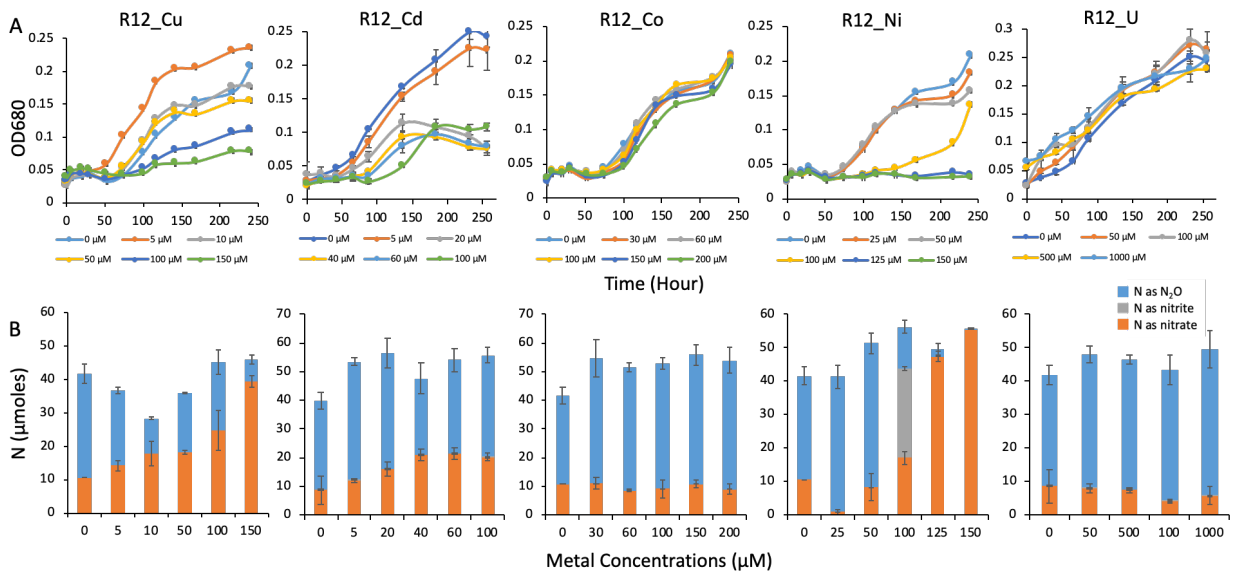


Figure 5.6 Nitrate reducing growth of *Rhodanobacter* R12 with Cu, Cd, Co, Ni and U. (A) Growth curves of R12 with increasing concentrations of Cu, Cd, Co, Ni and U, (B) nitrate, nitrite and $N_2O$ present in spent media or in the gas phase of R12 cultures in Hungate tubes. The amounts of nitrate (orange bars), nitrite (grey bars) and $N_2O$ (blue bars) are given in terms of µmoles of N.

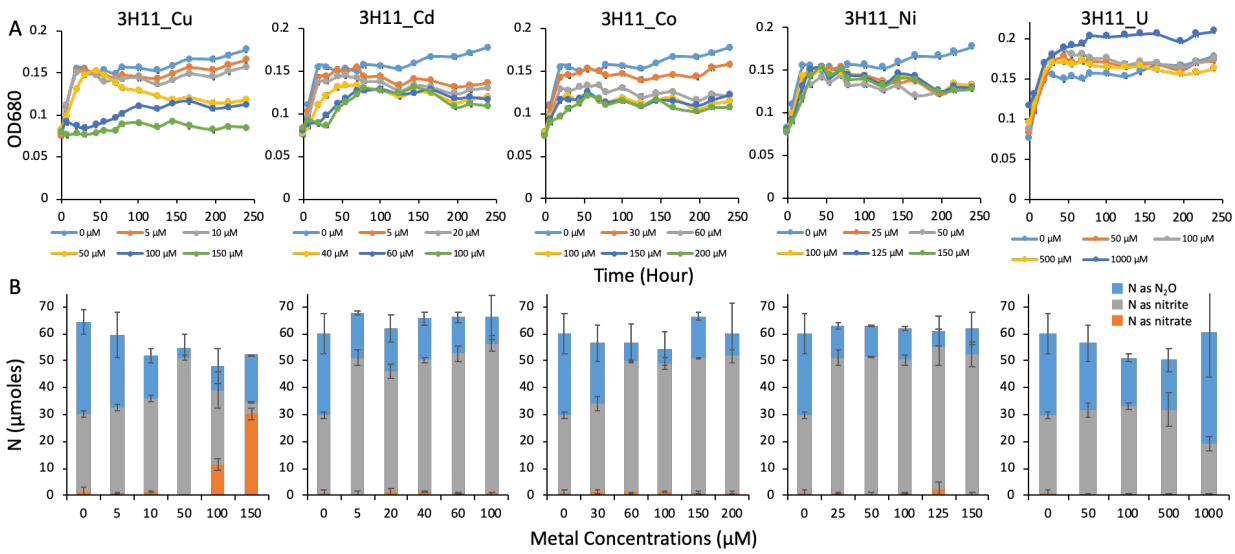


Figure 5.7 Nitrate reducing growth of *Acidovorax* 3H11 with Cu, Cd, Co, Ni and U. (A) Growth curves of 3H11 with increasing concentrations of Cu, Cd, Co, Ni and U, (B) nitrate, nitrite and $N_2O$ measured in spent media or in the gas phase of 3H11 cultures in Hungate tubes. The amounts of nitrate (orange bars), nitrite (grey bars) and $N_2O$ (blue bars) are given in terms of µmoles of N.

Table 5.1 $IC_{50}$ values of the ORR metal mix (MM) and individual metals on *Rhodanobacter* R12, *Acidovorax* 3H11 and the *Rhodanobacter* R12 and *Acidovorax* 3H11 co-culture.

| Strain | $Cu^{2+}$ (μM) | $Cd^{2+}$(μM) | $Co^{2+}$ (μM) | $Ni^{2+}$ (μM) | $U^{6+}$ (μM) | Metal Mix (×) |
|---|---|---|---|---|---|---|
| **R12** | 75.8 | 16.9 | > 200 | 114.9 | > 500 | 0.4 |
| **3H11** | 77.2 | 18.4 | 53.7 | 26.3 | > 500 | 0.6 |
| **Co-culture** | 47.0 | 37.8 | 72.3 | 67.6 | > 500 | 0.5 |

# CHAPTER 6

# DISCUSSION AND CONCLUSIONS

The contaminated site at the Oak Ridge Reservation (ORR) in Tennessee, USA, is very special. Millions of liters of waste containing nitric acid and toxic metals were disposed at this site by the US government for 32 years from the nuclear developing facilities at the Y-12 Plant (126). There are two locations that are highly acidic and contain high concentrations of nitrate and uranium (U) (Area 1 and Area 3), a site with much lower nitrate and U (Area 2) (233). As a major contaminant, nitrate is present at concentration as high as 74 g/L (1.2 M; (126)) and remains at a high level (up to 230 mM)) in some heavily contaminated wells even after the remediation in 1980s (127). Various metals still remain at high levels after the remediation (uranium up to 580 μM, aluminum up to 20709 μM, manganese up to 3150 μM, nickel up to 157 μM, cobalt up to 30 μM, cadmium up to 10 μM, copper up to 15 μM, chromium up to 11 μM, lead up to 0.5 μM and thorium up to 8 μM) in the most contaminated well FW126 (26, 126, 130). Meanwhile, the pH of the groundwater in the contaminated area range from very acidic about 2 to neutral level about 7, many of the contaminated groundwater samples are in the low end below pH 5 (26). A large plume of nitrate that extended approximately 1 km to a depth of over 100 m was detected in this area (128, 129). However, molybdenum (Mo), required by nitrate reductase to remove nitrate, was present at a lower median concentration (<<1 nM) in highly contaminated wells compared to those in pristine wells (up to 330 nM (26)).

In the research for this thesis, geochemical, microbiological, phylogenetic and biochemical analyses have been carried out to investigate why Mo is present at extremely low concentrations in contaminated ORR groundwater, the relationship between nitrate-reducing bacteria and the

heavy metal and high nitrate environment, and to determine mechanisms that enable microorganisms to survive in this unique and extreme environment. In chapter 2, analysis in the laboratory showed that Mo limitation in the highly contaminated groundwater is because of Fe/Al-precipitation when pH increases above 3 as the acidic and contaminated groundwater mixes with the surrounding groundwater. At the same time, it was shown that Mo depletion by Fe/Al-precipitation can dramatically inhibit nitrate reduction by microorganisms. This is important because Mo is required for biological nitrate reduction in nature. The environmental model described in this study can also be applied to other acidic, nitrate and/or metal-contaminated environments, such as acid mine drainage.

In chapter 3, the mechanism that enables a metal resistance nitrate-reducing *Bacillus* strain, isolated from ORR sediment, to survive in Mo-limited ORR environment was elucidated. *Bacillus sp*. EB106-08-02-XG196 was more resistant to heavy metals and much less sensitive to Mo-limitation under nitrate reducing conditions than other environmental strains from ORR. Its genome was sequenced, annotated and published (234). It was shown in this study that the molybdate binding affinity of the XG196 molybdate ABC transporter is very high ($K_D$ ~ 2 nM) and is proposed to be the reason why XG196 readily takes up Mo. Its $K_D$ value is the lowest reported for any ModA to date by about an order of magnitude. This is also the first ModA characterized from a *Bacillus* strain.

It was also shown experimentally in this study that $Fe^{3+}$ and $Al^{3+}$ are effective at removing molybdate from solution. However, $Fe^{3+}$ rather than $Al^{3+}$ is the main driver of Mo depletion in the ORR contaminated area because, based on our elemental analysis, $Fe^{3+}$ precipitation induced Mo depletion happened when pH < 5.0, consistent with the pH in many contaminated ORR wells, in which the concentrations of Fe are low (μM range) but Al are still high (mM range) and Mo is virtually undetectable. The sediment at ORR is rich in iron oxides (150, 151) and several of the highest concentrations of Mo (at 501 cm and 583 cm depth) that were measured are also rich in Fe in the contaminated core EB-106. We assume that these represent the pathways through which the

contaminated S-3 ponds liquids flowed leading to iron-based precipitation at these depths. Mo limitation is clearly another factor that could be impacting microbial nitrate reduction at ORR, besides the low pH and high concentrations of metals and nitrate, as well as of other anions such as sulfate and chloride. *Bacillus* strain XG196 isolated from EB-106 saturated zone is of great interest because it is both metal resistant and has a very high affinity for molybdate. XG196 was isolated from the EB-106 sediment at the depth that corresponds to the third Mo peak in the depth profile(235). However, strains like XG196 with a high molybdate binding ability can help it survive in an environment extremely limited for Mo (sub-pM levels) when nitrate is available as an electron acceptor. XG196 is only one representative of what are assumed to be many strains with special properties that enable them to survive in the extreme environment of the ORR sediments. Future enrichment and isolation and characterization should be carried out in the future to determine how such strains compare with XG196.

Many studies have been carried out to investigate the relationships of microbes and the special environment at the ORR contaminated area to search novel strains, mechanisms, bioproducts and other resources from, including by field geochemical analysis (127-129, 150, 188, 236, 237), metagenome analysis (138, 205, 238) and microbial isolation and characterization (26, 141, 234, 239). Community characterization of groundwater and sediment samples from ORR area 2 and area 3 by a suite of DNA- and RNA-based molecular tools revealed that denitrifying bacteria from the genus *Rhodanobacter* dominate at low pH (near 3; (232)). Relative abundance of *Rhodanobacter* in acidic groundwater from Area 3 can be more than 90% (232) and this was positively correlated with low pH conditions. Members of this genus were abundant and active in the most highly contaminated area 3, and their distribution was not affected by other factors, such as the concentration of nitrogen species, oxygen level, and sampling season (232). The role that *Rhodanobacter* plays in nitrogen related metabolism in high nitrate contaminated area at ORR is

currently being studied in depth by our collaborators on ENIGMA project (Ecosystems and Networks Integrated with Genes and Molecular Assemblies, https://enigma.lbl.gov/) in order to reveal the efficiency of nitrate reduction, $N_2O$ emission under conditions that simulate the ORR environment, their interactions with other microbes (e.g. *Acidovorax* 3H11) in nitrate reducing under various pH levels, ORR levels of metal concentrations. There is no doubt that laboratory work using ORR strains is critical to revealing what is happening in the field, although relating the results to what is actually happening in the field is a big challenge.

Seven nitrate-reducing strains that can grow in the presence of metals at concentrations found in the contaminated ORR environment were recently isolated in our laboratory (141). Of these, four (MT049 (*Serratia*), MT058 (*Pantoea*), MT066 (*Bacillus*), MT094 (*Bacillus*), and MT123 (*Castellaniella*).) were mapped back geographically to both non-contaminated and contaminated wells at ORR using exact sequence variant (ESV) analysis of metagenome data (141). These strains have the potential to be the model strains for understanding nitrate metabolism and related activities in the presence of various metals in this extremely contaminated ORR environment. The study of ORR-related microbes also faces other challenges, in particular, carbon source limitation and fluctuation. Enrichment and isolation work are fundamental and also important in environmental microbiology studies, but cultivation of diverse microorganisms from the field can also be very challenging because of what are termed 'unculturable' microbes. One key to isolate strains from their environment is to mimic their natural conditions in the laboratory, but the challenging part is reproducing the complex natural environment, for example, containing natural organic matter (NOM) and potential microbe-microbe interactions. One recent study showed that natural organic carbon sources such as NOM and bacterial cell lysates are very effective in enriching diverse bacteria (240). Future enrichment and isolation work using ORR

samples should focus on this but with an additional focus on both essential (Mo) and toxic metals at environmentally-relevant concentrations.

Metagenome analysis provides a comprehensive view of the composition of microbes in environments such as ORR, but genome annotations are sometimes not as precise as expected. For example, metagenome analysis uses the EggNOG mapper (EggNOG is evolutionary genealogy of genes: Non-supervised Orthologous Groups) and database, part of the international consortium Quest for Orthologs (241), was shown to work better at annotating genes than two widely used homology-based approaches: BLAST and InterProScan. For example, EggNOG mapper reduced by 7% the rate of false positive assignments and increased by 19% the ratio of curated terms recovered over all terms assigned per protein compared to BLAST and increased by 26% the rate of curated terms recovered over total term assignments per protein than InterProScan. In addition, the EggNOG-mapper is faster than BLAST(~15x) and InterProScan (> 2.5x) (207). In the research presented in this thesis, EggNOG mapper (v2) was used to identify annotated Mo-related proteins in metagenome data (234).

The ability to study soil microbial diversity and soil processes also requires technologies that differentiate active microbes from extracellular DNA fragments and non-active cells (238). Bioorthogonal non-canonical amino acid tagging (BONCAT) revealed that the phylogenetic composition of the active fraction is distinct from the total population of extractable cells in ORR sediments (238) and similar studies have been done in marine sediments (242, 243). This approach uses homopropargylglycine (HPG), a water-soluble analog of methionine containing an alkyne group which can be incorporated into newly synthesized proteins. Fluorescent dyes are then linked to HPG-containing proteins by azide-alkyne reaction. As a result, active cells are fluorescently labeled and can be sorted out by fluorescence-activated cell sorting (FACS) (238). It was revealed that in ORR sediments, the composition of active cells, which is about 25–70% of the extractable

cells, is different from the total extractable cells using BONCAT (238). BONCAT-FACS is an effective method to study the active population in microbial communities in situ and provides a more efficient way to uncover the relationship between soil activities and microbial communities. Proper enrichment and isolation work can identify many environmental strains relatively quickly and easily with the help of modern sequencing technologies. In addition, the work described here shows that the environmental conditions must play an important role in designing the appropriate experimental conditions for enrichments, in particular, the presence of essential and toxic metals.

One of the main obstacles is to assign phenotypes or functions to genes in a strain isolated from environments such as the ORR. RB-Tnseq (random bar code transposon-site sequencing) is a powerful tool to annotate gene functions in bacteria on a genome-wide basis (244-246). RB-Tnseq combines the advantages of TnSeq and DNA bar coding. First, a large transposon mutant population of each strain containing a unique DNA bar code is generated. Tnseq is then applied to generate corresponding a randomly bar-coded transposon mutant library of this strain. DNA barcodes are amplified and sequenced by Illumina sequencing. Competitive mutant fitness assays can then be carried out by comparing the abundance of the DNA bar codes with BarSeq before and after growth under selective conditions to reveal genes that show higher or lower fitness (245). Using this method, our laboratory showed that several proteins of unknown function are involved in resisting zinc and copper toxicity of *Pseudomonas stutzeri* RCH2, a model strain used in ORR related studies (246). RB-Tnseq is therefore a powerful tool that can definitely enable gene characterization work using ORR strains in the future.

Tungsten (W) and molybdenum (Mo) are chemically similar metals. The physiologically-relevant oxidation states of both W and Mo are +4, +5, and +6, and they are taken up and utilized by microbial cells in form of tungstate and molybdate, respectively (7). Mo-containing enzymes are usually absolutely exclusive in utilizing Mo for active catalytic processes, for example,

xanthine oxidase and sulfite oxidase can only use Mo. Similarly, the WOR family of enzymes only use W based on the studies to date (7, 68). However, some enzymes in DMSO reductase family are able to use W as well as Mo and the W-DMSOR found from *Rhodobacter capsulatus* is significantly more active than Mo-DMSOR in catalyzing the reduction of DMSO (247). An active W-containing nitrate reductase (Nar) has also been characterized from the hyperthermophilic denitrifying archaeon *Pyrobaculum aerophilum* when grown with tungstate concentrations that are completely inhibitory to nitrate-reducing bacteria, which is thought to be a result of this organism adapting to the high tungstate environments of volcanic vents (95). Heterologously expressed arsenate respiratory reductase (Arr) and thiosulfate reductase (Tsr) from the crenarchaeon *Pyrobaculum aerophilum* ($T_{opt}$ ~ 100°C) in the euryarchaeon *Pyrococcus furiosus* ($T_{opt}$ ~ 100°C) are proved to be active with both Mo and W, and both enzymes that contains Mo are more active than those with W (93, 248). Interestingly, both W- and Mo-forms produced are by *Pyrococcus furiosus*, which itself have five members of the WOR family, none of which will incorporate Mo, only W (80-86).

One question is whether in the Mo-limited ORR environment, are W-containing enzymes present that either substitute for Mo in certain Mo-enzymes (like DMSOR and nitrate reductase) or have completely new metabolic roles in the function and diversity of ORR microbes. In the study of the abundance of Mo-related proteins in the ORR environment, we also analyzed for genes representing the W-containing WOR family and also the tungstate transporter (TupABC) and were surprised to find that they were as abundant in ORR groundwater and sediment metagenomes as the genes representing Mo-enzymes and transporters (234). Uncharacterized members of the WOR family could therefore also be present in ORR microbes and this very intriguing topic should be the focus of a future study in the unique ORR environment.

The Archaea represent one of the three domains of cellular life and play important roles in biogeochemical cycles (249). Archaea are also widespread and diverse at ORR. About 60% of the archaea groups detected from ORR surface stream sediments were not similar to any cultivated isolate (250) and at least one archaeal 16S sequence was found in every 100-well survey well, a study in which groundwater samples were collected from about 100 ORR wells, including contaminated and non-contaminated ones, to study the effects of ORR contamination to the microbial communities, and over 20 families observed spanning all major branches (130). In addition, some of the archaeal 16S sequences have close relatives in the *Thermoproteales* that have been characterized but these grow at extreme temperatures (> 80°C) and no mesophilic member of the group, which is presumably present in the ORR environment, is known at present. Interesting anaerobic or facultatively anaerobic archaea that have uncharacterized metabolic pathways and have high resistance to metals or produce interesting bioproducts might survive in the extreme contaminated ORR environment, but no representative has yet been isolated. Enrichment and characterization of novel archaea strains could involve 16S rRNA sequencing using archaea-specific primers and archaeal specific fluorescent single cell probes can be used to screen groundwater and sediment samples in ORR (251, 252). In addition, as has been emphasized in the work presented in this thesis, isolation procedures for novel archaea should also take into account the availability of essential (Mo, and perhaps W) as well as toxic metals and do so at concentrations that these metals are present in the ORR environment.

## REFERENCES


1. Madsen EL. 2011. Microorganisms and their roles in fundamental biogeochemical cycles. Curr Opin Biotechnol 22:456-464.
2. Gadd GM. 2004. Mycotransformation of organic and inorganic substrates. Mycologist 18:60-70.
3. Ferguson SJ. 1998. Nitrogen cycle enzymology. Curr Opin Chem Biol 2:182-193.
4. Galloway JN, Dentener FJ, Capone DG, Boyer EW, Howarth RW, Seitzinger SP, Asner GP, Cleveland CC, Green P, Holland EA. 2004. Nitrogen cycles: past, present, and future. Biogeochemistry 70:153-226.
5. Maia LB, Moura JJ. 2014. How biology handles nitrite. Chem Rev 114:97.
6. Jetten MS. 2008. The microbial nitrogen cycle. Environ Microbiol 10:2903-2909.
7. Maia LB, Moura I, Moura JJ. 2017. Molybdenum and tungsten-containing enzymes: an overview, p 1-18. *In* Hille R, Schulzke C, Kirk ML (ed), Molybdenum and tungsten enzymes.
8. Moore H. 1977. The isotopic composition of ammonia, nitrogen dioxide and nitrate in the atmosphere. Atmos Environ (1967) 11:1239-1243.
9. Marty B, Zimmermann L, Pujol M, Burgess R, Philippot P. 2013. Nitrogen isotopic composition and density of the Archean atmosphere. Science 342:101-104.
10. Dixon R, Kahn D. 2004. Genetic regulation of biological nitrogen fixation. Nat Revie Microbiol 2:621-631.
11. Berman-Frank I, Lundgren P, Falkowski P. 2003. Nitrogen fixation and photosynthetic oxygen evolution in cyanobacteria. Res Microbiol 154:157-164.

12. Strous M, Kuenen JG, Jetten MS. 1999. Key physiology of anaerobic ammonium oxidation. Appl Environ Microbiol 65:3248-3250.

13. Mulder A, Van de Graaf AA, Robertson L, Kuenen J. 1995. Anaerobic ammonium oxidation discovered in a denitrifying fluidized bed reactor. FEMS Microbiol Ecol 16:177-183.

14. Kuypers MM, Sliekers AO, Lavik G, Schmid M, Jørgensen BB, Kuenen JG, Damsté JSS, Strous M, Jetten MS. 2003. Anaerobic ammonium oxidation by anammox bacteria in the Black Sea. Nature 422:608-611.

15. Thamdrup B, Dalsgaard T. 2002. Production of $N_2$ through anaerobic ammonium oxidation coupled to nitrate reduction in marine sediments. Appl Environ Microbiol 68:1312-1318.

16. Lisa JA, Song B, Tobias CR, Duernberger KA. 2014. Impacts of freshwater flushing on anammox community structure and activities in the New River Estuary, USA. Aquat Microb Ecol 72:17-31.

17. Galloway JN, Townsend AR, Erisman JW, Bekunda M, Cai Z, Freney JR, Martinelli LA, Seitzinger SP, Sutton MA. 2008. Transformation of the nitrogen cycle: recent trends, questions, and potential solutions. Science 320:889-892.

18. Gruber N, Galloway JN. 2008. An Earth-system perspective of the global nitrogen cycle. Nature 451:293-296.

19. Hille R. 1996. The mononuclear molybdenum enzymes. Chem Rev 96:2757-2816.

20. Zhang Y, Gladyshev VN. 2008. Molybdoproteomes and evolution of molybdenum utilization. J Mol Biol 379:881-99.

21. Kisker C, Schindelin H, Rees DC. 1997. Molybdenum-cofactor–containing enzymes: structure and mechanism. Annu Rev Biochem 66:233-267.

22. Hille R. 2002. Molybdenum and tungsten in biology. Trends Biochem Sci 27:360-367.

23. Glass JB, Axler RP, Chandra S, Goldman CR. 2012. Molybdenum limitation of microbial nitrogen assimilation in aquatic ecosystems and pure cultures. Front Microbiol 3.

24. Barron AR, Wurzburger N, Bellenger JP, Wright SJ, Kraepiel AM, Hedin LO. 2009. Molybdenum limitation of asymbiotic nitrogen fixation in tropical forest soils. Nat Geosci 2:42-45.

25. Howarth RW, Cole JJ. 1985. Molybdenum availability, nitrogen limitation, and phytoplankton growth in natural waters. Science 229:653-5.

26. Thorgersen MP, Lancaster WA, Vaccaro BJ, Poole FL, Rocha AM, Mehlhorn T, Pettenato A, Ray J, Waters RJ, Melnyk RA, Chakraborty R, Hazen TC, Deutschbauer AM, Arkin AP, Adams MWW. 2015. Molybdenum availability is key to nitrate removal in contaminated groundwater environments. Appl Environ Microbiol 81:4976-4983.

27. Bouchard DC, Williams MK, Surampalli RY. 1992. Nitrate contamination of groundwater: sources and potential health effects. J Am Water Works Associ 84:85-90.

28. Manassaram DM, Backer LC, Moll DM. 2006. A review of nitrates in drinking water: maternal exposure and adverse reproductive and developmental outcomes. Environ Health Perspect 114:320-327.

29. Mueller DK, Helsel DR, Kidd MA. 1996. Nutrients in the nation's waters: too much of a good thing? US Government Printing Office Washington, DC.

30. Almasri MN. 2007. Nitrate contamination of groundwater: A conceptual management framework. Environ Impact Assess Rev 27:220-242.

31. Heffer P, Prud'homme M. Global nitrogen fertilizer demand and supply: trend, current level and outlook, International Nitrogen Initiative Conference. Melbourne, Australia.

32. Norton R, Davidson E, Roberts T. 2015. Nitrogen use efficiency and nutrient performance indicators. Global Partnership on Nutrient Management 6.

33. Lassaletta L, Billen G, Grizzetti B, Anglade J, Garnier J. 2014. 50 year trends in nitrogen use efficiency of world cropping systems: the relationship between yield and nitrogen input to cropland. Environ Res Lett 9:105011.

34. Zhang X, Davidson EA, Mauzerall DL, Searchinger TD, Dumas P, Shen Y. 2015. Managing nitrogen for sustainable development. Nature 528:51-59.

35. Spalding RF, Exner ME. 1993. Occurrence of nitrate in groundwater—a review. J Environ Qual 22:392-402.

36. Böhlke J, Denver J. 1995. Combined use of groundwater dating, chemical, and isotopic analyses to resolve the history and fate of nitrate contamination in two agricultural watersheds, Atlantic coastal plain, Maryland. Water Resour Res 31:2319-2339.

37. Power J, Schepers J. 1989. Nitrate contamination of groundwater in North America. Agric, Ecosyst Environ 26:165-187.

38. Mahvi A, Nouri J, Babaei A, Nabizadeh R. 2005. Agricultural activities impact on groundwater nitrate pollution. Int J Environ Sci Technol (Tehran) 2:41-47.

39. Nolan BT, Ruddy BC, Hitt KJ, Helsel DR. 1998. A national look at nitrate contamination of ground water. Water Cond Purif 39:76-79.

40. Zhang W, Tian Z, Zhang N, Li X. 1996. Nitrate pollution of groundwater in northern China. Agric, Ecosyst Environ 59:223-231.

41. Rao NS. 2006. Nitrate pollution and its distribution in the groundwater of Srikakulam district, Andhra Pradesh, India. Environ Geol 51:631-645.

42. Nolan BT, Hitt KJ. 2006. Vulnerability of shallow groundwater and drinking-water wells to nitrate in the United States. Environ Sci Technol 40:7834-7840.

43. Diaz RJ, Rosenberg R. 2008. Spreading dead zones and consequences for marine ecosystems. Science 321:926-929.

44. Mallin MA, Johnson VL, Ensign SH, MacPherson TA. 2006. Factors contributing to hypoxia in rivers, lakes, and streams. Limnol Oceanogr 51:690-701.

45. Lenihan HS, Peterson CH. 1998. How habitat degradation through fishery disturbance enhances impacts of hypoxia on oyster reefs. Ecol Appl 8:128-140.

46. Diaz RJ, Rosenberg R. 1995. Marine benthic hypoxia: a review of its ecological effects and the behavioural responses of benthic macrofauna. Oceanogr Mar Biol 33:245-03.

47. Powlson DS, Addiscott TM, Benjamin N, Cassman KG, de Kok TM, van Grinsven H, L'hirondel J-L, Avery AA, Van Kessel C. 2008. When does nitrate become a risk for humans? J Environ Qual 37:291-295.

48. Edition F. 2011. Guidelines for drinking-water quality. WHO Chron 38:104-8.

49. Ward MH, Jones RR, Brender JD, De Kok TM, Weyer PJ, Nolan BT, Villanueva CM, Van Breda SG. 2018. Drinking water nitrate and human health: an updated review. Int J Env Res Public Health 15:1557.

50. Knowles R. 1982. Denitrification. Microbiol Rev 46:43.

51. He T, Li Z, Sun Q, Xu Y, Ye Q. 2016. Heterotrophic nitrification and aerobic denitrification by *Pseudomonas tolaasii* Y-11 without nitrite accumulation during nitrogen conversion. Bioresour Technol 200:493-499.

52. Robertson L, Cornelisse R, De Vos P, Hadioetomo R, Kuenen J. 1989. Aerobic denitrification in various heterotrophic nitrifiers. Antonie Van Leeuwenhoek 56:289-299.

53. Robertson LA, Kuenen JG. 1984. Aerobic denitrification: a controversy revived. Arch Microbiol 139:351-354.

54. Tiedje JM. 1988. Ecology of denitrification and dissimilatory nitrate reduction to ammonium. Biology of anaerobic microorganisms 717:179-244.

55. Tiedje J, Sørensen J, Chang Y-Y. 1981. Assimilatory and dissimilatory nitrate reduction: perspectives and methodology for simultaneous measurement of several nitrogen cycle processes. Ecol Bull:331-342.

56. Guerrero MG, Vega JM, Losada M. 1981. The assimilatory nitrate-reducing system and its regulation. Annu Rev Plant Physiol 32:169-204.

57. Richardson D, Berks B, Russell D, Spiro S, Taylor C. 2001. Functional, biochemical and genetic diversity of prokaryotic nitrate reductases. Cell Mol Life Sci 58:165-178.

58. Gonzalez P, Correia C, Moura I, Brondino C, Moura J. 2006. Bacterial nitrate reductases: molecular and biological aspects of nitrate reduction. J Inorg Biochem 100:1015-1023.

59. Hettmann T, Anemüller S, Borcherding H, Mathé L, Steinrücke P, Diekmann S. 2003. *Pseudomonas stutzeri* soluble nitrate reductase αβ-subunit is a soluble enzyme with a similar electronic structure at the active site as the inner membrane-bound αβγ holoenzyme. FEBS Lett 534:143-150.

60. Bertero MG, Rothery RA, Palak M, Hou C, Lim D, Blasco F, Weiner JH, Strynadka NC. 2003. Insights into the respiratory electron transfer pathway from the structure of nitrate reductase A. Nat Struct Mol Biol 10:681-687.

61. Rothery RA, Blasco F, Magalon A, Weiner JH. 2001. The diheme cytochrome b subunit (Narl) of *Escherichia coli* nitrate reductase A (NarGHI): structure, function, and interaction with quinols. J Mol Microbiol Biotechnol 3:273-283.

62. Hettmann T, Siddiqui RA, Frey C, Santos-Silva T, Romão MJ, Diekmann S. 2004. Mutagenesis study on amino acids around the molybdenum centre of the periplasmic

nitrate reductase from Ralstonia eutropha. Biochem Biophys Res Commun 320:1211-1219.

63. Brigé A, Leys D, Meyer TE, Cusanovich MA, Van Beeumen JJ. 2002. The 1.25 Å resolution structure of the diheme NapB subunit of soluble nitrate reductase reveals a novel cytochrome c fold with a stacked heme arrangement. Biochemistry 41:4827-4836.

64. Brondijk THC, Nilavongse A, Filenko N, Richardson DJ, Cole JA. 2004. NapGH components of the periplasmic nitrate reductase of *Escherichia coli* K-12: location, topology and physiological roles in quinol oxidation and redox balancing. Biochem J 379:47-55.

65. Smedley PL, Kinniburgh DG. 2017. Molybdenum in natural waters: A review of occurrence, distributions and controls. Appl Geochem 84:387-432.

66. L'vov N, Nosikov A, Antipov A. 2002. Tungsten-containing enzymes. Biochemistry (Moscow) 67:196-200.

67. Peng T, Xu Y, Zhang Y. 2018. Comparative genomics of molybdenum utilization in prokaryotes and eukaryotes. BMC Genomics 19:691.

68. Hille R, Hall J, Basu P. 2014. The mononuclear molybdenum enzymes. Chem Rev 114:3963-4038.

69. Schwarz G, Mendel RR, Ribbe MW. 2009. Molybdenum cofactors, enzymes and pathways. Nature 460:839-847.

70. Seelmann CS, Willistein M, Heider J, Boll M. 2020. Tungstoenzymes: occurrence, catalytic diversity and cofactor synthesis. Inorganics 8:44.

71. Truglio JJ, Theis K, Leimkühler S, Rappa R, Rajagopalan K, Kisker C. 2002. Crystal structures of the active and alloxanthine-inhibited forms of xanthine dehydrogenase from *Rhodobacter capsulatus*. Structure 10:115-125.

72. Magalon A, Fedor JG, Walburger A, Weiner JH. 2011. Molybdenum enzymes in bacteria and their maturation. Coord Chem Rev 255:1159-1178.

73. Kappler U, Bennett B, Rethmeier J, Schwarz G, Deutzmann R, McEwan AG, Dahl C. 2000. Sulfite: Cytochrome c Oxidoreductase from *Thiobacillus novellus* purification, characterization, and molecular biology of a heterodimeric member of the sulfite oxidase family. J Biol Chem 275:13202-13212.

74. Miralles-Robledillo JM, Torregrosa-Crespo J, Martínez-Espinosa RM, Pire C. 2019. DMSO reductase family: phylogenetics and applications of extremophiles. Int J Mol Sci 20:3349.

75. Wells M, Kanmanii NJ, Janecka JE, Basu P, Oremland RS, Stolz JF. 2020. Methane, arsenic, selenium and the origins of the DMSO reductase family. Sci Rep 10:1-14.

76. Fourmond V, Burlat B, Dementin S, Arnoux P, Sabaty M, Boiry S, Guigliarelli B, Bertrand P, Pignol D, Léger C. 2008. Major Mo (V) EPR signature of *Rhodobacter sphaeroides* periplasmic nitrate reductase arising from a dead-end species that activates upon reduction. Relation to other molybdoenzymes from the DMSO reductase family. J Phys Chem B 112:15478-15486.

77. Weiner JH, Rothery RA, Sambasivarao D, Trieber CA. 1992. Molecular analysis of dimethylsulfoxide reductase: a complex iron-sulfur molybdoenzyme of *Escherichia coli*. BBA Bioenergetics 1102:1-18.

78. Bauer S, Conrad S, Ingri J. 2018. Geochemistry of tungsten and molybdenum during freshwater transport and estuarine mixing. Appl Geochem 93:36-48.

79. Gaillardet J, Viers J, Dupré B. 2003. Trace elements in river waters. TrGeo 5:605.

80. Mukund S, Adams M. 1991. The novel tungsten-iron-sulfur protein of the hyperthermophilic archaebacterium, *Pyrococcus furiosus*, is an aldehyde ferredoxin

oxidoreductase. Evidence for its participation in a unique glycolytic pathway. J Biol Chem 266:14208-14216.

81. Mukund S, Adams M. 1993. Characterization of a novel tungsten-containing formaldehyde ferredoxin oxidoreductase from the hyperthermophilic archaeon, Thermococcus litoralis. A role for tungsten in peptide catabolism. J Biol Chem 268:13592-13600.

82. Mukund S, Adams MW. 1995. Glyceraldehyde-3-phosphate ferredoxin oxidoreductase, a novel tungsten-containing enzyme with a potential glycolytic role in the hyperthermophilic archaeon *Pyrococcus furiosus*. J Biol Chem 270:8389-8392.

83. Roy R, Mukund S, Schut GJ, Dunn DM, Weiss R, Adams MW. 1999. Purification and molecular characterization of the tungsten-containing formaldehyde ferredoxin oxidoreductase from the hyperthermophilic archaeon *Pyrococcus furiosus*: the third of a putative five-member tungstoenzyme family. J Bacteriol 181:1171-1180.

84. Roy R, Adams MW. 2002. Characterization of a fourth tungsten-containing enzyme from the hyperthermophilic archaeon *Pyrococcus furiosus*. J Bacteriol 184:6952-6956.

85. Bevers LE, Bol E, Hagedoorn P-L, Hagen WR. 2005. WOR5, a novel tungsten-containing aldehyde oxidoreductase from *Pyrococcus furiosus* with a broad substrate specificity. J Bacteriol 187:7056-7061.

86. Heider J, Ma K, Adams M. 1995. Purification, characterization, and metabolic function of tungsten-containing aldehyde ferredoxin oxidoreductase from the hyperthermophilic and proteolytic archaeon *Thermococcus* strain ES-1. J Bacteriol 177:4757-4764.

87. Ma K, Hutchins A, Sung S-JS, Adams MW. 1997. Pyruvate ferredoxin oxidoreductase from the hyperthermophilic archaeon, *Pyrococcus furiosus*, functions as a CoA-dependent pyruvate decarboxylase. Proc Natl Acad Sci USA 94:9608-9613.

88. van der Oost J, Schut G, Kengen SM, Hagen WR, Thomm M, de Vos WM. 1998. The ferredoxin-dependent conversion of glyceraldehyde-3-phosphate in the hyperthermophilic archaeon *Pyrococcus furiosus* represents a novel site of glycolytic regulation. J Biol Chem 273:28149-28154.

89. Meckenstock RU, Krieger R, Ensign S, Kroneck PM, Schink B. 1999. Acetylene hydratase of *Pelobacter acetylenicus*: molecular and spectroscopic properties of the tungsten iron–sulfur enzyme. Eur J Biochem 264:176-182.

90. Hartmann T, Schwanhold N, Leimkühler S. 2015. Assembly and catalysis of molybdenum or tungsten-containing formate dehydrogenases from bacteria. Biochim Biophys Acta Proteins Proteom 1854:1090-1100.

91. Niks D, Hille R. 2019. Molybdenum‐and tungsten‐containing formate dehydrogenases and formylmethanofuran dehydrogenases: structure, mechanism, and cofactor insertion. Protein Sci 28:111-122.

92. Hochheimer A, Hedderich R, Thauer RK. 1998. The formylmethanofuran dehydrogenase isoenzymes in *Methanobacterium wolfei* and *Methanobacterium thermoautotrophicum*: induction of the molybdenum isoenzyme by molybdate and constitutive synthesis of the tungsten isoenzyme. Arch Microbiol 170:389-393.

93. Haja DK, Wu C-H, Poole FL, Sugar J, Williams SG, Jones AK, Adams MW. 2020. Characterization of thiosulfate reductase from *Pyrobaculum aerophilum* heterologously produced in *Pyrococcus furiosus*. Extremophiles 24:53-62.

94. Pacheco J, Niks D, Hille R. 2018. Kinetic and spectroscopic characterization of tungsten-substituted DMSO reductase from *Rhodobacter sphaeroides*. J Biol Inorg 23:295-301.

95. de Vries S, Momcilovic M, Strampraad MJ, Whitelegge JP, Baghai A, Schröder I. 2010. Adaptation to a high-tungsten environment: *Pyrobaculum aerophilum* contains an active tungsten nitrate reductase. Biochemistry 49:9911-9921.

96. Gates AJ, Hughes RO, Sharp SR, Millington PD, Nilavongse A, Cole JA, Leach E-R, Jepson B, Richardson DJ, Butler CS. 2003. Properties of the periplasmic nitrate reductases from *Paracoccus pantotrophus* and *Escherichia coli* after growth in tungsten-supplemented media. FEMS Microbiol Lett 220:261-269.

97. Self WT, Grunden AM, Hasona A, Shanmugam KT. 2001. Molybdate transport. Res Microbiol 152:311-321.

98. Rosentel JK, Healy F, Maupin-Furlow JA, Lee JH, Shanmugam K. 1995. Molybdate and regulation of mod (molybdate transport), fdhF, and hyc (formate hydrogenlyase) operons in *Escherichia coli*. J Bacteriol 177:4857-4864.

99. Hollenstein K, Frei DC, Locher KP. 2007. Structure of an ABC transporter in complex with its binding protein. Nature 446:213-216.

100. Hu Y, Rech S, Gunsalus RP, Rees DC. 1997. Crystal structure of the molybdate binding protein ModA. Nat Struct Biol 4:703-707.

101. Santacruz C, Balan A, Ferreira LCdS, Barbosa J. 2006. Crystallization, data collection and phasing of the molybdate-binding protein of the phytopathogen *Xanthomonas axonopodis pv. citri*. Acta Crystallogr F 62:289-291.

102. Lawson DM, Williams CE, Mitchenall LA, Pau RN. 1998. Ligand size is a major determinant of specificity in periplasmic oxyanion-binding proteins: the 1.2 Å resolution crystal structure of *Azotobacter vinelandii* ModA. Structure 6:1529-1539.

103. Hollenstein K, Comellas-Bigler M, Bevers LE, Feiters MC, Meyer-Klaucke W, Hagedoorn P-L, Locher KP. 2009. Distorted octahedral coordination of tungstate in a subfamily of specific binding proteins. J Biol Inorg 14:663-672.

104. Imperial J, Hadi M, Amy NK. 1998. Molybdate binding by ModA, the periplasmic component of the *Escherichia coli* mod molybdate transport system. Biochim Biophys Acta Biomembr 1370:337-346.

105. Aryal BP, Brugarolas P, He C. 2012. Binding of $ReO_4^-$ with an engineered $MoO_4^{2-}$-binding protein: towards a new approach in radiopharmaceutical applications. J Biol Inorg 17:97-106.

106. Balan A, Santacruz-Pérez C, Moutran A, Ferreira LCS, Neshich G, Barbosa JARG. 2008. Crystallographic structure and substrate-binding interactions of the molybdate-binding protein of the phytopathogen *Xanthomonas axonopodis pv. citri*. Biochimica et Biochim Biophys Acta Proteins Proteom 1784:393-399.

107. Maier RJ, Graham L. 1988. Molybdate transport by *Bradyrhizobium japonicum* bacteroids. J Bacteriol 170:5613-5619.

108. Bevers LE, Hagedoorn P-L, Krijger GC, Hagen WR. 2006. Tungsten transport protein A (WtpA) in *Pyrococcus furiosus*: the first member of a new class of tungstate and molybdate transporters. J Bacteriol 188:6498-6505.

109. Otrelo-Cardoso AR, Nair RR, Correia MA, Cordeiro RSC, Panjkovich A, Svergun DI, Santos-Silva T, Rivas MG. 2017. Highly selective tungstate transporter protein TupA from *Desulfovibrio alaskensis* G20. Sci Rep 7:1-12.

110. Sohrin Y, Matsui M, Nakayama E. 1999. Contrasting behavior of tungsten and molybdenum in the Okinawa Trough, the East China Sea and the Yellow Sea. Geochim Cosmochim Acta 63:3457-3466.

111. Malinovsky D, Hammarlund D, Ilyashuk B, Martinsson O, Gelting J. 2007. Variations in the isotopic composition of molybdenum in freshwater lake systems. Chem. Geol. 236:181-198.

112. Organization WH. 2004. Back ground document or development of WHO Guidelines for drinking-water quality. Fax 41:791.

113. Khanna S, Udas AC, Kumar GK, Suvarna S, Karjodkar FR. 2013. Trace elements (copper, zinc, selenium and molybdenum) as markers in oral sub mucous fibrosis and oral squamous cell carcinoma. J Trace Elem Med Biol 27:307-311.

114. Jackson ML, Zhang JZ, Li CS, Martin DF. 1986. The geochemical availability of soil Zn and Mo in relation to stomach and esophageal cancer in the People's Republic of China and U.S.A. Appl Geochem 1:487-492.

115. Nouri M, Chalian H, Bahman A, Mollahajian H, Ahmadi-Faghih M, Fakheri H, Soroush A. 2008. Nail molybdenum and zinc contents in populations with low and moderate incidence of esophageal cancer. Arch Iran Med 11:392-6.

116. Cao G-H, Yan S-M, Yuan Z-K, Wu L, Liu Y-F. 1998. A study of the relationship between trace element Mo and gastric cancer. World J Gastroenterol 4:55-56.

117. Rajagopalan K. 1988. Molybdenum: an essential trace element in human nutrition. Annu Rev Nutr 8:401-427.

118. Helz GR, Miller CV, Charnock JM, Mosselmans JFW, Pattrick RAD, Garner CD, Vaughan DJ. 1996. Mechanism of molybdenum removal from the sea and its concentration in black shales: EXAFS evidence. Geochim Cosmochim Acta 60:3631-3642.

119. Wichard T, Mishra B, Kraepiel A, Myneni S. 2008. Molybdenum speciation and bioavailability in soils. Geochim Cosmochim Acta 72:A1019.

120. Wichard T, Mishra B, Myneni SC, Bellenger J-P, Kraepiel AM. 2009. Storage and bioavailability of molybdenum in soils increased by organic matter complexation. Nat Geosci 2:625-629.

121. Smith HD, Parkinson GM, Hart RD. 2005. In situ absorption of molybdate and vanadate during precipitation of hydrotalcite from sodium aluminate solutions. J Cryst Growth 275:e1665-e1671.

122. Paikaray S, Hendry MJ. 2013. In situ incorporation of arsenic, molybdenum, and selenium during precipitation of hydrotalcite-like layered double hydroxides. Appl Clay Sci 77:33-39.

123. Allada RK, Navrotsky A, Berbeco HT, Casey WH. 2002. Thermochemistry and aqueous solubilities of hydrotalcite-like solids. Science 296:721-723.

124. Gustafsson JP. 2003. Modelling molybdate and tungstate adsorption to ferrihydrite. Chem Geol 200:105-115.

125. Goldberg S. 2010. Competitive adsorption of molybdenum in the presence of phosphorus or sulfur on gibbsite. Soil Sci 175:105-110.

126. Brooks SC. 2001. Waste characteristics of the former S-3 ponds and outline of uranium chemistry relevant to NABIR Field Research Center studies. ORNL Oak Ridge National Laboratory (US).

127. Revil A, Skold M, Karaoulis M, Schmutz M, Hubbard SS, Mehlhorn TL, Watson DB. 2013. Hydrogeophysical investigations of the former S-3 ponds contaminant plumes, Oak Ridge Integrated Field Research Challenge site, Tennessee. Geophysics 78:EN29-EN41.

128. Kornegay F, West D, McMahon L, Murphy J, Shipe L, Koncinski W. 1994. Oak Ridge reservation annual site environmental report for 1993. ES/ESH-47, Martin Marietta Energy Systems, Inc,

129. Jones S. 1998. Evaluation of Calendar Year 1997 Groundwater and Surface Water Quality Data For The Upper East Fork Poplar Creek Hydrogeologic Regime At The US Department of Energy Y-12 Plant, Oak Ridge, Tennessee. Oak Ridge Y-12 Plant, Oak Ridge, TN,

130. Smith MB, Rocha AM, Smillie CS, Olesen SW, Paradis C, Wu L, Campbell JH, Fortney JL, Mehlhorn TL, Lowe KA. 2015. Natural bacterial communities serve as quantitative geochemical biosensors. MBio 6:e00326-15.

131. He Z, Zhang P, Wu L, Rocha AM, Tu Q, Shi Z, Wu B, Qin Y, Wang J, Yan Q. 2018. Microbial functional gene diversity predicts groundwater contamination and ecosystem functioning. MBio 9.

132. Shcherbak I, Millar N, Robertson GP. 2014. Global metaanalysis of the nonlinear response of soil nitrous oxide ($N_2O$) emissions to fertilizer nitrogen. Proc Natl Acad Sci USA 111:9199-9204.

133. Solomon S, Manning M, Marquis M, Qin D. 2007. Climate change 2007-the physical science basis: working group I contribution to the fourth assessment report of the IPCC, vol 4. Cambridge university press.

134. Su Q, Domingo-Félez C, Jensen MM, Smets BF. 2019. Abiotic nitrous oxide ($N_2O$) production is strongly pH dependent, but contributes little to overall $N_2O$ emissions in biological nitrogen removal systems. Environ Sci Technol 53:3508-3516.

135. Khalil K, Mary B, Renault P. 2004. Nitrous oxide production by nitrification and denitrification in soil aggregates as affected by $O_2$ concentration. Soil Biol Biochem 36:687-699.

136. Shaaban M, Peng Q-a, Bashir S, Wu Y, Younas A, Xu X, Rashti MR, Abid M, Zafar-ul-Hye M, Núñez-Delgado A. 2019. Restoring effect of soil acidity and Cu on $N_2O$ emissions from an acidic soil. J Environ Manage 250:109535.

137. Cavazos AR. 2020. Interactions between reactive nitrogen and manganese: implications for marine nitrous oxide cycling, Georgia Institute of Technology.

138. Wilpiszeski RL, Gionfriddo CM, Wymore AM, Moon J-W, Lowe KA, Podar ML, Fields MW, Hazen TC, Ge X, Poole F. 2020. In-field bioreactors demonstrate dynamic shifts in microbial communities in response to geochemical perturbations. bioRxiv.

139. Wu X, Wu L, Liu Y, Zhang P, Li Q, Zhou J, Hess NJ, Hazen TC, Yang W, Chakraborty R. 2018. Microbial interactions with dissolved organic matter drive carbon dynamics and community succession. Front Microbiol 9:1234.

140. Wu X, Spencer S, Gushgari-Doyle S, Yee MO, Voriskova J, Li Y, Alm EJ, Chakraborty R. 2020. Culturing of “unculturable" subsurface microbes: Natural organic carbon source fuels the growth of diverse and distinct bacteria from groundwater. bioRxiv.

141. Thorgersen MP, Ge X, Poole FL, Price MN, Arkin AP, Adams MW. 2019. Nitrate-utilizing microorganisms resistant to multiple metals from the heavily contaminated Oak Ridge Reservation. Appl Environ Microbiol 85:e00896-19.

142. Moura JJG, Brondino CD, Trincao J, Romao MJ. 2004. Mo and W bis-MGD enzymes: nitrate reductases and formate dehydrogenases. J Biol Inorg Chem 9:791-799.

143. Istok J, Senko J, Krumholz LR, Watson D, Bogle MA, Peacock A, Chang Y-J, White DC. 2004. In situ bioreduction of technetium and uranium in a nitrate-contaminated aquifer. Environ Sci Technol 38:468-475.

144. Rauret G. 1998. Extraction procedures for the determination of heavy metals in contaminated soil and sediment. Talanta 46:449-455.

145. Giles M, Morley N, Baggs EM, Daniell TJ. 2012. Soil nitrate reducing processes drivers, mechanisms for spatial variation, and significance for nitrous oxide production. Front Microbiol 3.

146. Zumft WG. 1997. Cell biology and molecular basis of denitrification. Microbiol Mol Biol Rev 61:533-616.

147. Vergnes A, Gouffi-Belhabich K, Blasco F, Giordano G, Magalon A. 2004. Involvement of the molybdenum cofactor biosynthetic machinery in the maturation of the *Escherichia coli* nitrate reductase A. J Biol Chem 279:41398-41403.

148. Showe MK, DeMoss J. 1968. Localization and regulation of synthesis of nitrate reductase in *Escherichia coli*. J Bacteriol 95:1305-1313.

149. Härtig E, Schiek U, Vollack K-U, Zumft WG. 1999. Nitrate and nitrite control of respiratory nitrate reduction in denitrifying *Pseudomonas stutzeri* by a two-component regulatory system homologous to NarXL of *Escherichia coli*. J Bacteriol 181:3658-3665.

150. Watson D, Kostka J, Fields M, Jardine P. 2004. The Oak Ridge field research center conceptual model. NABIR Field Research Center, Oak Ridge, TN.

151. Wu W-M, Carley J, Fienen M, Mehlhorn T, Lowe K, Nyman J, Luo J, Gentile ME, Rajan R, Wagner D. 2006. Pilot-scale in situ bioremediation of uranium in a highly contaminated aquifer. 1. Conditioning of a treatment zone. Environ Sci Technol 40:3978-3985.

152. Salmimies R, Mannila M, Juha J, Häkkinen A. 2011. Acidic dissolution of magnetite: experimental study on the effects of acid concentration and temperature. Clays Clay Miner 59:136-146.

153. Salmimies R. 2012. Acidic dissolution of iron oxides and regeneration of a ceramic filter medium. Acta Universitatis Lappeenrantaensis.

154. Qu Z, Bakken LR, Molstad L, Frostegård Å, Bergaust LL. 2016. Transcriptional and metabolic regulation of denitrification in *P. aracoccus* denitrificans allows low but significant activity of nitrous oxide reductase under oxic conditions. Environ Microbiol 18:2951-2963.

155. Hug LA, Thomas BC, Sharon I, Brown CT, Sharma R, Hettich RL, Wilkins MJ, Williams KH, Singh A, Banfield JF. 2016. Critical biogeochemical functions in the subsurface are associated with bacteria from new phyla and little studied lineages. Environ Microbiol 18:159-173.

156. Klotz MG, Stein LY. 2008. Nitrifier genomics and evolution of the nitrogen cycle. FEMS Microbiol Lett 278:146-156.

157. Palmer K, Biasi C, Horn MA. 2012. Contrasting denitrifier communities relate to contrasting $N_2O$ emission patterns from acidic peat soils in arctic tundra. ISME J 6:1058.

158. Palmer K, Drake HL, Horn MA. 2010. Association of novel and highly diverse acid-tolerant denitrifiers with $N_2O$ fluxes of an acidic fen. Appl Environ Microbiol 76:1125-1134.

159. Watanabe T, Motoyama H, Kuroda M. 2001. Denitrification and neutralization treatment by direct feeding of an acidic wastewater containing copper ion and high-strength nitrate to a bio-electrochemical reactor process. Water Res 35:4102-4110.

160. Hemme CL, Deng Y, Gentry TJ, Fields MW, Wu L, Barua S, Barry K, Tringe SG, Watson DB, He Z. 2010. Metagenomic insights into evolution of a heavy metal-contaminated groundwater microbial community. ISME J 4:660-672.

161. Morford JL, Martin WR, Kalnejais LH, François R, Bothner M, Karle I-M. 2007. Insights on geochemical cycling of U, Re and Mo from seasonal sampling in Boston Harbor, Massachusetts, USA. Geochim Cosmochim Acta 71:895-917.

162. Beck M, Dellwig O, Schnetger B, Brumsack H-J. 2008. Cycling of trace metals (Mn, Fe, Mo, U, V, Cr) in deep pore waters of intertidal flat sediments. Geochim Cosmochim Acta 72:2822-2840.

163. Smedley PL, Edmunds WM. 2002. Redox patterns and trace‐element behavior in the east midlands triassic sandstone aquifer, UK. Groundwater 40:44-58.

164. Nordstrom DK. 2015. Baseline and premining geochemical characterization of mined sites. Appl Geochem 57:17-34.

165. Sánchez-España J, Yusta I, Gray J, Burgos WD. 2016. Geochemistry of dissolved aluminum at low pH: Extent and significance of Al–Fe (III) coprecipitation below pH 4.0. Geochim Cosmochim Acta 175:128-149.

166. Cronan CS, Schofield CL. 1979. Aluminum leaching response to acid precipitation: effects on high-elevation watersheds in the northeast. Science 204:304-306.

167. Johnson DB, Hallberg KB. 2005. Acid mine drainage remediation options: a review. Sci Total Environ 338:3-14.

168. Baeseman J, Smith R, Silverstein J. 2006. Denitrification potential in stream sediments impacted by acid mine drainage: effects of pH, various electron donors, and iron. Microb Ecol 51:232-241.

169. Colman DR, Poudel S, Stamps BW, Boyd ES, Spear JR. 2017. The deep, hot biosphere: twenty-five years of retrospection. Proc Natl Acad Sci USA 114:6895-6903.

170. Smith VH, Tilman GD, Nekola JC. 1999. Eutrophication: impacts of excess nutrient inputs on freshwater, marine, and terrestrial ecosystems. Environ Pollut 100:179-196.

171. Widdel F, Bak F. 1992. Gram-negative mesophilic sulfate-reducing bacteria, p 3352-3378. *In* Balows A, Trüper H, Dworkin M, Harder W, Schleifer K-H (ed), The Prokaryotes. Springer New York.

172. Miranda KM, Espey MG, Wink DA. 2001. A rapid, simple spectrophotometric method for simultaneous detection of nitrate and nitrite. Nitric Oxide 5:62-71.

173. Nason A, Lee K-Y, Pan S-S, Ketchum PA, Lamberti A, DeVries J. 1971. *In vitro* formation of assimilatory reduced nicotinamide adenine dinucleotide phosphate: nitrate reductase from a Neurospora mutant and a component of molybdenum-enzymes. Proc Natl Acad Sci USA 68:3242-3246.

174. Moon JW, Roh Y, Phelps TJ, Phillips DH, Watson DB, Kim YJ, Brooks SC. 2006. Physicochemical and mineralogical characterization of soil-saprolite cores from a field research site, Tennessee. J Environ Qual 35:1731-1741.

175. Li B, Wu WM, Watson DB, Cardenas E, Chao YQ, Phillips DH, Mehlhorn T, Lowe K, Kelly SD, Li PS, Tao HC, Tiedje JM, Criddle CS, Zhang T. 2018. Bacterial community shift and coexisting/coexcluding patterns revealed by network analysis in a uranium-contaminated site after bioreduction followed by reoxidation. Appl Environ Microbiol 84.

176. Kazi T, Jamali M, Kazi G, Arain M, Afridi H, Siddiqui A. 2005. Evaluating the mobility of toxic metals in untreated industrial wastewater sludge using a BCR sequential extraction procedure and a leaching test. Anal Bioanal Chem 383:297-304.

177. Link DD, Walter PJ, Kingston H. 1998. Development and validation of the new EPA microwave-assisted leach method 3051A. Environ Sci Technol 32:3628-3632.

178. Ge X, Vaccaro BJ, Thorgersen MP, Poole FL, Majumder EL, Zane GM, De León KB, Lancaster WA, Moon JW, Paradis CJ. 2019. Iron- and aluminium‐induced depletion of molybdenum in acidic environments impedes the nitrogen cycle. Environ Microbiol 21:152-163.

179. Bolger AM, Lohse M, Usadel B. 2014. Trimmomatic: a flexible trimmer for Illumina sequence data. Bioinformatics 30:2114-2120.

180. Bankevich A, Nurk S, Antipov D, Gurevich AA, Dvorkin M, Kulikov AS, Lesin VM, Nikolenko SI, Pham S, Prjibelski AD. 2012. SPAdes: a new genome assembly algorithm and its applications to single-cell sequencing. J Comput Biol 19:455-477.

181. Seemann T. 2014. Prokka: rapid prokaryotic genome annotation. Bioinformatics 30:2068-2069.

182. Arkin AP, Cottingham RW, Henry CS, Harris NL, Stevens RL, Maslov S, Dehal P, Ware D, Perez F, Canon S. 2018. KBase: the United States department of energy systems biology knowledgebase. Nat Biotechnol 36:566.

183. Schwarz G. 2016. Molybdenum cofactor and human disease. Curr Opin Chem Biol 31:179-187.

184. Hamlin RL. 2016. Molybdenum, p 391-410, Handbook of Plant Nutrition. CRC Press.

185. Grunden AM, Shanmugam K. 1997. Molybdate transport and regulation in bacteria. Arch Microbiol 168:345-354.

186. Zhang Q, Sun J, Liu J, Huang G, Lu C, Zhang Y. 2015. Driving mechanism and sources of groundwater nitrate contamination in the rapidly urbanized region of south China. J Contam Hydrol 182:221-230.

187. Kellman L, Hillaire-Marcel C. 2003. Evaluation of nitrogen isotopes as indicators of nitrate contamination sources in an agricultural watershed. Agric, Ecosyst Environ 95:87-102.

188. Moon J-W, Paradis CJ, Joyner DC, von Netzer F, Majumder EL, Dixon ER, Podar M, Ge X, Walian PJ, Smith HJ. 2020. Characterization of subsurface media from locations up- and down-gradient of a uranium-contaminated aquifer. Chemosphere:126951.

189. Altschul SF, Gish W, Miller W, Myers EW, Lipman DJ. 1990. Basic local alignment search tool. J Mol Biol 215:403-410.

190. Filiatrault MJ, Tombline G, Wagner VE, Van Alst N, Rumbaugh K, Sokol P, Schwingel J, Iglewski BH. 2013. *Pseudomonas aeruginosa* PA1006, which plays a role in molybdenum homeostasis, is required for nitrate utilization, biofilm formation, and virulence. PLoS One 8.

191. Scott IM, Rubinstein GM, Lipscomb GL, Basen M, Schut GJ, Rhaesa AM, Lancaster WA, Poole FL, Kelly RM, Adams MW. 2015. A new class of tungsten-containing oxidoreductase in *Caldicellulosiruptor*, a genus of plant biomass-degrading thermophilic bacteria. Appl Environ Microbiol 81:7339-7347.

192. Lancaster WA, Menon AL, Scott I, Poole FL, Vaccaro BJ, Thorgersen MP, Geller J, Hazen TC, Hurt RA, Brown SD. 2014. Metallomics of two microorganisms relevant to heavy metal bioremediation reveal fundamental differences in metal assimilation and utilization. Metallomics 6:1004-1013.

193. Kahm M, Hasenbrink G, Lichtenberg-Fraté H, Ludwig J, Kschischo M. 2010. grofit: fitting biological growth curves with R. J Stat Softw 33:1-21.

194. Cole JR, Wang Q, Fish JA, Chai B, McGarrell DM, Sun Y, Brown CT, Porras-Alfaro A, Kuske CR, Tiedje JM. 2013. Ribosomal Database Project: data and tools for high throughput rRNA analysis. Nucleic Acids Res 42:D633-D642.

195. Nguyen L-T, Schmidt HA, von Haeseler A, Minh BQ. 2014. IQ-TREE: a fast and effective stochastic algorithm for estimating maximum-likelihood phylogenies. Mol Biol Evol 32:268-274.

196. Kalyaanamoorthy S, Minh BQ, Wong TK, von Haeseler A, Jermiin LS. 2017. ModelFinder: fast model selection for accurate phylogenetic estimates. Nat Methods 14:587.

197. Hoang DT, Chernomor O, Von Haeseler A, Minh BQ, Vinh LS. 2017. UFBoot2: improving the ultrafast bootstrap approximation. Mol Biol Evol 35:518-522.

198. Mitchell AL, Attwood TK, Babbitt PC, Blum M, Bork P, Bridge A, Brown SD, Chang H-Y, El-Gebali S, Fraser MI. 2018. InterPro in 2019: improving coverage, classification and access to protein sequence annotations. Nucleic Acids Res 47:D351-D360.

199. Huang Y, Niu B, Gao Y, Fu L, Li W. 2010. CD-HIT Suite: a web server for clustering and comparing biological sequences. Bioinformatics 26:680-682.

200. Madeira F, Lee J, Buso N, Gur T, Madhusoodanan N, Basutkar P, Tivey A, Potter SC, Finn RD, Lopez R. 2019. The EMBL-EBI search and sequence analysis tools APIs in 2019. Nucleic Acids Res 47:W636-W641.

201. Armenteros JJA, Tsirigos KD, Sønderby CK, Petersen TN, Winther O, Brunak S, von Heijne G, Nielsen H. 2019. SignalP 5.0 improves signal peptide predictions using deep neural networks. Nat Biotechnol 37:420.

202. Robert X, Gouet P. 2014. Deciphering key features in protein structures with the new ENDscript server. Nucleic Acids Res 42:W320-W324.

203. Pettersen EF, Goddard TD, Huang CC, Couch GS, Greenblatt DM, Meng EC, Ferrin TE. 2004. UCSF Chimera—a visualization system for exploratory research and analysis. J Comput Chem 25:1605-1612.

204. Sigurskjold BW. 2000. Exact analysis of competition ligand binding by displacement isothermal titration calorimetry. Anal Biochem 277:260-266.

205. Tian R, Ning D, He Z, Zhang P, Spencer SJ, Gao S, Shi W, Wu L, Zhang Y, Yang Y. 2020. Small and mighty: adaptation of superphylum *Patescibacteria* to groundwater environment drives their genome simplicity. Microbiome 8:1-15.

206. Hyatt D, Chen G-L, LoCascio PF, Land ML, Larimer FW, Hauser LJ. 2010. Prodigal: prokaryotic gene recognition and translation initiation site identification. BMC Bioinformatics 11:119.

207. Huerta-Cepas J, Forslund K, Coelho LP, Szklarczyk D, Jensen LJ, Von Mering C, Bork P. 2017. Fast genome-wide functional annotation through orthology assignment by eggNOG-mapper. Mol Biol Evol 34:2115-2122.

208. MacGregor CH, Schnaitman CA, Normansell DE, Hodgins MG. 1974. Purification and properties of nitrate reductase from *Escherichia coli* K12. J Biol Chem 249:5321-5327.

209. Cabello P, Roldan MD, Moreno-Vivian C. 2004. Nitrate reduction and the nitrogen cycle in archaea. Microbiology 150:3527-3546.

210. Krainer G, Keller S. 2015. Single-experiment displacement assay for quantifying high-affinity binding by isothermal titration calorimetry. Methods 76:116-123.

211. Abulencia CB, Wyborski DL, Garcia JA, Podar M, Chen W, Chang SH, Chang HW, Watson D, Brodie EL, Hazen TC. 2006. Environmental whole-genome amplification to access microbial populations in contaminated sediments. Appl Environ Microbiol 72:3291-3301.

212. Vishnivetskaya TA, Mosher JJ, Palumbo AV, Yang ZK, Podar M, Brown SD, Brooks SC, Gu B, Southworth GR, Drake MM. 2011. Mercury and other heavy metals influence bacterial community structure in contaminated Tennessee streams. Appl Environ Microbiol 77:302-311.

213. Corcuera GL, Bastidas M, Dubourdieu M. 1993. Molybdenum uptake in *Escherichia coli* K12. Microbiology 139:1869-1875.

214. Smart JP, Cliff MJ, Kelly DJ. 2009. A role for tungsten in the biology of *Campylobacter jejuni*: Tungstate stimulates formate dehydrogenase activity and is transported via an

ultra‐high affinity ABC system distinct from the molybdate transporter. Mol Microbiol 74:742-757.

215. Rech S, Wolin C, Gunsalus RP. 1996. Properties of the periplasmic ModA molybdate-binding protein of *Escherichia coli*. J Biol Chem 271:2557-2562.

216. Nielsen H, Tsirigos KD, Brunak S, von Heijne G. 2019. A brief history of protein sorting prediction. The protein journal:1-17.

217. Sutcliffe IC, Russell R. 1995. Lipoproteins of gram-positive bacteria. J Bacteriol 177:1123.

218. Hutchings MI, Palmer T, Harrington DJ, Sutcliffe IC. 2009. Lipoprotein biogenesis in Gram-positive bacteria: knowing when to hold ‘em, knowing when to fold ‘em. Trends Microbiol 17:13-21.

219. Schwarz G, Mendel RR. 2006. Molybdenum cofactor biosynthesis and molybdenum enzymes. Annu Rev Plant Biol 57:623-647.

220. Pienkos PT, Brill W. 1981. Molybdenum accumulation and storage in *Klebsiella pneumoniae* and *Azotobacter vinelandii*. J Bacteriol 145:743-751.

221. Smedley P, Cooper D, Ander E, Milne C, Lapworth D. 2014. Occurrence of molybdenum in British surface water and groundwater: distributions, controls and implications for water supply. Appl Geochem 40:144-154.

222. Wallenstein MD, Myrold DD, Firestone M, Voytek M. 2006. Environmental controls on denitrifying communities and denitrification rates: insights from molecular methods. Ecol Appl 16:2143-2152.

223. Heggeset TM, Krog A, Balzer S, Wentzel A, Ellingsen TE, Brautaset T. 2012. Genome sequence of thermotolerant *Bacillus methanolicus*: features and regulation related to

methylotrophy and production of L-lysine and L-glutamate from methanol. Appl Environ Microbiol 78:5170-5181.

224. Lapidus A, Goltsman E, Auger S, Galleron N, Ségurens B, Dossat C, Land ML, Broussolle V, Brillard J, Guinebretiere M-H. 2008. Extending the *Bacillus cereus* group genomics to putative food-borne pathogens of different toxicity. Chem-Biol Interact 171:236-249.

225. Guan P, Ai P, Dai X, Zhang J, Xu L, Zhu J, Li Q, Deng Q, Li S, Wang S. 2012. Complete genome sequence of *Bacillus thuringiensis serovar Sichuansis* strain MC28. J Bacteriol 194:6975-6975.

226. Djukic M, Brzuszkiewicz E, Fünfhaus A, Voss J, Gollnow K, Poppinga L, Liesegang H, Garcia-Gonzalez E, Genersch E, Daniel R. 2014. How to kill the honey bee larva: genomic potential and virulence mechanisms of *Paenibacillus larvae*. PloS One 9.

227. Zeigler DR, Prágai Z, Rodriguez S, Chevreux B, Muffler A, Albert T, Bai R, Wyss M, Perkins JB. 2008. The origins of 168, W23, and other *Bacillus subtilis* legacy strains. J Bacteriol 190:6983-6995.

228. Burkholder PR, Giles Jr NH. 1947. Induced biochemical mutations in *Bacillus subtilis*. Am J Bot:345-348.

229. Mohapatra BR, La Duc MT. 2012. Rapid detection of viable *Bacillus pumilus* SAFR-032 encapsulated spores using novel propidium monoazide-linked fluorescence in situ hybridization. J Microbiol Methods 90:15-19.

230. Zhu X, Burger M, Doane TA, Horwath WR. 2013. Ammonia oxidation pathways and nitrifier denitrification are significant sources of $N_2O$ and NO under low oxygen availability. Proc Natl Acad Sci USA 110:6328-6333.

231. Cuevas JG, Paulino L, Dörner J. 2020. Pathways for nitrous oxide generation in forested and agricultural zones growing on volcanic ash soils. J Soil Sci Plant Nutr:1-13.

232. Green SJ, Prakash O, Jasrotia P, Overholt WA, Cardenas E, Hubbard D, Tiedje JM, Watson DB, Schadt CW, Brooks SC. 2012. Denitrifying bacteria from the genus *Rhodanobacter* dominate bacterial communities in the highly contaminated subsurface of a nuclear legacy waste site. Appl Environ Microbiol 78:1039-1047.

233. Spain AM, Krumholz LR. 2011. Nitrate-reducing bacteria at the nitrate and radionuclide contaminated Oak Ridge Integrated Field Research Challenge site: a review. Geomicrobiol J 28:418-429.

234. Ge X, Thorgersen MP, Poole FL, Deutschbauer AM, Chandonia J-M, Novichkov PS, Adams PD, Arkin AP, Hazen TC, Adams MWW. 2020. Draft genome sequence of *Bacillus sp*. EB106-08-02-XG196 isolated from high nitrate contaminated sediment. Microbiol Resour Announc 9:e01149-20.

235. Ge X, Thorgersen MP, Poole FL, Deutschbauer AM, Chandonia J-M, Novichkov PS, Gushgari-Doyle S, Lui LM, Nielsen T, Chakraborty R, Adams PD, Arkin AP, Hazen TC, Adams MWW. 2020. Characterization of a metal-resistant *Bacillus* strain with a high molybdate affinity ModA from contaminated sediments at the Oak Ridge Reservation. Front Microbiol 11:2543.

236. Dixon E, Walker KF, Williams D, Hazen T. 2019. Modeling dynamic geochemical processes: How diurnal and seasonal water table fluctuations influence contaminated groundwater geochemistry. AGUFM 2019:H41S-2008.

237. Wu X, Lui L, Liu Y, Justice N, Simmons T, Nielsen T, Jagadamma S, Hess NJ, Hazen T, Arkin AP. 2019. Insights into the depth-resolved geochemical constraints on microbial

community structure and metabolic potential for carbon cycling in shallow subsurface sediment. AGUFM 2019:B53L-2567.

238. Couradeau E, Sasse J, Goudeau D, Nath N, Hazen TC, Bowen BP, Chakraborty R, Malmstrom RR, Northen TR. 2019. Probing the active fraction of soil microbiomes using BONCAT-FACS. Nat Commun 10:1-10.

239. Thorgersen MP, Lancaster WA, Rajeev L, Ge X, Vaccaro BJ, Poole FL, Arkin AP, Mukhopadhyay A, Adams MW. 2017. A highly expressed high-molecular-weight S-layer complex of *Pelosinus sp.* strain ufo1 binds uranium. Appl Environ Microbiol 83.

240. Wu X, Spencer S, Gushgari-Doyle S, Yee MO, Voriskova J, Li Y, Alm EJ, Chakraborty R. 2020. Culturing of" Unculturable" Subsurface Microbes: Natural Organic Carbon Source Fuels the Growth of Diverse and Distinct Bacteria from Groundwater. bioRxiv.

241. Huerta-Cepas J, Szklarczyk D, Heller D, Hernández-Plaza A, Forslund SK, Cook H, Mende DR, Letunic I, Rattei T, Jensen LJ. 2019. eggNOG 5.0: a hierarchical, functionally and phylogenetically annotated orthology resource based on 5090 organisms and 2502 viruses. Nucleic Acids Res 47:D309-D314.

242. Hatzenpichler R, Scheller S, Tavormina PL, Babin BM, Tirrell DA, Orphan VJ. 2014. In situ visualization of newly synthesized proteins in environmental microbes using amino acid tagging and click chemistry. Environ Microbiol 16:2568-2590.

243. Hatzenpichler R, Connon SA, Goudeau D, Malmstrom RR, Woyke T, Orphan VJ. 2016. Visualizing in situ translational activity for identifying and sorting slow-growing archaeal− bacterial consortia. Proc Natl Acad Sci USA 113:E4069-E4078.

244. Price MN, Wetmore KM, Waters RJ, Callaghan M, Ray J, Liu H, Kuehl JV, Melnyk RA, Lamson JS, Suh Y. 2018. Mutant phenotypes for thousands of bacterial genes of unknown function. Nature 557:503-509.

245. Wetmore KM, Price MN, Waters RJ, Lamson JS, He J, Hoover CA, Blow MJ, Bristow J, Butland G, Arkin AP. 2015. Rapid quantification of mutant fitness in diverse bacteria by sequencing randomly bar-coded transposons. MBio 6.

246. Vaccaro BJ, Lancaster WA, Thorgersen MP, Zane GM, Younkin AD, Kazakov AE, Wetmore KM, Deutschbauer A, Arkin AP, Novichkov PS. 2016. Novel metal cation resistance systems from mutant fitness analysis of denitrifying Pseudomonas stutzeri. Appl Environ Microbiol 82:6046-6056.

247. Stewart LJ, Bailey S, Bennett B, Charnock JM, Garner CD, McAlpine AS. 2000. Dimethylsulfoxide reductase: an enzyme capable of catalysis with either molybdenum or tungsten at the active site. J Mol Biol 299:593-600.

248. Haja DK, Wu C-H, Ponomarenko O, Poole FL, George GN, Adams MW. 2020. Improving arsenic tolerance of *Pyrococcus furiosus* by the heterologous expression of a respiratory arsenate reductase. Appl Environ Microbiol.

249. Williams TA, Szöllősi GJ, Spang A, Foster PG, Heaps SE, Boussau B, Ettema TJ, Embley TM. 2017. Integrative modeling of gene and genome evolution roots the archaeal tree of life. Proc Natl Acad Sci USA s 114:E4602-E4611.

250. Porat I, Vishnivetskaya TA, Mosher JJ, Brandt CC, Yang ZK, Brooks SC, Liang L, Drake MM, Podar M, Brown SD. 2010. Characterization of archaeal community in contaminated and uncontaminated surface stream sediments. Microb Ecol 60:784-795.

251. Guillou L, Eikrem W, Chrétiennot-Dinet M-J, Le Gall F, Massana R, Romari K, Pedrós-Alió C, Vaulot D. 2004. Diversity of picoplanktonic prasinophytes assessed by direct nuclear SSU rDNA sequencing of environmental samples and novel isolates retrieved from oceanic and coastal marine ecosystems. Protist 155:193-214.

252. Fuhrman JA, Ouverney CC. 1998. Marine microbial diversity studied via 16S rRNA sequences: cloning results from coastal waters and counting of native archaea with fluorescent single cell probes. Aquat Ecol 32:3-15.